GCA-TR-68-7-N

EXPERIMENTAL AND THEORETICAL STUDIES IN PLANETARY AERONOMY

PRINCIPAL INVESTIGATOR: F. F. MARMO

GCA CORPORATION

Bedford, Massachusetts

FINAL REPORT

CONTRACT NO. NASW-1283

PREPARED FOR

NATIONAL AERONAUTICS AND SPACE ADMINISTRATION

HEADQUARTERS

WASHINGTON, D. C.

JULY 1968

GCA-TR-68-7-N

EXPERIMENTAL AND THEORETICAL STUDIES IN PLANETARY AERONOMY

Principal Investigator: F. F. Marmo

GCA CORPORATION
GCA TECHNOLOGY DIVISION
Bedford, Massachusetts

FINAL REPORT

Contract No. NASW-1283

July 1968

Prepared for:

NATIONAL AERONAUTICS AND SPACE ADMINISTRATION
Headquarters
Washington, D. C.

TABLE OF CONTENTS

I. INTRODUCTION

This Final Report summarizes the work performed under Contract No. NASW-1283 for the period 17 September 1966 through 1 March 1968. The overall problems associated with the physics of planetary atmosphere and the broad variety of scientific areas which have been considered are discussed most conveniently under the following major categories:

A. Photochemistry of planetary atmospheres
B. Theoretical studies
C. Laboratory investigations in the VUV (2000-1000Å) and the EUV (below 1000Å) spectral regions
D. Planetary aeronomy

During the performance of the subject contract, a number of reports were generated which have been submitted and accepted for publication in accredited journals. In some cases, a more detailed discussion of the material is available in the form of published GCA Technical Reports. In any event, the pertinent information concerning the journal publication is presented below for each of the categories previously cited:

A. Photochemistry of Planetary Atmospheres

"Laboratory Rate Coefficients for Positive Ion-Neutral Reactions in the Ionosphere," by P. Warneck, J. Geophys. Res. 72, 1651 (1967).

"Reactions of ^1D Oxygen Atoms III. Ozone Formation in the 1470Å Photolysis of O_2," by P. Warneck and J. O. Sullivan, J. Chem. Phys. 46, 953 (1967).

"Gas Analysis by Photoionization Mass Spectrometry," by W. Poschenrieder and P. Warneck, J. Appl. Phys. 37, 2812 (1966).

"On the Quenching of the 6300Å," by P. Warneck and J. O. Sullivan, Planet. Space Sci. 14, 1225 (1966).

"Studies of Ion-Neutral Reactions by a Photoionization Mass Spectrometer Technique, II. Charge Transfer Reactions of Argon Ions at Near Thermal Energies," by P. Warneck, J. Chem. Phys. 46, 513 (1967).

"Studies of Ion-Neutral Reactions by a Photoionization Mass Spectrometer, III. Several Ionospheric Reactions," by P. Warneck, Planet. Sci. 15, 1349 (1967).

"Studies of Ion-Neutral Reactions by a Photoionization Mass Spectrometer. IV. Reactions of He^+ with Nitrogen and Oxygen," by P. Warneck, J. Chem. Phys. 47, 4279 (1967).

"Primary Processes in the Photolysis of SO_2 at 1849Å," by J. N. Driscoll and P. Warneck, J. Chem. Phys. (submitted April 1968).

B. Theoretical Studies

"The Diurnal Variation of Ionospheric Temperatures," by A. Dalgarno, M. B. McElroy and J. C. G. Walker, Planet. Space Sci. 15, 331 (1967).

"Ion Temperatures in the Topside Ionosphere," by A. Dalgarno and J. C. G. Walker, Planet. Space Sci. 15, 200 (1967).

"Atom-Atom Collision Processes in Astrophysics: Theoretical Studies," by A. Dalgarno, Rev. Mod. Phys. 39, 850 (1967).

"Some Problems in Planetary Atmospheres Involving Collision Processes," by A. Dalgarno, Rev. Mod. Phys. 39, 858 (1967).

"Dipole Properties of Molecular Nitrogen," by A. Dalgarno, T. C. Degges and D. A. Williams, Proc. Phys. Soc. (London) 92, 291 (1967).

"Electron Cooling in the Upper Atmosphere," by A. Dalgarno and T. C. Degges, Planet. Space Sci. 16, 125 (1968).

"Optical Properties of Molecular Hydrogen," by G. A. Victor, J. C. Browne and A. Dalgarno, Proc. Phys. Soc. (London) 92, 42 (1967).

"Electron Impact Excitation of the Dayglow," by A. Dalgarno, M. B. McElroy and A. I. Stewart, Planet. and Space Sci. (submitted April 1968).

C. Laboratory Investigations in the VUV (2000-1000Å) and the EUV (below 1000Å) Spectral Regions

"Photoabsorption Studies of Hydrogen Discharges," by R. B. Cairns and J. A. R. Samson, Proc. Phys. Soc. (London) 90, 879 (1967).

"Vacuum Ultraviolet Research," by J. A. R. Samson, Appl. Opt. 6, 403 (1967).

"The Relative Photoelectric Yield and Transmittance of Aℓ Films," by R. B. Cairns and J. A. R. Samson, J. Opt. Soc. Am. 90, 879 (1967).

"Ionization Potential of O_2," by J. A. R. Samson and R. B. Cairns, J. Opt. Soc. Am. 56, 769 (1966).

"Ionization Potential of Molecular Xenon and Krypton," by J. A. R. Samson and R. B. Cairns, J. Opt. Soc. Am. 56, 1140 (1966).

"Total Absorption Cross Sections of CO and CO_2 in the Region 550-200Å," by R. B. Cairns and J. A. R. Samson, J. Opt. Soc. Am. 56, 526 (1966).

"Reflectance and Relative Transmittance of Laser Deposited Iridium in the Vacuum Ultraviolet," by J. A. R. Samson, J. P. Padur, and A. Sharma, J. Opt. Soc. Am. 57, 966 (1967).

"Metal Photocathodes as Secondary Standards for Absolute Intensity Measurements in the Vacuum Ultraviolet," by R. B. Cairns and J. A. R. Samson, J. Opt. Soc. Am. 56, 1568 (1966).

"Photoelectron Spectroscopy of the Rare Gases," by J. A. R. Samson and R. B. Cairns, Phys. Rev. (submitted April 1968).

D. Planetary Aeronomy

"Experimental Evidence for Xe_2 Molecules," by Shardanand, Phys. Rev. 160, 67 (1967).

"Photon Scattering Cross Sections at Lyman-α (1215.7Å) for He and Ne," by Shardanand and Y. Mikawa, J. Quant. Spectry. Radia. Trans. 7, 605 (1967).

"Scattering Cross Sections of Argon and Krypton in the VUV," by R. B. Cairns, F. F. Marmo and J. A. R. Samson, J. Opt. Soc. Am. (submitted April 1968).

A significant portion of the research results generated under the subject contract have been presented at various scientific and technical meetings. This information is presented below.

E. Technical Papers Presented at Scientific and/or Professional Meetings

"Charge Transfer Reactions of Argon Ions at Near Thermal Energies," by P. Warneck at the 19th Annual Gaseous Electronics Conference held at the Atlanta Americana Motor Hotel, Atlanta, Georgia on October 12-14, 1966.

"The Kinetic Energies of Photoelectrons," by J. A. R. Samson, invited talk delivered at the NASA-Ames Research Center, 10 January 1967.

"Photoelectron Spectroscopy," by J. A. R. Samson, invited talk delivered at the University of Southern California, 13 January 1967.

Conference on the Atmospheres of Mars and Venus (F. F. Marmo), sponsored by NASA-Goddard Space Flight Center (ISS) and Kitt Peak National Observatory, and held in Tucson, Arizona, February 28 - March 2, 1967.

"Photoelectron Spectroscopy," by J. A. R. Samson, invited talk delivered at seminar held at the Air Force Cambridge Research Laboratory, April 10, 1967.

"The Scattering Cross Section of Argon in the Vacuum Ultraviolet," by R. B. Cairns, J. A. R. Samson, and F. F. Marmo, contributed paper presented by R. B. Cairns at Meeting of the Optical Society of America, Columbus, Ohio, April 12, 1967.

"Vacuum Ultraviolet Radiation," by J. A. R. Samson, invited talk delivered at seminar held at Syracuse University, April 21, 1967.

"Laboratory Studies Employing a Photoionization Mass Spectrometer," by P. Warneck, invited talk delivered at seminar held at the Air Force Cambridge Research Laboratories, May 4, 1967.

"Specific Photoionization Cross Sections of Xe, Dr, and Ar," by J. A. R. Samson, invited talk delivered at Fifteenth Annual Conference on Mass Spectroscopy and Allied Topics, Denver, Colorado, May 14, 1967.

"Ultraviolet Satellite Observation of Noctilucent Clouds," by F. F. Marmo, A. Engelman, and H. A. Miranda, Jr., contributed paper presented by F. F. Marmo at AGU Meeting held in Washington, D. C., 17-20 April 1967.

"Specific Photoionization Cross Sections of Atoms and Molecules," by J. A. R. Samson and R. B. Cairns, contributed paper presented by J. A. R. Samson at American Physical Society Meeting, Toronto, Canada, June 21, 1967.

"Reactions of ^1D Oxygen Atoms, Reactions with N_2O, N_2, and CO_2," by P. Warneck, presented at International Conference on Photochemistry, Munich, Germany, September 6-9, 1967. (No travel expense on the current contract involved.)

"Photoionization Mass Spectrometry and Its Applications to Chemical Physics," by P. Warneck, presented paper, Department of Chemistry, Northeastern University, March 25, 1968.

"Photon Scattering in the VUV," by F. F. Marmo, R. B. Cairns, and J. A. R. Samson, Forty-ninth Annual Meeting of AGU, Washington, D. C., April 10, 1968.

The remainder of this report describes the results of the several planetary physics investigations which have been performed under the present contract effort. These discussions are brief since a more comprehensive description of the work is available in the cited references. As such, the ensemble of publications are summarized by technical areas, accompanied by a tabulation of the published papers. For convenience, a dual reference system is employed in which the published material generated under the current program is indicated by an appropriate letter-number designation, whereas other references are designated by Arabic numerals.

II. SUMMARY OF TECHNICAL WORK PERFORMED FOR THE PERIOD 15 SEPTEMBER 1966 THROUGH 29 FEBRUARY 1968

The technical progress accomplished under the program is described in the present section in four general categories: (A) photochemistry of planetary atmospheric constituents, (B) theoretical studies, (C) experimental investigations in the VUV (2000-1000Å) and EUV (below 1000Å) spectral regions, and (D) planetary aeronomy. Specifically, the brief discussions under each category include comprehensive bibliographies on the scientific material published elsewhere. In this manner, the interested reader can obtain detailed accounts on any specific topic of special interest. However, in order to present the general scope and nature of the problems investigated, brief technical summaries are included for each major topic for which the key data are presented along with cogent comments on the analysis, utility and scientific value of the data pertinent to current problems on planetary aeronomy.

A. Photochemistry of Planetary Atmospheric Constituents

The detailed results of the photochemical studies accomplished under the present contract effort are available in the several published reports included in the following bibliographies:

A-1. "Mass Analysis of Photoionization Products in the VUV and EUV Spectral Regions," by P. Warneck and F. F. Marmo, Quarterly Progress Report No. 9, June 1967, pp. 8-18.

A-2. "Gas Analysis by Photoionization Mass Spectrometer," by W. Poschenrieder and P. Warneck, J. Appl. Phys. 37, 2813 (1966).

A-3. "On the Quenching of the 6300Å Radiation," by P. Warneck and J. O. Sullivan, Planet. Space Sci. 14, 1225 (1966).

A-4. "Photochemical Studies of Minor Constituents in Planetary Atmospheres: Photolysis of H_2O and $HC\ell$," by P. Warneck and F. F. Marmo, Quarterly Progress Report No. 10, pp. 13-15 and Quarterly Progress Report No. 11, December 1967, pp. 8-12.

A-5. "Photochemical Generation of Precursors to Sulfur Containing Amino Acids," by P. Warneck and F. F. Marmo, Quarterly Progress Report No. 12, March 1968, pp. 12-16, and Quarterly Progress Report No. 10, September 1967.

A-6. "Reactions of ^1D Oxygen Atoms III. Ozone Formation in the 1470Å Photolysis of O_2," by P. Warneck and J. O. Sullivan, J. Chem. Phys. 46, 953 (1967).

A-7. "Primary Processes in the Photolysis of SO_2 at 1849Å," by J. N. Driscoll and P. Warneck, J. Chem. Phys. (submitted April 1968) and Quarterly Progress Report No. 12, March 1968, pp. 4-12.

A-8. "Photochemistry of Planetary Gases in the EUV (below 1000Å)," by P. Warneck, Quarterly Progress Report No. 7, December 1966, pp. 3-5 and Quarterly Progress Report No. 11, December 1967, pp. 4-8.

A-9. "Studies of Ion-Neutral Reactions by a Photoionization Mass Spectrometer Technique, II. Charge Transfer Reactions of Argon Ions at Near Thermal Energies," by P. Warneck, J. Chem. Phys. 46, 513 (1967) and Quarterly Progress Report No. 7, December 1966, pp. 5-13.

A-10. "Studies of Ion Neutral Reactions by a Photoionization Mass Spectrometer Technique, III. Several Ionospheric Reactions," by P. Warneck, Planet. Space Sci. 15, 1349-1359 (1967) and Quarterly Progress Report No. 7, December 1967, pp. 7-13.

A-11. "Studies of Ion-Neutral Reactions by a Photoionization Mass Spectrometer Technique, IV. Reactions of He^+ with Nitrogen and Oxygen," by P. Warneck, J. Chem. Phys. 47 (10), 4279-4281 (15 November 1967); Quarterly Progress Report No. 8, March 1967, pp. 4-10 and Quarterly Progress Report No. 9, June 1967, pp. 3-8.

A-12. "Laboratory Rate Coefficients for Positive Ion-Neutral Reactions in the Ionosphere," by P. Warneck, J. Geophys. Res. 72, 1651 (1967) and Quarterly Progress Report No. 10, September 1967, pp. 3-7.

The major content of the material discussed in these publications is briefly summarized below. For this purpose, it is convenient to note that the overall results are discussed in terms of the four following subtopics: (1) VUV photochemical investigations involving minor constituents in the atmospheres of Earth, Mars, and Venus, (2) photochemistry of planetary atmospheric gases in solar EUV radiation, (3) laboratory measurements of ion-molecule reactions and mechanisms occurring in planetary ionospheres, and (4) mass and ion energy determinations of photoionization products due to solar VUV (1000-2000Å) and EUV ($\lambda < 1000$Å) radiation.

1. VUV photochemical investigations involving minor constituents in planetary atmospheres. – It has been well established that the presence of minor constituents in planetary atmospheres may play a major role in establishing specific atmospheric and/or ionospheric parameters. This is usually a consequence of the initial interaction between the minor constituent and the VUV and/or EUV incident solar flux, i.e., the EUV-VUV photochemistry of minor constituents. A portion of the current program effort has involved investigation of the VUV photochemistry in the following three problem areas: (a) the photochemistry of simulated

planetary atmospheres containing trace amounts of HCℓ and/or H_2O in CO and/or CO_2 (A-4),* (b) the role of SO_2 VUV (λ = 1849Å) photolysis in the Earth's atmosphere (A-7) and, (c) the VUV photochemical generation of precursors to sulfur containing amino acids (A-5). Since the detailed results and analyses are described in the sources cited above, only brief summary discussions are presented below.

a. VUV photochemical investigations on the role of minor constituents in the atmospheres of Mars and Venus. – Recent interferometric investigations [1]** on the atmospheres of Mars and Venus have demonstrated unambiguously the presence of water vapor, hydrogen chloride, and hydrogen fluoride. Although these species represent minor constituents, they may play significant roles in the aeronomy of these atmospheres. It is interesting to note that none of the identified or suspect major constituents (i.e., CO_2, N_2, Ar, Ne, and CO) absorb radiation for $\lambda > 1750$Å. On the other hand, water vapor, HCℓ, and HF absorb radiation at these longer wavelengths where the major solar UV flux is located. Thus, in the planetary atmospheres considered, it is expected that solar photodecomposition of these minor constituents should occur; furthermore, since the major constituents are transparent to these radiations, the photochemical reactions can occur at relatively low altitudes or, indeed, in the case of Mars, perhaps down to the planetary surface. In order to better evaluate the role of minor constituents in planetary atmospheres, a laboratory study was initiated for the express purpose of measuring the photodecomposition products associated with simulated atmospheres containing controlled amounts of H_2O and/or HCℓ (HF involves a number of experimental difficulties which precluded it from the present investigation).

Laboratory studies of H_2O or HCℓ photodecomposition in the presence of CO_2 and/or CO are complicated by several factors: (i) the quantum yields for decomposition of pure H_2O and HCℓ are low (of the order of 0.01, presumably due to back reactions); (ii) the absorption is of an intermediate strength; (iii) no readily available light sources exist in the spectral region $\lambda\lambda$ 1700-1800Å, where both minor species absorb strongly.

For the present purpose, the relatively low intensity 1745Å atomic nitrogen (doublet) resonance lines were generated in a discharged mixture of argon and nitrogen. Experimental descriptions involving the irradiation of H_2O and HCℓ in the presence of CO_2 and CO are presented below even though only negative results were obtained.

The light source employed for the photolysis experiments was a microwave-powered discharge lamp [2] operated with a flow of 20 percent nitrogen in argon at a pressure of 2 torr. Impurities in the gas stream were removed by passage through a liquid nitrogen trap. The emission

*Bibliography

**Numbers in [ ] represent reference numbers.

spectrum of this lamp was examined by Okabe [3], who found strong line groups at 1493-1495Å and 1743-1745Å. The short wavelength line group (1493Å) was removed by using a GE quartz window between the lamp and the photolysis vessel. The lamp intensity was determined with the ozone actinometer [4]. Oxygen, at atmospheric pressure and a flow rate of 5 cc/sec, was irradiated with the argon-nitrogen lamp, and the ozone produced was trapped in an acidic solution of potassium iodide. Ozone oxidizes the iodide ion to I_2 which, in iodide solution, exists as I_3^-. The absorbence of the solution was measured at 3530Å in a 5-cm cell with a Perkin-Elmer 4000Å spectrophotometer. The concentration of the tri-iodide ion was calculated using Beer's law and an extinction coefficient of 26400 $M^{-1}cm^{-1}$ [5]. The blank absorbence (light source off) was sufficiently small to be negligible for these measurements.

The light flux from the lamp, as determined by actinometry, was about 10^{14} quanta/sec, which is in good agreement with the results of Okabe [3]. At 1743-1745Å, only the minor constituents such as H_2O [6] and $HC\ell$ [7] in this region are approximately 100 and 35 $atm^{-1}\ cm^{-1}$, respectively. Because of the divergence of the light source beam and the low partial pressures of the absorbing species (H_2O or $HC\ell$), a 150 mℓ, 6-mm diameter hemispherical reactor was employed to ensure that all the radiation from the lamp was absorbed by the sample.

The photolysis vessel and vacuum system were evacuated with a diffusion pump prior to irradiation. The system was filled to about 750 torr with CO_2 or CO, whereupon the photolysis vessel was sealed off from the main system with a stopcock and 1.5 $\mu\ell$ (approximately 10 torr) of distilled water was added with a syringe through a vacuum-tight septum. Following irradiation, the sample was expanded into an evacuated transfer cell for gas chromatographic analysis with an F & M Model 700 gas chromatograph. A number of simulated planetary atmospheric mixtures containing between 1 and 10 torr of H_2O in carbon monoxide were irradiated for periods of one to three hours in the spectral region where water vapor represents the only absorber (λ = 1744Å). Decomposition products could not be detected by gas chromatography owing to the relatively low intensity of the microwave powered light source employed in the experiment (20 percent N_2 in argon) and to the limited sensitivity of the chromatograph (100 ppm). On this basis, additional emphasis was applied both in optimizing the source intensity and increasing the detection capability of the system. Concerning the former, the additional effort resulted in the increase of source intensity from about 1×10^{14} to 5×10^{14} quanta/sec. Additionally, the reaction vessel was redesigned to eliminate the transfer cell and to decrease the total volume of the reaction vessel. The new reactor consists of a 1.75-cm diameter Pyrex tube, 10 cm in length, with a suprasil quartz window cemented on one end. This tube was fused onto a 34/35 standard taper joint which can be inserted directly into the lamp housing. Following evacuation with a diffusion pump, the vessel was filled to atmospheric pressure with carbon monoxide, sealed by a teflon stopcock, and placed

in the lamp housing for irradiation. The minor constituent (H_2O) was added through a vacuum-tight septum incorporated into the vessel. After irradiation for one to three hours with the argon-nitrogen lamp, the vessel was removed and the sample was expanded into an evacuated sample loop on the gas chromatograph.

The F & M Model 700 chromatograph is equipped with a thermal conductivity detector with a temperature programming capability. The chromatograph was operated at maximum sensitivity (filament current 275 mA) with the sample being introduced through the gas sampling valve. The original 0.5-cc sample loop was replaced by a 10-cc loop to increase the sensitivity to a detection limit of 5 ppm.

Since the structures of the possible photolysis products exhibited considerable variation, good separation could not be obtained with a single column. Therefore, the two best suited columns were selected from F & M Company (Hewlett Packard), the first of which was a 6-foot molecular sieve 5A column. Although oxygen, hydrogen, carbon oxides, alkanes, etc. are easily separated, aldehydes or ketones are not. The second column was selected because of its ability to separate formaldehyde or other carbonyl compounds. The experimental results employing either column indicated that no other new products were detected.

If it is assumed that the quantum yield ≈ 0.01 for the photochemical process, then irradiation of the sample for one hour would be expected to produce product concentrations of about 50 ppm. This is an order of magnitude above the detection line of approximately 5 ppm. This is an indication that the quantum yield of this process is either extremely low (i.e., < 0.01) or nonexistent. The new improved system was then also employed to investigate CO-$HC\ell$ and CO_2-$HC\ell$ mixtures. The procedure adopted essentially duplicated that employed for the H_2O photochemistry studies. Here again, although runs were performed for periods as long as three hours, no new products were detected. Thus, the comments that apply to the negative results observed for the CO-H_2O and CO_2-H_2O cases apply here as well. No further experimental effort was performed since the negative results indicated that (at least for solar radiation in the wavelength vicinity of 1700-1800Å) the photochemistry of the minor constituents (in the atmospheres of Mars and Venus) $HC\ell$ and H_2O does not significantly affect any of the major atmospheric parameters which can be measured with present experimental capability.

b. Photochemical generation of precursors to essential sulfur containing amino acids. – A number of sulfur containing amino acids (e.g., crysteine, methionine, etc.) are essential to the origin, development, and sustenance of life. For this reason, it is of interest to inquire as to the source of these ingredients in primitive atmospheres. For example, it is possible that these compounds (or their precursors) are readily produced under conditions which reasonably simulate the pertinent environmental conditions that obtain for solar-illuminated primitive planetary atmospheres. On the basis of present evidence, it

appears that these atmospheres were reducing in character (i.e., NH_3, CH_4, C_2H_4, H_2, etc.) and could have contained trace elements such as H_2S (due to volcanism) [8] which absorbs strongly at wavelenths greater than 2500Å [9]. Concerning the latter, the photochemically active ultraviolet solar flux represents the strongest available source in primitive times [10]. On the basis of energetic considerations, the bulk of this UV radiation resides at wavelengths exceeding 2500Å. Thus, the presence of H_2S in the primitive atmosphere makes available an ultraviolet sensitizer (absorbs incident [$\lambda > 2500$Å] photons, then transfers this energy to other molecular constituents by collisions) so that the solar energy can be efficiently transferred into the generation of new chemical species (no other likely constituents absorb $\lambda >$ 2500Å). Previous irradiation (1849Å and 2537Å) experiments (A-5) involving simulated (CH_4, NH_3, H_2O and H_2) primitive atmospheres [8] have demonstrated the photochemical generation of amino acids. The exposure of simulated atmospheres containing H_2S to an intense 2537Å radiation source could yield sulfur containing amino acids which are essential to the development of life under primitive conditions. The above experiments were performed under the current program, the results of which are summarized briefly below.

A mercury light source with 10 watts output was employed with 96 percent of the radiation residing in the 2537Å mercury line. The source was located in the central well of a 5-liter quartz vessel. A complete glass magnetic piston pump of the Watson design was incorporated to circulate the gas mixtures successively through the reaction vessel, a condenser, and over a water reservoir where the photolytic products were washed out. In this manner, the products were removed from the gas phase before the mixture was recirculated through the reaction vessel. A photograph of this system is reproduced in Figure 1. The system is attached to a vacuum and gas handling manifold, only a portion of which is shown in the photograph.

The experiments were performed at 710-torr pressure involving a mixture of 30 percent methane, 30 percent ammonia, 30 percent hydrogen sulfide and 2.1 percent water vapor. The irradiation was performed with water cooling of the mercury lamp, so that only the 2537Å lines was active and H_2S constituted the only interacting species. The irradiation time employed was 14 hours, with gas samples being withdrawn at various intervals during this period for detailed examination by fractional distillation, infrared spectroscopy, mass spectrometry, and gas chromatography. The liquid sample was examined by paper chromatography, mass spectrometry, and melting point determination of extractable precipitates.

The results obtained can be summarized as follows: after the termination of the photolysis, only 1380 cc of gas remained as compared to 3450 cc introduced into the reaction vessel. Only a portion of the consumed gas underwent photochemical reactions, while the remainder was

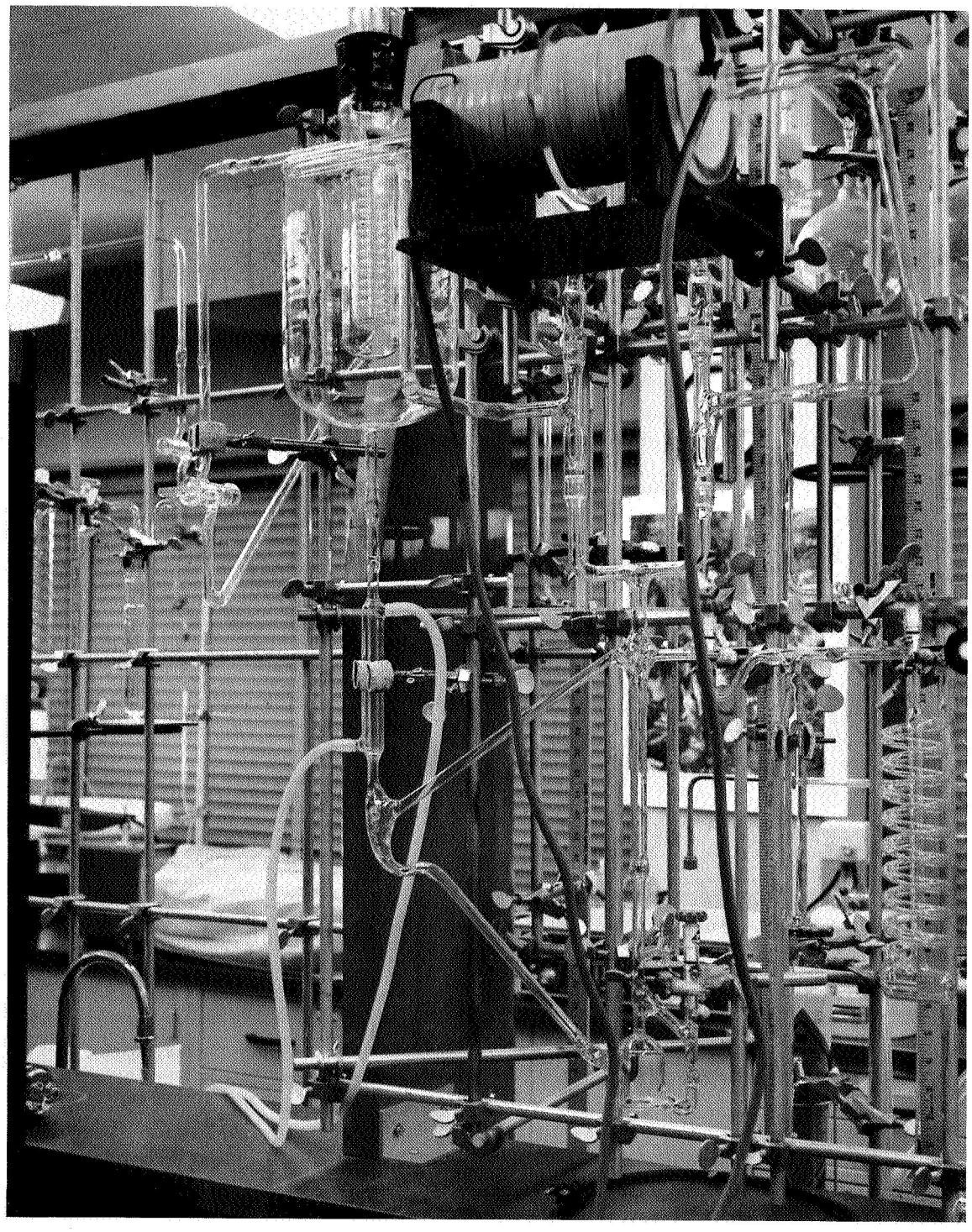

Figure 1. Experimental apparatus for investigations on the photochemical generation of amino acids.

simply dissolved in the water reservoir. Of the remaining gas 903 cc were noncondensable with liquid nitrogen, indicating that appreciable amounts of hydrogen were formed. The infrared analysis of the gas samples indicated only the presence of the initial reactants and the formation of no new products. Mass spectrometry and gas chromatography indicated the formation of minor products in the 10 ppm range. No definite identification of these products could be established, but the mass spectrometer traces are consistent with the products $(NH_4)HS$ and $(NH_4)_2S$ which result from the admixture of ammonia and H_2S.

During irradiation the liquid underwent a color change from colorless to yellow. Melting point determination and mass spectrometry of the extractable precipitate indicated the presence of sulfur in the form S_1 through S_7 which confirms that dissociation of H_2S has indeed occurred.

Paper chromatography showed a ninhydrin positive spot suggesting that one or more amino acids may have been formed. Repeated rinsing of the reaction vessel resulted in the collection of 0.33 grams of sulfur from the vessel walls, which together with the sulfur found in the solution, constituted 22 percent of the initial H_2S. This implies that about 253 cc of the H_2 evolved originated from H_2S, whereas $\sim$ (900 - 250) = 650 cc H_2 must have originated from other sources, i.e., reactions with methane and/or ammonia. Other products resulting from these reactions must have accummulated in the solution, since none were found in the gas phase.

c. Primary processes in the photolysis of SO_2 at 1849Å. – As noted previously, it is widely accepted that minor constituents can play a major role in establishing many of the important characteristics of a planetary atmosphere. A known terrestrial atmospheric minor constituent which is suspected to be present in the atmospheres of Venus and Mars is SO_2. The results of a previous experimental program [11] indicated that SO_2 begins to absorb strongly for $\lambda\lambda < 3000$Å. Specifically, for $\lambda\lambda < 2280$Å the spectrum is characterized by a continuum attributed to the formation of SO and O in their ground states. Thus, under the present effort, an investigation was performed to determine the pertinent photochemical processes involved when atmospheric SO_2 is exposed to this solar photodissociating photon flux.

The experimental apparatus and procedure employed are discussed in detail elsewhere (A-7) so that only a brief review of this aspect of the investigation is included here. The present arrangement employed a flow system whereby product SO_3 was removed continuously from the absorption region. The light source employed was a U-shaped Hanovia medium pressure mercury lamp coupled with a Baird interference filter to isolate the 1850Å region. Ferrioxalate actinometry was performed indirectly wherein the 1849Å region ligh flux was determined to be $7.2 \pm 0.3 \times 10^{13}$ photons/sec. For a typical run, the purified SO_2 was photolyzed for 2 to 4 hours

at atmospheric pressure fed at a flow rate of 150 cm^3/min. The barium chloranilate method [12] was employed to deduce the SO_3 content of the photolyzed sample. The resultant data are shown in Figure 2. The data were analyzed in terms of the following primary and dark reactions:

(P_1)	$SO_2 + h\nu \rightarrow SO + O$	Continuum $\varphi_1 = 0.27$
(P_2)	$SO_2 + h\nu \rightarrow SO_2^*$	Excitation $1-\varphi_1 = 0.73$
(1)	$SO_2^* + SO_2 \rightarrow SO_2 + SO_2$	k_1
(2)	$SO_2^* + SO_2 \rightarrow SO_3 + SO$	k_2
(P_3)	$SO^* \rightarrow SO + O$	Predissociation φ_3
(P_4)	$SO_2^* \rightarrow S + O_2$	Predissociation φ_4
(3)	$O + SO_2 + M \rightarrow SO_3 + M$	k_3

On the basis of the measured quantum yield $\varphi(SO_3) = 0.5$ and the previously determined quantum yield of direct dissociation of SO_2 due to the continuum absorption, $\varphi_1 = 0.27$, upper limits were derived for the other primary processes. Of the total excited SO_2^* production $1 - \varphi_1 = \varphi_2 + \varphi_3 + \varphi_4 = 0.73$, simple quenching assumes $k_1\varphi_2/(k_1+k_2) \leq 0.5$, and quenching with SO_3 formation $k_2\varphi_2/(k_1+k_2) \leq 0.23$, and that for predissociation into $S + O_2$ is $\varphi_4 \leq 0.5$. Supplementary information concerning the relative contributions of these primary processes were obtained from the results for $SO_2 - O_2$ by considering the following reactions:

(4) $SO_2 + O_2 \rightarrow SO_2 + O_2$

(5) $SO_2^* + O_2 \rightarrow SO_3 + O$

(6) $SO + O_2 \rightarrow SO_2 + O$

(7) $SO + O_2 + M \rightarrow SO_3 + M$

(8) $S + O_2 \rightarrow SO + O$

(9) $O + O_2 + M \rightarrow O_3 + M$

The plateau observed for the SO_3 quantum yields in mixtures containing about equal quantities of SO_2 and oxygen shows that the reactions responsible for the additional SO_3 formation essentially go to completion. It is interesting to note the reaction (8), involving sulfur atoms from the primary process (P_4) results in equal amounts of SO radicals and oxygen

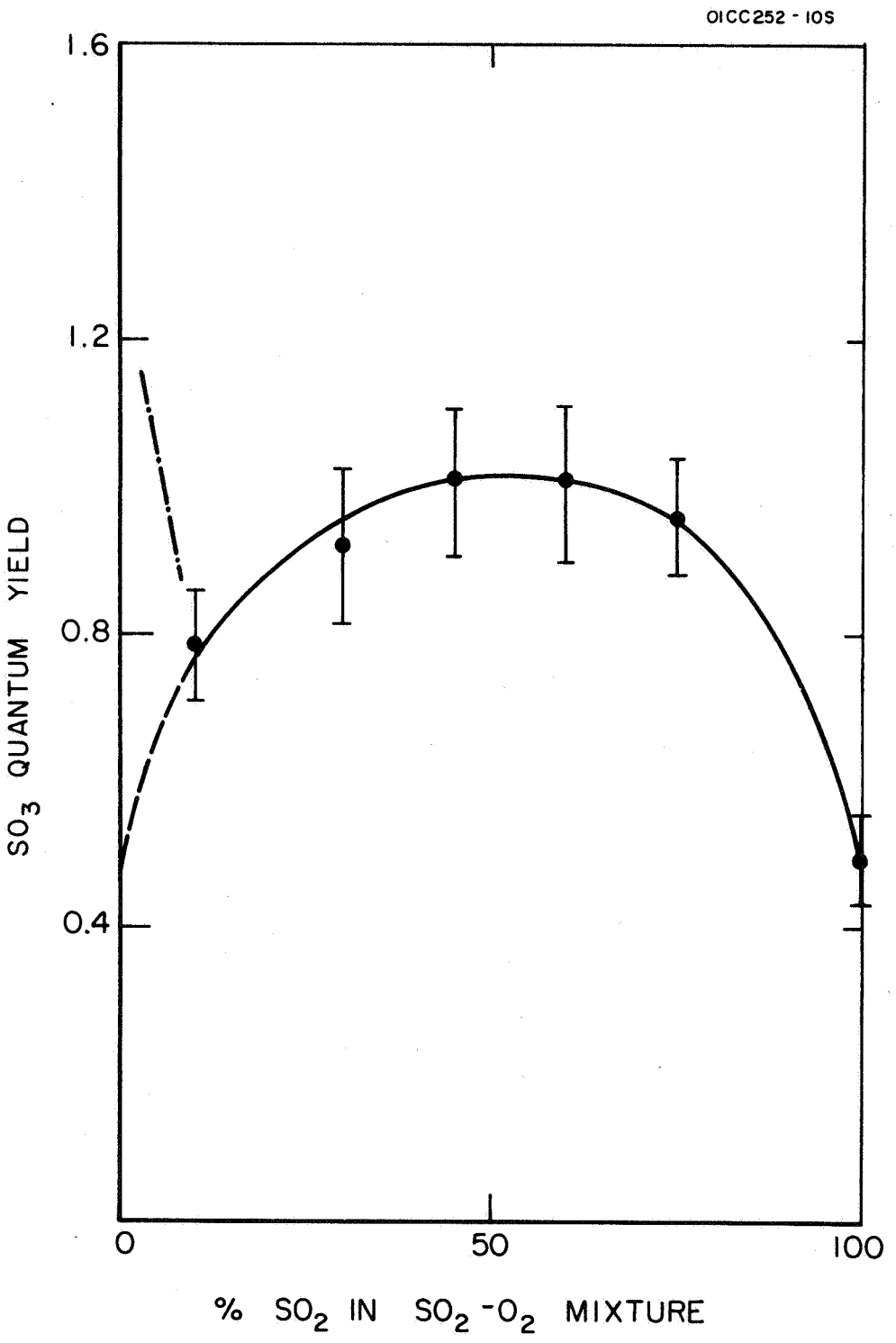

Figure 2. SO_3 quantum yield as a function of percentage of SO_2 in sulfur dioxide-oxygen mixture. Dashed line indicates extrapolation to limiting value. (The data due to Chen [13] and shown as -·-·- are discussed in the original paper.)

atoms, thereby making it impossible to distinguish between primary processes (P_3) and (P_4) on the basis of SO_3 evolution. The observed decline in the SO_3 φ-value yield (when the SO_2 concentration in the SO_2 - O_2 mixture is decreased below 30 percent) can be explained by involving Equation (9) in a relatively complex argument given in the original paper (A-7). Finally, it has been shown that based on the values of φ (0) = φ_o (SO_2) = 0.53 it is possible to derive the corresponding upper limit quantum yield for predissociation of $\varphi_3 + \varphi_4 < 0.26$. On this basis, in the detailed analyses it was shown that neither predissociation nor quenching could singly account for the fate of SO_2^*. Thus, it was concluded that both processes (quenching and predissociation) contribute significantly to its removal.

2. Photochemistry of planetary atmospheric gases in the EUV (below 1000Å). – Essentially all gases absorb strongly in the EUV (i.e., $\lambda < 1000$Å). Owing to the high energy photons involved, the initial absorption act can result in predissociation, direct photodissociation, and/or photoionization. Furthermore, EUV photon energies often considerably exceed the photodissociation and photoionization thresholds so that the corresponding products can be formed with significant excess kinetic energy. The solar flux incident on a planetary atmosphere includes a large number of relatively intense lines in the EUV spectral region. Thus, the interaction of this radiation with constituents in the upper atmosphere results in a host of primary processes intimately related to the aeronomy of the planet involved. Since little or no experimental data exist for this spectral region, a laboratory investigation was performed on the EUV photochemistry of planetary gases as summarized briefly below.

Two major sources of difficulty encountered in the conduct of the photochemical investigations in the EUV spectral region are (1) the general lack of optical windows and (2) the variety of problems involved in conjunction with high vacuum systems. Alternatively, in principle several suitable light sources are available including the helium resonance emission at 584Å and the neon emissions at 736 and 744Å. In practice, a suitable light source was developed wherein it was demonstrated that the photon flux generated in conjunction with a 125-watt microtherm unit can be as high as 10^{16} photons cm^{-2} sec^{-1}, which is considered sufficient output for the EUV photochemical investigations. However, an additional major experimental problem involved the location and suitable employment of a thin film metallic window which transmits selectively in the region of the rare gas resonance lines. In this regard, it should be recognized that only a small select number of materials can be made sufficiently mechanically self-supporting to offset the adverse effects of stress, brittleness, etc. Published data suggest that both aluminum and indium thin films possess the desired mechanical characteristics. With respect to the optical properties of aluminum film, an 800Å thick film transmits about 20 percent of the incident radiation at 584Å and less than 5 percent at 740Å. Indium transmits only in the spectral region

λλ 750 to 1050Å so that the lower wavelength limit is just beyond the two cited neon resonance lines, i.e., 736 and 744Å. Additionally, recent investigations indicate that tin and lead also transmit in the spectral region containing the two neon resonance lines, although their mechanical characteristics are not as suitable as those of aluminum and indium.

In view of these and other detailed requirements, a suitable photochemical reaction cell was designed and fabricated as shown in Figure 3. It was decided to perform the initial EUV photochemical experiments with air samples and using the neon source emissions (736 and 744Å) for the following reasons. The energy of the helium radiation at 584Å is sufficient to ionize all gases except neon and helium. Furthermore, the ionization efficiencies at 584Å are essentially unity for most gases of interest, so that the resultant primary products are ionic in nature. The chemistry of such a system is governed by (1) the primary ion distribution, (2) the subsequent series of ion reactions with the neutral constituents, and (3) the recombination of the final long-lived positive ions with electrons or negative ions formed by electron attachment. While it should be possible to obtain a considerable amount of information on these processes from a detailed final product analysis, precise information on items (1) and (2), above can be obtained both more conveniently and accurately by other techniques, e.g., by the photoionization mass spectrometer experiments described elsewhere in this report.

In contrast, a different situation exists with respect to using the neon resonance emissions at 736 and 744Å. At these wavelengths, the ionization efficiencies are generally less than unity, so that an appreciable portion of the energy is utilized in the formation of superexcited molecules, which subsequently either dissociate or react with the other constituents in the system. In contrast to the chemical reactions of the ions, there presently exists only scant information on the reactivity behavior of those highly excited neutral species which are produced by the energetic radiation in the EUV spectral region. Accordingly, the more fruitful investigative area for experimentation involved the use of a neon rather than a helium light source. On the basis of the above arguments, it was decided to employ the neon source and the indium optical films in the initial EUV photochemical investigation.

The indium film fabrication was predicated on a well-known procedure involving evaporation of indium onto a water soluble substrate Victawet which was sprayed onto a glass slide. Conditions of high vacuum and cleanliness were observed in order to obtain smooth and uniform films. Following desposition, the glass slide was immersed slowly in water so that the substrate was dissolved and the indium film floated off. The film was then lifted off the water surface with a piece of 80 percent transparent steel mesh, which subsequently served as the holder and mechanical support for the film.

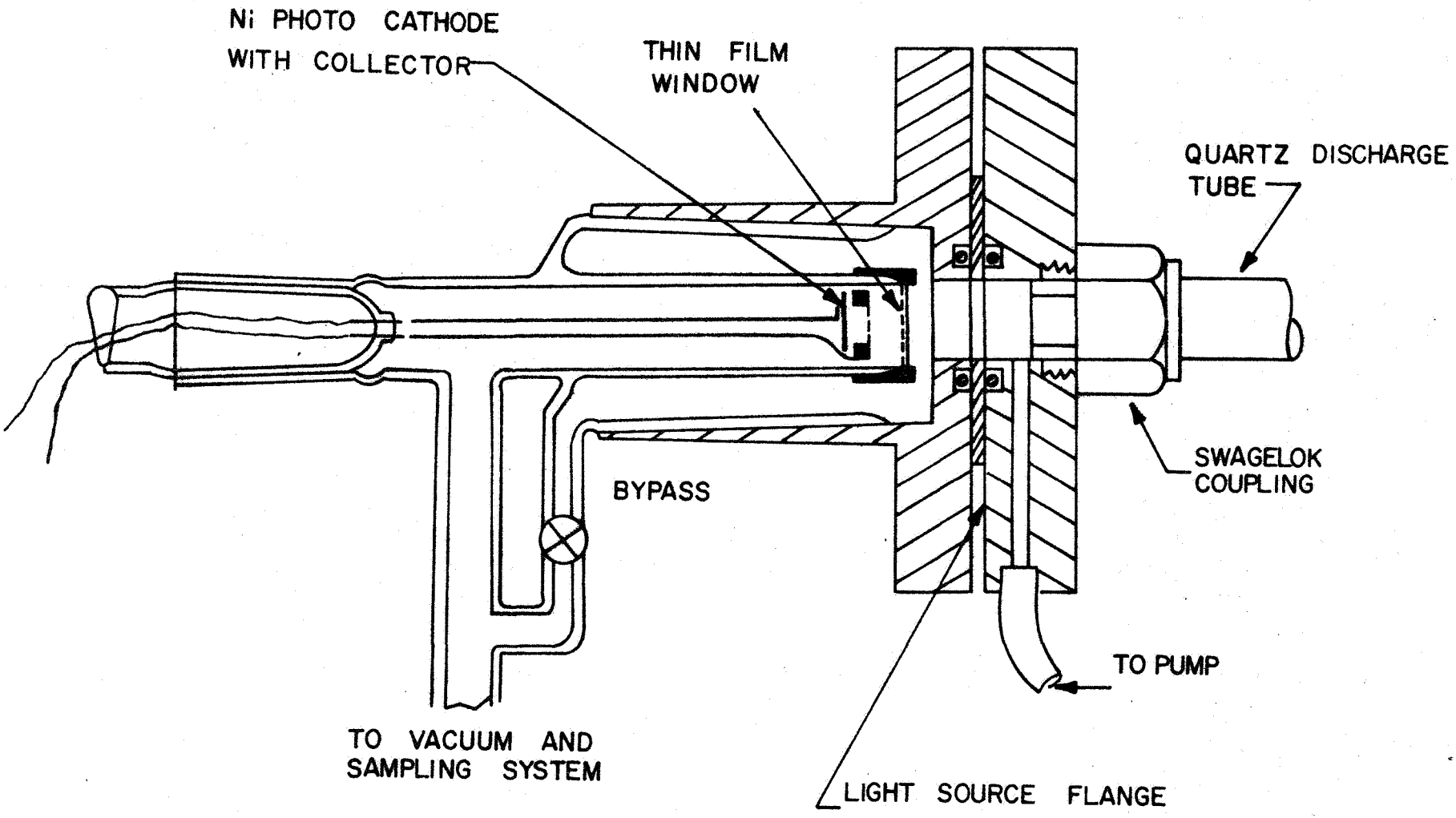

Figure 3. Photochemical setup used in conjunction with extreme ultraviolet light source. Note inserted photoelectric detector.

It was found that, although films of approximately 2000Å thickness had sufficient mechanical strength to withstand the required pressure differences of about 1 torr, their optical properties were unsuitable. For example, the required transmittance measurements indicated that radiation of an argon spark source through a 2000Å thick indium filter suffered a tenfold reduction of intensity in the peak transmission region, 770 to 980Å. At the desired wavelengths, i.e., 736 and 744Å, the resultant transmissions were only about 5 percent. Although these observed reduced transmissivities were not excessively critical, separate experiments encompassing the 1000-1300Å spectral region indicated that the unfiltered intensity of the Lyman-alpha line at 1216Å was essentially equivalent to that of the primary neon lines. On the basis of the above, it was concluded that the indium filter did not provide the required spectral discrimination.

At this point, the experimental situation was reappraised. A further search of the literature indicated that a lead filter might possess the required suitable optical properties. In this case, the absorption edge occurs in the vicinity of 690Å, so that the positions of the neon lines are located close to the transmission maximum. With respect to longer wavelengths, the tail extends to about 1100Å which is similar to the case of indium. A number of appropriate experiments were performed to verify both the mechanical properties and the absolute transmittance of lead as compared to indium. The lead films were fabricated with special care to insure a thickness of only about 1000Å. Subsequent experimental results employing these samples demonstrated that these lead thin films also did not possess the required mechanical strength, and in addition, even for the 1000Å thick case, the EUV (neon lines) transmittance was only 3 percent. In any case, on the basis of the above findings, it appeared that a proper solution to the problem of EUV optical filters would involve a considerable development effort involving new techniques on thin film deposition. The required effort was estimated to exceed the scope of the present work requirements. Thus, no additional effort was devoted to this area of investigation.

3. Laboratory measurements of ion-molecule reactions and mechanisms occurring in planetary ionospheres. – The significance of ion-neutral reactions in controlling the abundance and distribution of ions in planetary ionospheres has been widely discussed so that it is now evident that the local concentrations of specific ionic species depend not only upon their diffusion properties and drift velocities but also on the rates and mechanisms associated with specific ion-neutral reactions owing to the solar VUV and/or EUV flux incident on a planetary ionosphere. Clear evidence for the predominant effects of ionic reactions has been acquired in recent rocket probe mass spectrometric experiments wherein ion density attitude profiles have been measured [14]. However, until recently, the relative importance of many reactions in the ionosphere could not be assessed because a detailed knowledge of the individual thermal rate coefficients was either lacking or relatively uncertain as a review by

Paulson [15] demonstrated. Since then, the considerable effort reported herein has resulted in the experimental determination of many of the required rate constant values thereby providing a set of acceptable pertinent data. The major experimental features and the resultant data are briefly summarized below since detailed descriptions have been presented elsewhere (A-12).

The present laboratory investigation involved the coupled VUV monochromator-mass spectrometer apparatus shown photographically in Figure 4, and schematically in Figure 5. This configuration avoids a host of disadvantages inherent to common mass spectrometric studies of ion-neutral reactions. For example, the employment of the common ion sources is usually complicated by the fact that electron impact results in many different primary ions in undefined energetic states. The technique developed and applied in the present investigation differs from that employed previously in two respects: (1) photoionization replaces the more commonly employed electron-impact mode of ion formation, and (2) a pulse delay measurement is used to determine ion residence times in the mass spectrometer source in the presence of a constant repeller field. The ensuing advantages are: (1) the state of the primary ions is well-defined since the ionizing wavelength is selected by a VUV monochromator, and (2) residence times can be obtained without detailed knowledge of the electric field configuration in the ion source.

For the present specific purpose, the apparatus involved a pulsed spark light source, a 1/2-meter Seya monochromator exit, a 180-degree magnetic analyzer with a wedge-shaped air gauge for stigmatic focusing, a 20-stage electron multiplier ion detector, and associated electronics. Differential pumping was employed to achieve ion-source pressures up to 200 microns while maintaining the analyzer pressure in the 10^{-6} torr range and the monochromator chamber at about 10^{-4} torr. Further description of the experimental apparatus is not presented herein.

Ion residence times are determined from the time delay between the formation of the ions in the source and their arrival at the mass spectrometer collector using a calibrated oscilloscope (Tektronix Type 545). Since the total delay time is a composite of the residence time in the source and the ion flight time in the spectrometer, measurements are performed at various repeller fields, and an extrapolation to infinite repeller fields is performed to obtain the ion flight time in the spectrometer independently. Residence times can then be deduced by different measurements. Since the ion flight time in the spectrometer is independent of the repeller field only within certain limits, the method requires a correction which can be calculated from the applied acceleration potentials and the known ion orbits. Details of the procedure have been described in previous publications (A-9). In any event, application of the experimental apparatus and procedures outlined above resulted in the measurement of a significant number of ion-molecule reactions directly

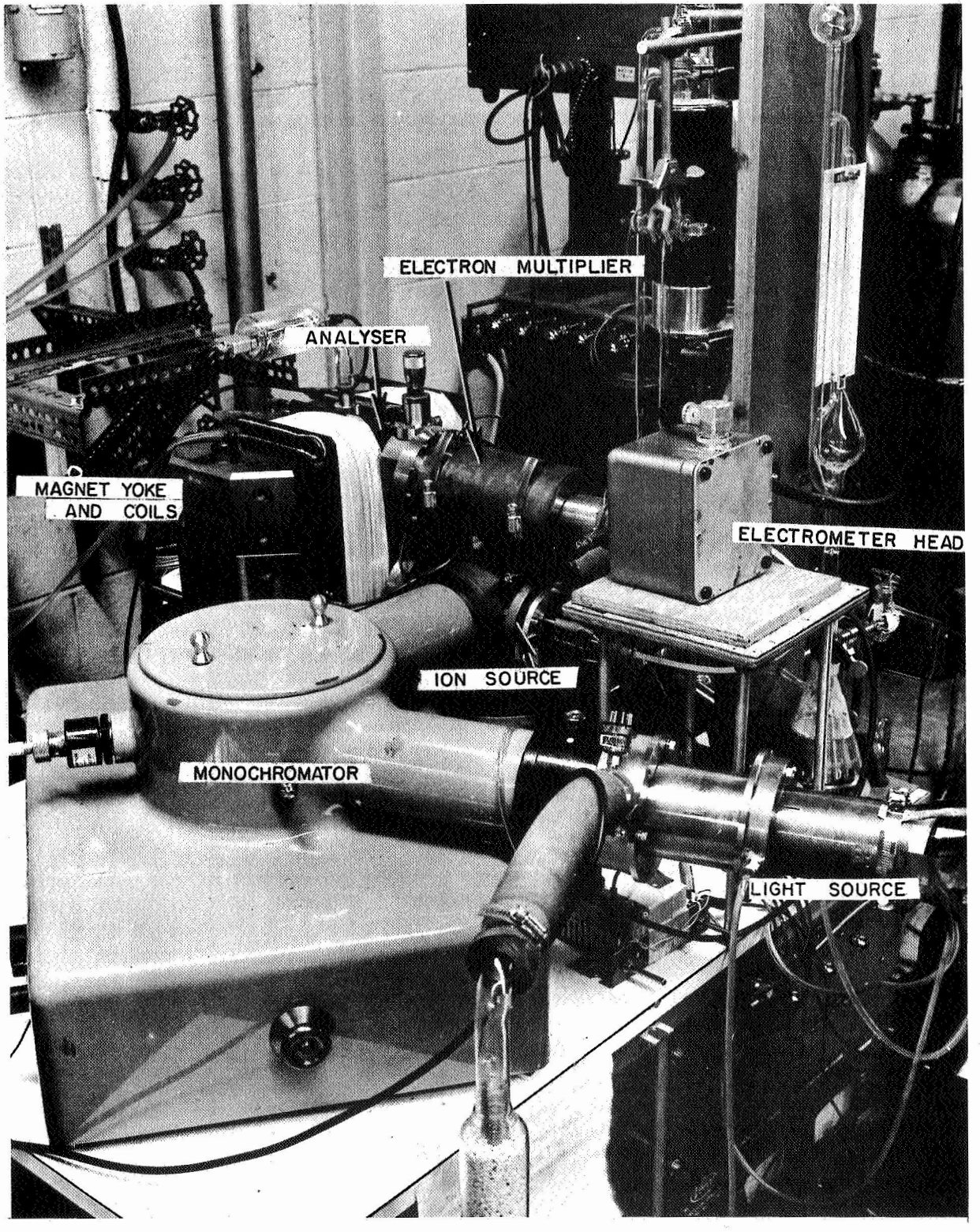

Figure 4. Photograph of photoionization-mass spectrometer setup.

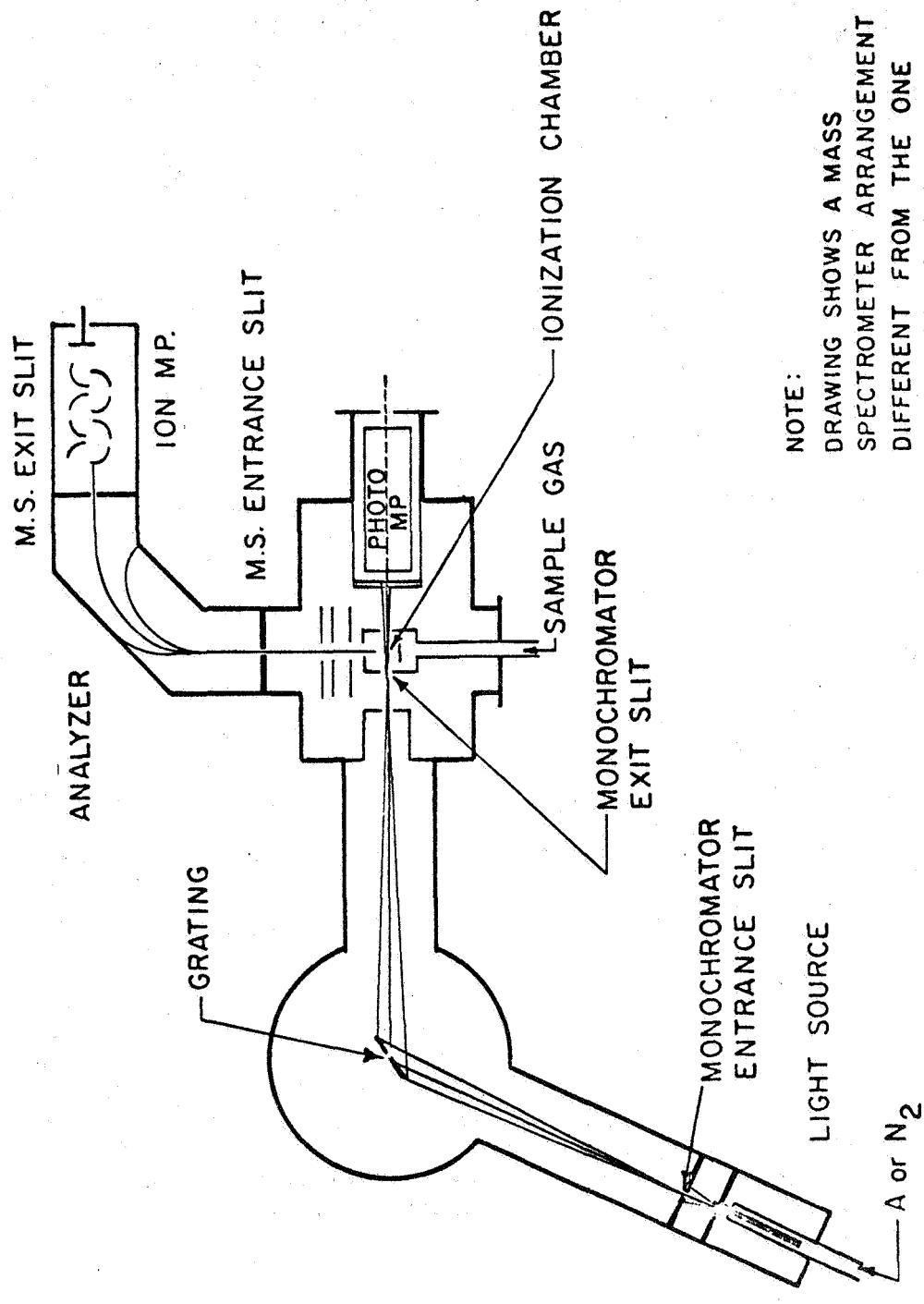

Figure 5. Schematic of setup shown photographically in Figure 4.

pertinent to planetary ionospheres. Previous published reports (A-9, A-10) contain detailed analyses and interpretations of the experimental data as well as suggested mechanisms appropriate to studies in planetary ionospheres.

The extensive data presented in Table 1 were compared to corresponding data, where possible, from other major investigating teams. In general, good agreement was achieved so that it appears that a satisfactory working set of ion-molecule rate constant values are now available for application to current problems on planetary ionospheres.

4. Mass and ion kinetic energy determinations of VUV and EUV photoionization products. – The VUV and EUV solar radiation incident on a planetary ionosphere gives rise to photoionization processes which result in the production of energetic (superthermal) photoelectrons as well as ion products with excess kinetic energy. The theoretical and laboratory studies (performed under this program) associated with the role of superthermal electrons are discussed in Sections B5 and C3 respectively of this report. For planetary ionospheric studies, it is equally important to measure the degree and efficiency of the photoionization fragmentation into specific ion products since these represent critical parameters in establishing atmospheric ion production rates. An early GCA investigation (A-2) involved the successful coupling of a mass spectrometer and a VUV-EUV monochromator for the purpose of performing mass identification and analyses of photoionization products (see Figures 4 and 5). The ion source used in this investigation was similar to that employed in conventional mass spectrometers, involving a simple box-like structure with orifices providing for passage of the light beam and extraction of ions as shown schematically in Figure 6. This source has provided valuable service in the studies of ion-neutral reactions (as discussed in the previous section) since it allows the maintenance of relatively high pressures in the system. However, investigations of the balance between products and consumed reactants in ion-molecule reactions had indicated that the box source discriminates severely against fast ions. Further, it was shown by some specific retardation measurements of photoionization products that fragment ions can be formed with considerable excess kinetic energy. Since essentially all previous mass spectrometric measurements were obtained with box sources, it turns out that these existing data are now suspect, since, to the best of the writer's knowledge this problem has not been recognized previously.

To demonstrate the extent of energetic ion formation, the box source was fitted with a retarding grid located between the exit orifice and the first accelerator plate as shown in Figure 6. Retardation measurements were performed for the fragment ion O^+ produced by photoionization of O_2. The results shown in Figures 7 and 8 demonstrate that (1) the kinetic energy of O^+ ions is inversely proportional to wavelength and (2) that increasing the pressure in the ion source moderates the energy of the O^+ ions toward thermal energies. One possibility for the unambiguous determination of the ion fragmentation ratio, therefore, is to

TABLE 1

ION-MOLECULE REACTION RATES MEASURED BY THE PHOTOIONIZATION-MASS SPECTROMETER TECHNIQUE

Ion-Molecule Reaction	Measured Rate Constant, $k(cm^3/sec)$
Reactions Involving O^+	
1. $O^+ + O_2 \rightarrow O_2^+ + O$	$k_1 = 2.0 \times 10^{-11}$
2. $O^+ + N_2 \rightarrow NO^+ + N$	$k_2 = 4.6 \times 10^{-12}$
Reactions Involving N_2^+	
3. $N_2^+ + O_2 \rightarrow O_2^+ + N_2$	$k_3 = 1.1 \times 10^{-10}$
4. $N_2^+ + O_2 \rightarrow NO^+ + NO$	$k_4 = < 3 \times 10^{-14}$
5. $N_2^+ + 2N_2 \rightarrow N_4^+ + N_2$	$k_5 = 8.5 \times 10^{-29}$ (cm^6/sec)
6. $N_2^+ + NO \rightarrow NO^+ + N_2$	$k_6 = 4.8 \times 10^{-10}$
7. $N_2^+ + CO_2 \rightarrow CO_2^+ + N_2$	$k_7 = 9.1 \times 10^{-10}$
8. $N_2^+ + H_2 \rightarrow N_2H^+ + H$	$k_8 = 1.4 \times 10^{-9}$
9. $N_2^+ + CH_4 \rightarrow CH_3^+ + N_2H$	$k_9 = 1.3 \times 10^{-9}$
10. $N_2^+ + N_2O \rightarrow N_2O^+ + N_2$	$k_{10} = 6.8 \times 10^{-10}$
11. $N_2^+ + SO_2 \rightarrow SO_2^+ + N_2$	$k_{11} = 4.1 \times 10^{-10}$
12. $N_2^+ + C_2H_2 \rightarrow C_2H_2^+ + N_2$	$k_{12} = 4.3 \times 10^{-10}$
13. $N_2^+ + COS \rightarrow S^+ + N_2 + CO$	$k_{13} = 1.4 \times 10^{-9}$
Reactions Involving O_2^+	
14. $O_2^+ + N_2 \rightarrow NO^+ + NO$	$k_{14} < 3 \times 10^{-15}$
15. $O_2^+ + NO \rightarrow NO^+ + O$	$k_{15} = 7.7 \times 10^{-10}$
Reactions Involving N^+	
16. $N^+ + O_2 \rightarrow NO^+ + O$	$k_{16} = 1.6 \times 10^{-10}$
17. $N^2 + O_2 \rightarrow O_2^+ + N$	$k_{17} = 4.5 \times 10^{-10}$
18. $N^+ + NO \rightarrow NO + N$	$k_{18} = 6.5 \times 10^{-10}$

TABLE 1 (continued)

Ion-Molecule Reaction	Measured Rate Constant, $k(cm^3/sec)$
Reactions Involving Ar^+	
19. $Ar^+ + O_2 \rightarrow O_2^+ + Ar$	$k_{19} = 1.1 \times 10^{-10}$
20. $Ar^+ + CO \rightarrow CO^+ + Ar$	$k_{20} = 1.2 \times 10^{-10}$
21. $Ar^+ + CO_2 \rightarrow CO_2^+ + Ar$	$k_{21} = 7.0 \times 10^{-10}$
22. $Ar^+ + NO \rightarrow NO^+ + Ar$	$k_{22} = 3.9 \times 10^{-10}$
23. $Ar^+ + N_2 \rightarrow N_2^+ + Ar$	$k_{23} = 0.6 \times 10^{-10}$
Reactions Involving CO_2^+	
24. $CO_2^+ + H_2 \rightarrow COH^+ + OH$	$k_{24} = 1.4 \times 10^{-9}$
25. $CO_2^+ + CO_2 \rightarrow CO_2^+ + CO_2$	$k_{25} = 1.1 \times 10^{-9}$
26. $CO_2^+ + O_2 \rightarrow O_2^+ + CO_2$	$k_{26} = 2.0 \times 10^{-10}$
27. $CO_2^+ + C_2H_2 \rightarrow C_2H_2^+ + CO_2$	$k_{27} = 4.1 \times 10^{-10}$
28. $CO_2^+ + COS \rightarrow COS^+ + CO_2$	$k_{28} = 1.6 \times 10^{-9}$
29. $CO_2^+ + NO \rightarrow NO^+ + CO_2$	$k_{29} = 5.0 \times 10^{-10}$
30. $CO_2^+ + CH_4 \rightarrow$ Major Products:	
$[COH^+(80\%)\ CH_4^+(20\%)]^*$	$k_{30} = 1.3 \times 10^{-9}$
31. $CO_2^+ + N_2O \rightarrow [N_2O^+(60\%)\ NO^+(40\%)]^*$	$k_{31} = 1.1 \times 10^{-9}$
32. $CO_2^+ + SO_2 \rightarrow [SO_2^+(40\%)\ SO^+(60\%)]^*$	$k_{32} = 3.1 \times 10^{-9}$
Reactions Involving He^+	
33. $He^+ + N_2 \rightarrow$ Major Products:	
$[N_2^+(48\%)\ N^+(52\%)]^*$	$k_{33} = 1.5 \times 10^{-9}$
34. $He^+ + N_2 \rightarrow$ [only $O^+(16\%)$ observed]*	$k_{34} = 1.2 \times 10^{-9}$

*see original publication (A-9) for details.

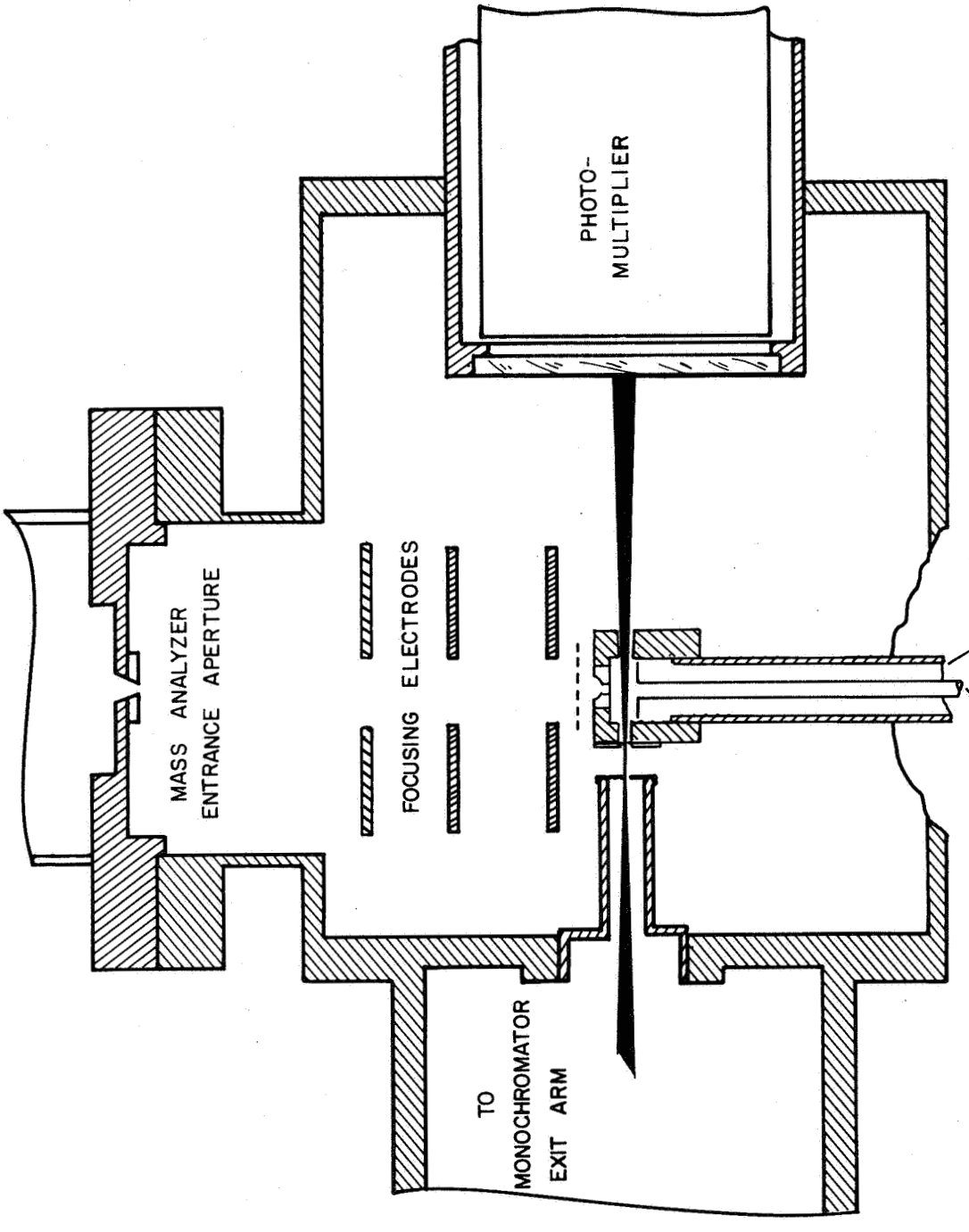

Figure 6. Box-like ion source geometry.

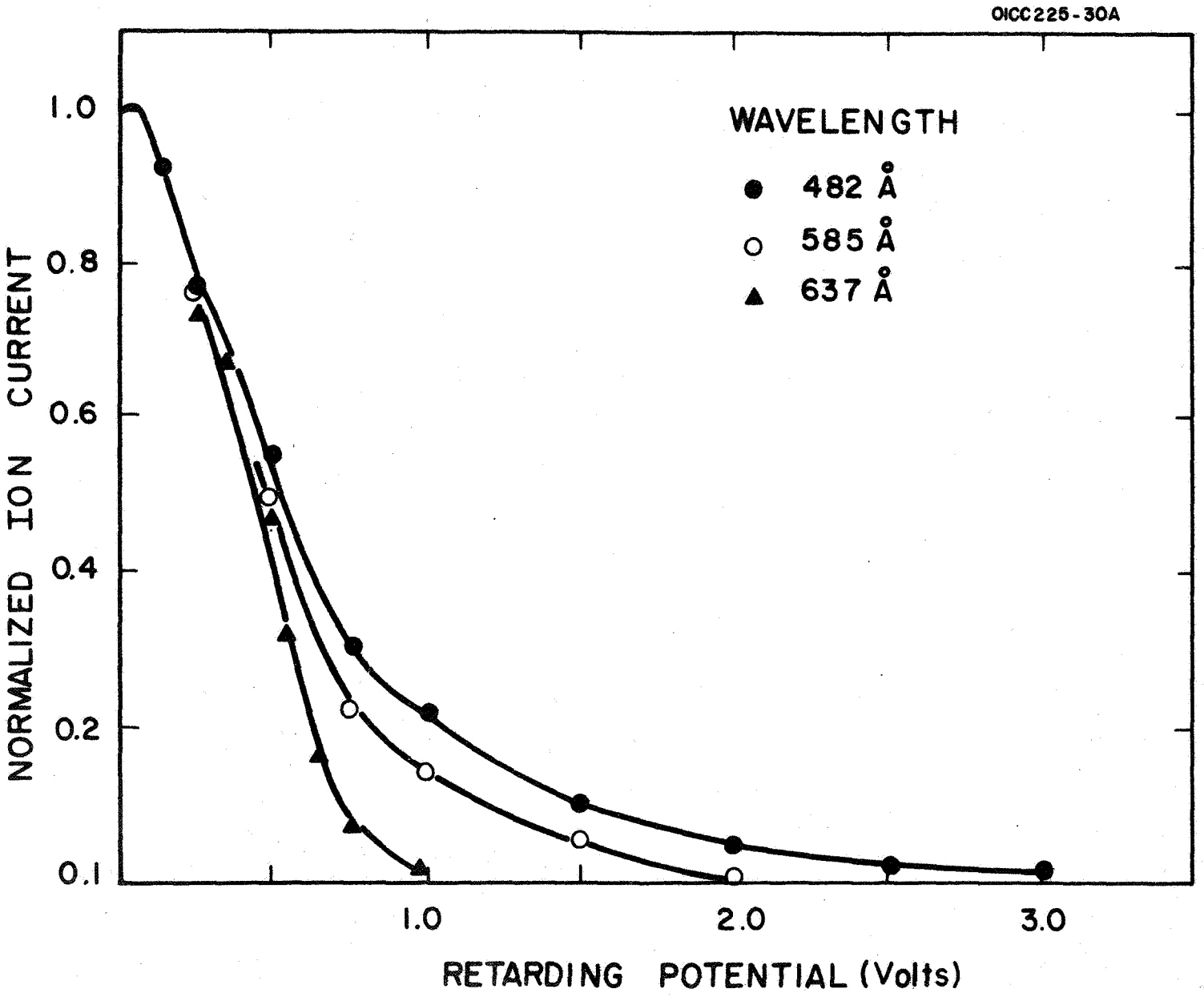

Figure 7. Retarding potential curve for O^+ produced by photoionization as a function of wavelength.

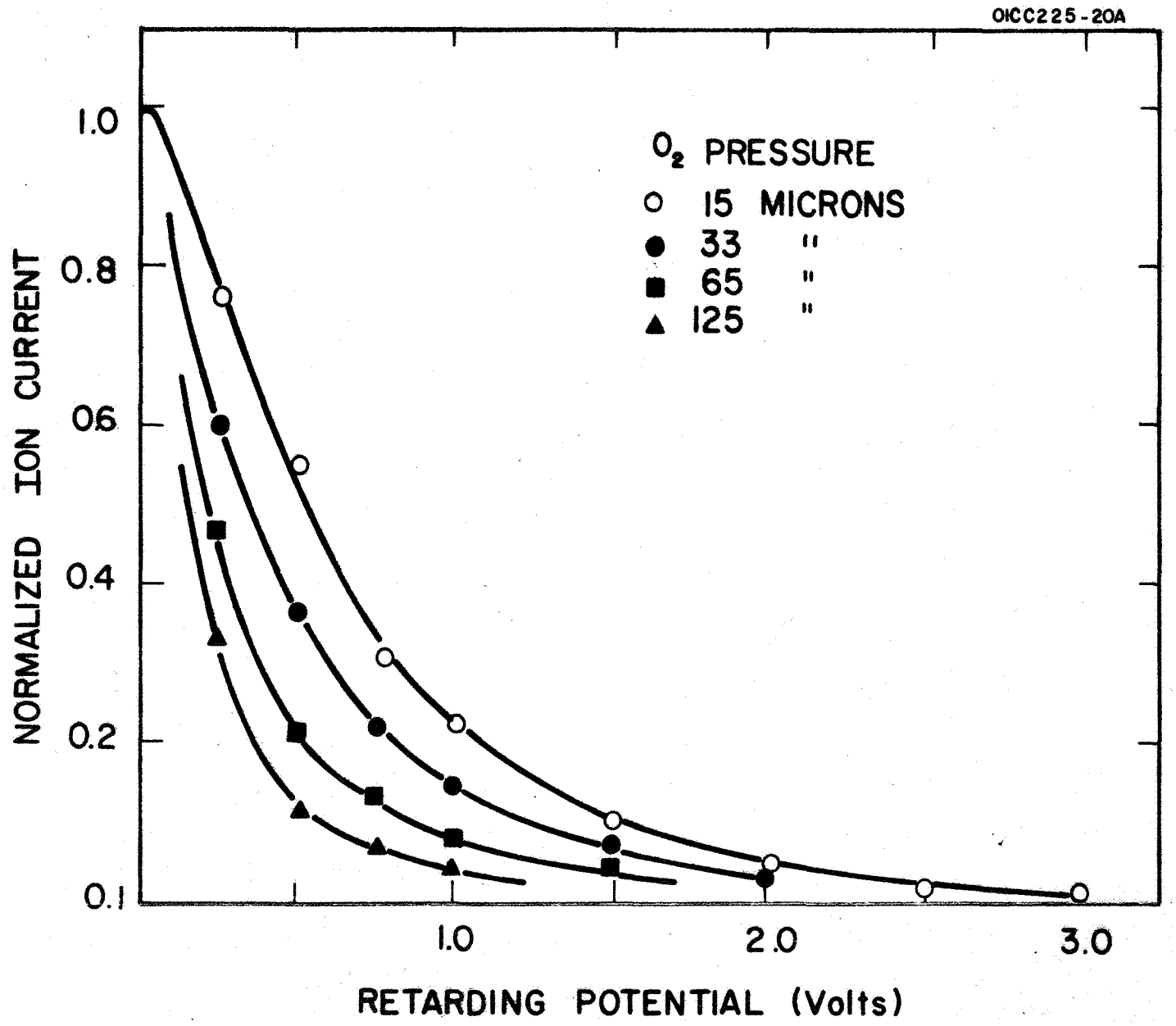

Figure 8. Retarding potential curves for O^+ produced by photoionization at 492Å as a function of ion source pressure.

operate at higher pressures in the source. While this procedure is appropriate for source gases, the general occurrence of ion-neutral reactions is correspondingly enhanced, thereby complicating the data interpretation. Even in the case of oxygen, for which the interaction between O^+ and O_2 is relatively slow, the results obtained are doubtful.

Recognition of all the factors involved indicated that a new type of ion source was required. The optimum source would provide both complete collection of all formed ions as well as a minimum dimension reaction region. It was envisioned that this ideal situation might be realized in a practical system by crossing a photon beam with a molecular beam. An ion source involving this concept has been developed, and tests have demonstrated that the approach is feasible. Front and top schematic views of the final configuration of the ion source which has been developed, fabricated, tested, and employed in the current investigation are shown in Figure 9. The source has been coupled to the monochromator exit slit at the position indicated in the figure. The gas jet molecular beam is formed at the terminus of the brass capillary (16 mm long x 1 mm internal diameter). The gas beam direction is perpendicular to the intersecting light beam and parallel to the monochromator exit slit. Ions created by the interaction of monochromatic UV light with the gas beam are extracted by the strongly inhomogeneous field established between the spherical repeller plate and a concentric drawout grid; thereafter, they are focused upon the entrance aperture of the 180-degree magnetic analyzer of the mass spectrometer. The inhomogeneous extraction field has two advantages: (1) it provides a favorable collection efficiency and (2) the ions are accelerated mainly near the fringe of the gas beam where densities are much lower than in the center, so that energy losses by collisions become negligible. To achieve the desired field configuration, the extraction region is shielded from the drawout electrode – except for the 1/2-inch grid aperture – and the shield potential is equivalent to that of the repeller. The potential of the jet inlet is adjusted appropriately to a value between that of the repeller and the drawout potential. The position of the jet relative to the light beam is maximized by means of a micrometer screw. Additional details are not presented here since they are available elsewhere (A-1).

One of the more important characteristics of the ion source is the resultant extent and density distribution of the gas beam. These beam dimensions were determined experimentally by application of the ram effect. Plots of pressure differences observed as a function of detector position are shown in Figure 10 for several inlet pressures, using air as the gas sample. Owing to the pressure drop produced by the viscous flow in the inlet line, the indicated values do not represent the pressures existing at the start of the jet capillary. Nevertheless, the best estimate indicates that the pressures at that point are still higher than compatible with free molecular flow for the given capillary dimension. The gas beam profiles, therefore, are not calculable, and no attempt has been made to compare the measured and theoretical profiles. At

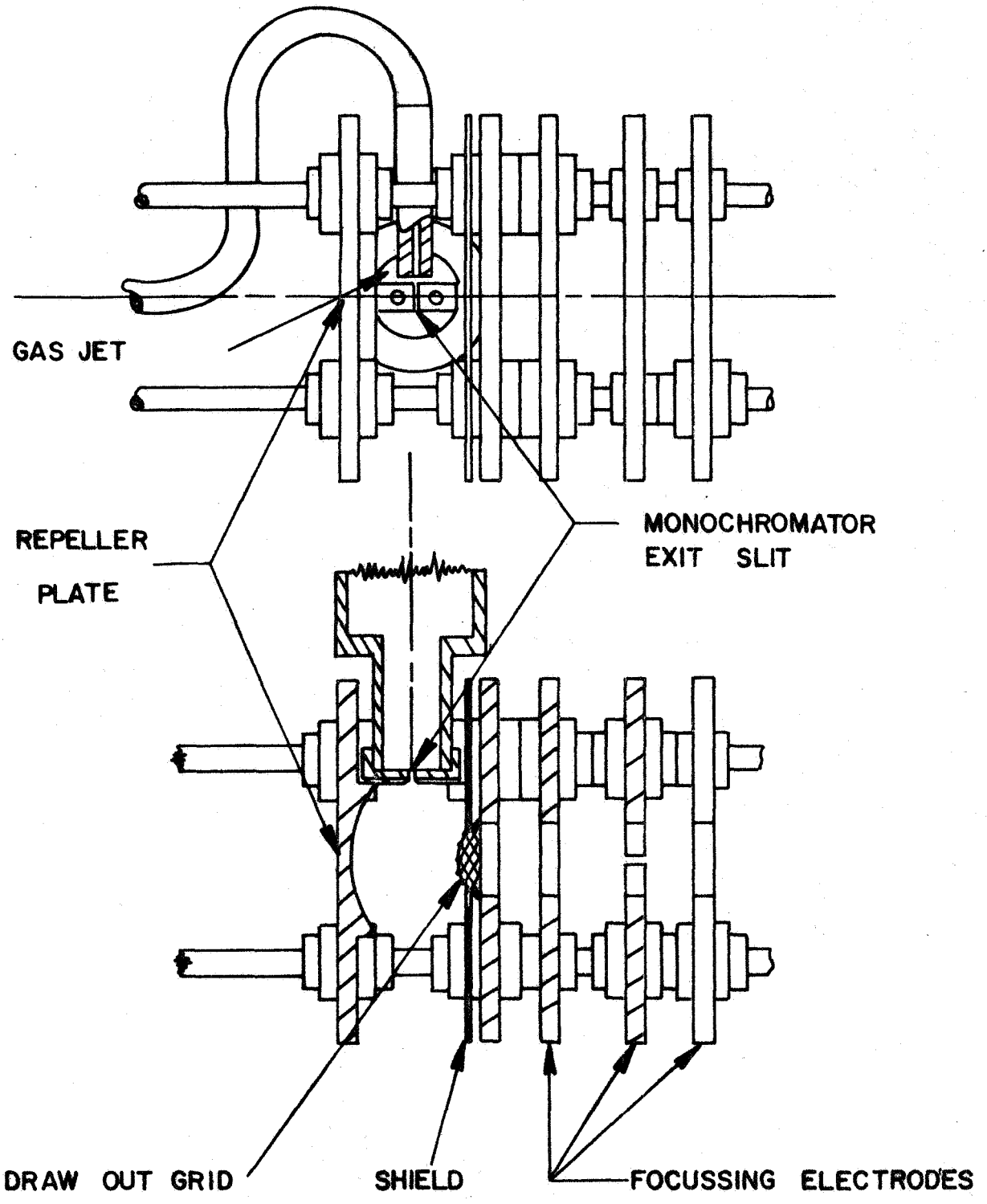

Figure 9. Front and top schematic views of the fragmentation ion source.

inlet pressures for which molecular flow is achieved, the resulting beam densities are insufficient. For the pressures actually employed, the existing flow is probably in the transition region from free molecular motion to a many collision behavior, since well-defined gas beams are observed. In this respect, it is important to note that the beam probing was performed relatively close to the origin. The data in Figure 10 show that the beams are symmetrical and that the total width (for 900 micron inlet pressure) is about 13 mm. For an intersecting light beam 5 mm in height, the maximum ionization region would be 5 x 13 mm. However, by integration it is found that nine-tenths of the entire beam density is located within 3.5 mm of the center, so that in the practice the significant ionization region is 5 x 7 mm wide. This area is larger than the orifices employed previously in conjunction with the box source, and proper allowance must be made in this regard when total ion collection is desired.

To test the ion source with respect to its collection efficiency for fast fragment ions, the currents obtained from the photoionization of oxygen were investigated at two different wavelengths. Near 490Å, the O^+ ions formed are endowed with considerable kinetic energy whereas near 640Å, their kinetic energy excess is minimal. Any difference in behavior, therefore, would indicate a discrimination against fast ions. The results revealed that the new ion source functioned properly with little or no discrimination experienced, but owing to the larger exposed source area, the aperture of the mass spectrometer analyzer was insufficient to accept all ions. Therefore, a limited amount of discrimination against fast O^+ ions was evident. This situation was improved by enlarging the analyzer entrance and exit orifices from 1 x 1 mm to 2.5 x 5 mm. This increased the analyzer acceptance aperture sufficiently to match it to the new source area and to allow collection of all ions with energies up to 3 eV.

For a precise measurement of fragment ion abundances, the conversion efficiencies of the ion-electron multiplier detector must also be taken into account. In view of the small ion current encountered, the measurement of conversion efficiencies requires an auxiliary electron impact source. Appropriate instrumentation has been designed and constructed, but performance tests have not yet been undertaken.

B. Theoretical Studies

Detailed discussions of the results obtained in the theoretical study phase of the present program are contained in the following publications:

B-1. "The Diurnal Variation of Ionospheric Temperature," by A. Dalgarno, M. B. McElroy and J. C. G. Walker, Planet. Space Sci. 15, 331 (1967), and Quarterly Progress Report No. 7, December 1966, pp. 4-14.

B-2. "Electron Cooling in the Upper Atmosphere," by A. Dalgarno and T. C. Degges, Planet. Space Sci. 16 (1), 125-127 (1968), and Quarterly Progress Report No. 10, September 1967, pp. 36-43.

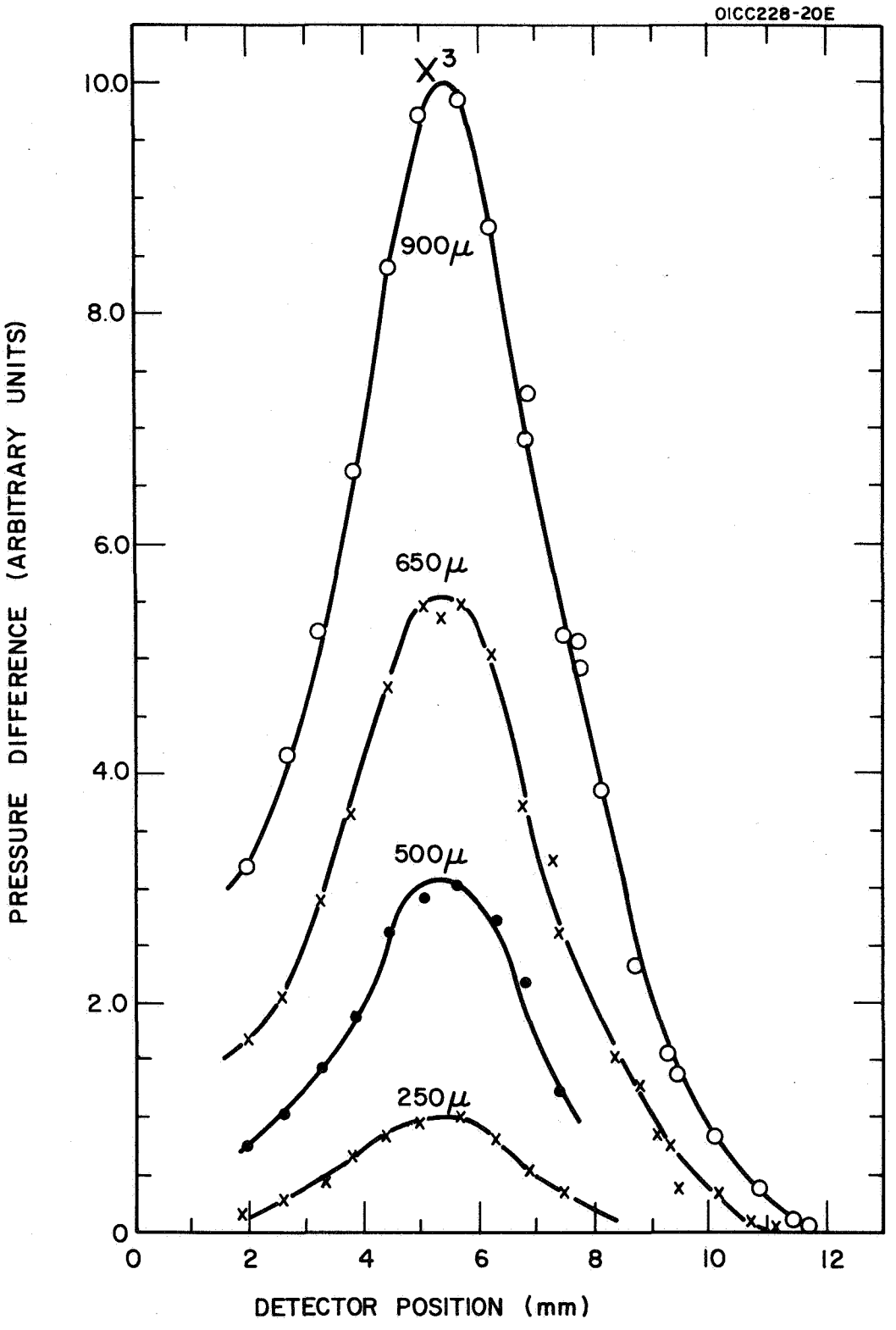

Figure 10. Gas beam profile for air sample.

B-3. "Ion Temperatures in the Topside Ionosphere," by A. Dalgarno and J. C. G. Walker, Planet. Space Sci. 15, 200 (1967).

B-4. "Dipole Properties of Molecular Nitrogen," by A. Dalgarno, T. C. Degges, and D. A. Williams, Proc. Phys. Soc. (London) 92, 291-295, and Quarterly Progress Report No. 9, June 1967, pp. 19-27.

B-5. "Optical Properties of Molecular Hydrogen," by A. Dalgarno and G. Victor, Proc. Phys. Soc. (London) 92, 42-49, and Quarterly Progress Report No. 10, September 1967, pp. 19-44.

B-6. "Electron Impact Excitation of the Dayglow," by A. Dalgarno, M. B. McElroy and A. I. Stewart, Planet. Space Sci. (submitted April 1968); Quarterly Progress Report No. 11, December 1967, pp. 13-19 and Quarterly Progress Report No. 12, March 1968, pp. 17-30.

Brief summaries are presented below in the order indicated in the above bibliography.

1. The diurnal variation of ionospheric temperatures. — It has been established by direct measurements using probes carried on rockets and satellites [16-22] that the electron temperature exceeds the neutral particle temperature at altitudes above about 120 km during the day. Measurements using the backscatter technique also indicate that the ion temperature exceeds the neutral particle temperature above about 300 km and apparently tends towards the electron temperature at extended altitudes.

Theoretical studies [23-25] indicate that solar UV raidation represents a major heat source. The ambient electrons are heated by elastic collisions with fast photoelectrons and the positive ions are heated by collisions with hot ambient electrons [24,25] while early theoretical studies were predicated on the assumption of local equilibrium. Hanson [24] noted that thermal conduction in the electron gas would modify the temperature profile at extended altitudes and Geisler and Bowhill [26] confirmed the importance of conduction.

The present investigation was stimulated by the availability of detailed observational data on the diurnal variations of the electron and ion temperatures. Simultaneous measurements of electron density are also available and afford an opportunity of extensively testing the theoretical model. In particular, it was propitious to ascertain whether additional heat sources were required to explain the data discrepancies.

This possibility was examined by developing a new theoretical procedure which is described elsewhere in detail (B-1). Briefly, the technique involved the generation of model atmospheres for the earth neutral and ionospheric components which were employed subsequently to calculate the electron heating and cooling rates in accordance with a technique due to Dalgarno [24]. The theory assumes heating by solar ultraviolet radiation, cooling by collisions and also allows for heat transport by conduction.

The appropriate form of the heat balance equation was solved numerically using the Runge-Kutta technique. The calculations performed yielded prediction data on the average diurnal variations of ionospheric electron and ion temperatures for April, July, and November 1963 at a typical mid-latitude station. The magnitudes of the predicted temperatures agree satisfactorily with observation but there are also some specific significant differences between measured and computed profiles of electron temperature. In general, the present results are consistent (above 140 km) with results of rocket flights but not for altitudes below 140 km and not with results derived from measurements of incoherent back scatter. On the basis of these results, it may be necessary to postulate and additional heat source at low altitudes.

2. Electron cooling in the earth's upper atmosphere. — In studies of the electron temperature in the terrestrial ionosphere, it has been assumed that cooling by collisions of the thermal electron gas occurs through elastic scattering by positive ions, through excitation of the rotational and vibrational levels of molecular nitrogen and oxygen, and through excitation of the ^1D level of atomic oxygen. There is, however, another collision process,

$$e + O\ (^3P_J) \rightarrow e + O\ (^3P_{J'}), \qquad (1)$$

which may be the dominant cooling mechanism over certain temperature and altitude ranges in the atmosphere. This interesting and important possibility was investigated by performing theoretical calculations which are described in detail elsewhere (B-2). The results of this investigation are presented in the curves of Figure 11 showing the calculated mean cooling rates for electron temperatures up to 10,000°K and for neutral-particles temperatures between 100°K and 3000°K. In order to obtain cooling rates for electron temperatures above 2000°K, it was assumed, that above a velocity corresponding to 10,000°K, the cross sections either remained constant or decreased as e^{-1}. The actual behavior probably lies between these two limits.

The relatively high electron cooling rates shown in Figure 11 indicates that process (1) is the dominant cooling mechanism over a wide range of temperatures throughout the E and F regions of the ionosphere. This represents an important conclusion since, on this basis, it can be stated that all previous calculations of electron temperatures are quantitatively incorrect below about 300 km. In particular, the inclusion of process (1) may resolve the discrepancies that exist, at altitudes between 200 and 300 km, between the backscatter data of Evans [27] and the theoretical predictions of Dalgarno, et al. [28].

3. Ion temperatures in the topside ionosphere. — Analysis of backscatter observations [27] has established that the positive ion temperature

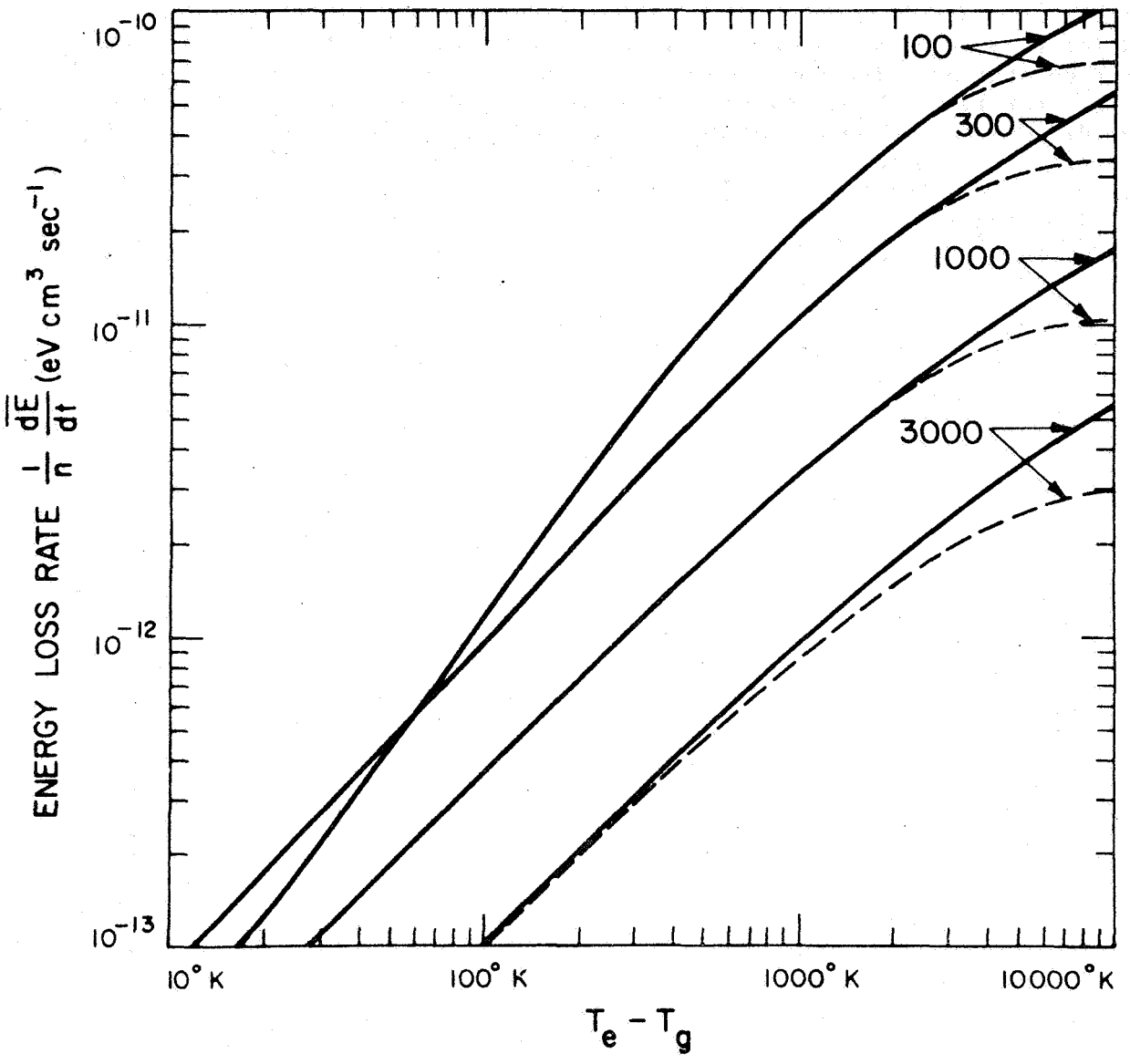

Figure 11. Cooling rates $\frac{1}{N}\overline{\frac{dE}{dt}}$ in eV cm^{-3} sec^{-1} for electron-impact-induced fine-structure transitions in atomic oxygen. The solid curves assume that the cross sections are constant at high velocities and the dashed curves assume that they decrease as E^{-1}. The curves are labeled by the neutral-particle gas temperature T_g in °K.

in the ionosphere exceeds the neutral particle temperature at altitudes above 300 km during the daytime, and the results are in general accord with theoretical predictions which assume that the ions are heated by collisions with the hot ambient electrons and cooled by collisions with the neutral particles [28]. Since the efficiency of the heating and cooling mechanisms depends upon the ionic species involved, the various positive ions may be characterized by different temperatures. This possibility was examined by performing a theoretical analysis of a variety of heating and cooling processes associated with the ions O^+, He^+, and H^+ resident in the earth topside ionosphere.

Equating the heating and cooling rates of the above ions results in a set of coupled equations for the ion temperature which can be solved iteratively. The resulting ion temperature profiles are illustrated in Figure 12. Owing to the high efficiency of energy exchange in ion-ion collisions, the H^+ - O^+ temperature difference does not exceed 200°K. and the He^+ - O^+ temperature difference does not exceed 50°K. In most circumstances it will suffice to characterize the ionic distribution by a single ion temperature.

The heat flow from electrons to neutrals at 700 km is shown in Figure 13. At this altitude the H^+ and O^+ ions are of approximately equal importance. At lower altitudes the heat flows principally to O^+ and then to O, and H^+ loses most of its heat to O^+. At higher altitudes, heat flows principally to H^+ and then to H and He, and O^+ receives most of its heat from H^+. The role of He^+ is negligible at all altitudes.

4. Theoretical investigations on VUV photon scattering by planetary gases - molecular nitrogen and molecular hydrogen. — A new semi-empirical model of the dipole spectrum of molecules was developed and applied to the determination of dipole properties of molecular nitrogen (B-4). With the techniques developed herein, VUV molecular scattering cross sections were derived wherein the resultant model extrapolates to shorter wavelengths (where laboratory measurements are available) and long wavelengths without using the conventional assumption that the cross section varies as the inverse fourth power of the wavelength. The results indicate that a marked increase appears in the cross section toward shorter wavelengths.

Owing to the severe experimental difficulties involved in performing absolute measurement of VUV molecular scattering, an effort was made to calculate the molecular scattering cross sections from first principles (i.e., without resorting to laboratory data). A new and suitable method was developed which is, in principle, capable of achieving this goal (B-5). Initial results were obtained for molecular hydrogen for $\lambda > 2500$Å since this model is more applicable to long wavelengths; specifically, numerical uncertainties existing at present have prevented the application of the method at shorter wavelengths. However, more refined procedures can be developed as required, so that the above theoretical approach should be capable of yielding cross section values with an accuracy not achievable

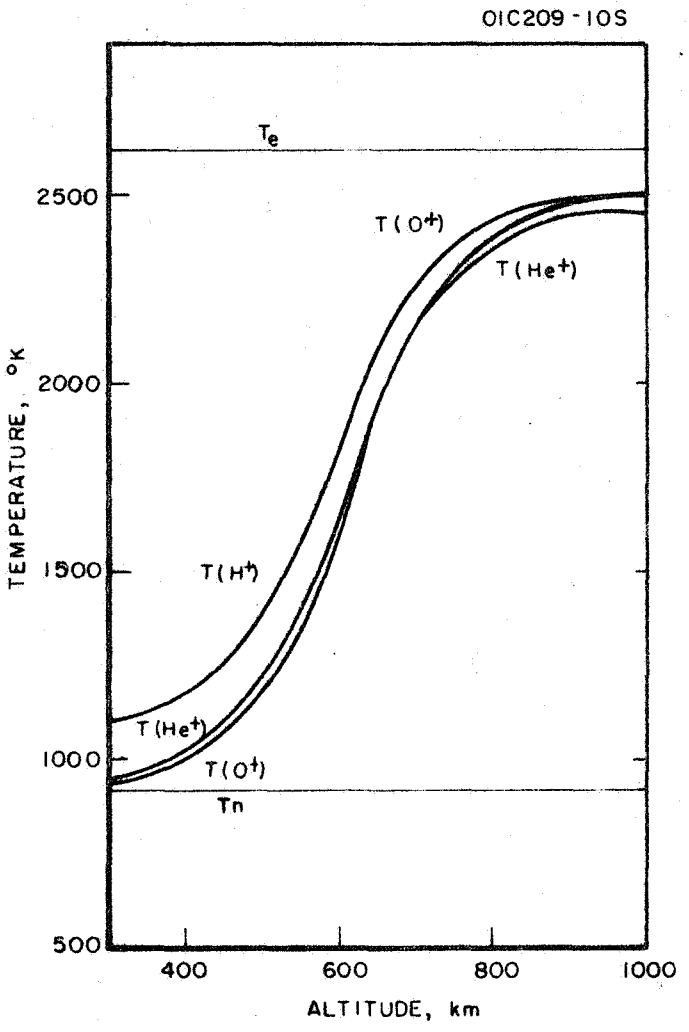

Figure 12. Electron temperature, T_e, ion temperatures, $T(X^+)$, and neutral temperature, T_n, as a function of altitude.

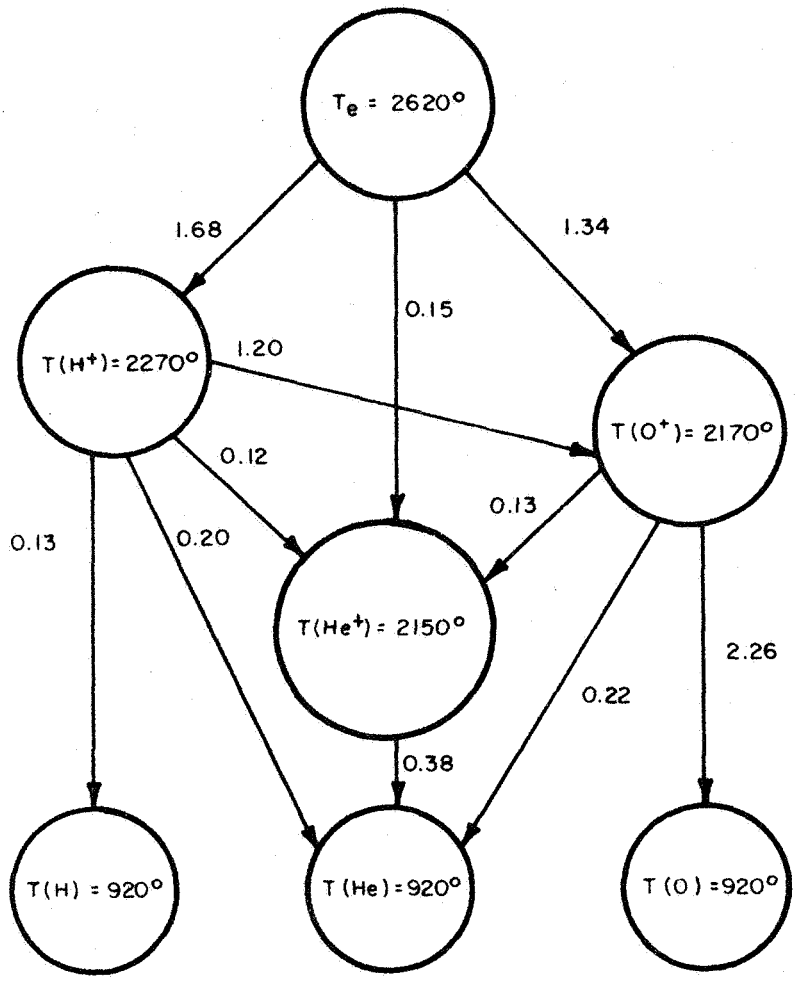

Figure 13. Flow of heat from electrons to neutrals at 700 km. The units are eV cm^{-3} sec^{-1}.

to date. The new model can be applied to H_2 (to below 1000Å) and the experience gained from this study in an absorbing region should indicate an explicit procedure for calculating absolute cross section values for the planetary gases N_2, O_2 and CO_2. Since it is certain that the relative VUV scattering cross sections of these gases will be measured in the laboratory in the near future, the new theory should be of particular value in establishing absolute values. In any event, even the results for H_2 should be useful for direct application to calculations on the VUV albedo of Jupiter. For completeness, brief summaries are included here of the material contained in the original publications (B-4,B-5).

a. Dipole properties of molecular nitrogen. – Experimental data available on the oscillator strength distribution of molecular nitrogen which, supplemented by refractive index data and sum rules, can be employed to construct a model of the complete dipole spectrum. On the other hand, no experimental data or absolute molecular scattering cross sections are available for the VUV region. Theoretical methods have been developed and applied to calculate the molecular nitrogen scattering cross section in the VUV spectral region. These data are important in the interpretation of ultraviolet observations of the atmospheres of the planets Earth, Venus, and possibly Mars. In addition, the calculated dipole spectrum can also be employed to calculate the leading term in the spherical component of the long range interaction between a pair of nitrogen molecules and to calculate the average excitation energy which controls the absorption of fast charged particles by nitrogen gas. In the original paper (B-4) the theoretical development is described in detail whereby calculations are performed to obtain estimates on the dipole spectrum of molecular nitrogen. The resultant spectrum was used to calculate various dipole properties including the spherically symmetric van de Waals coefficient for a pair of nitrogen molecules (73.4 a.u.), the mean excitation energy describing the deceleration of fast particles (82.1 eV), and the molecular scattering cross section of Lyman-α (5.6×10^{-24} cm^2). The vibrational Raman scattering at Lyman-α is estimated at between 10^{-27} and 10^{-26} cm^2. Finally, the molecular scattering cross section values for $\lambda\lambda$ 10,000 - 1200Å were calculated, and since these are of direct interest to the current program, the results are presented in Table 2.

b. Optical properties of molecular hydrogen. – Variational methods were employed to calculate the parallel and perpendicular dynamic dipole polarizabilities, the refractive index, the Verdet constant, the molecular and Raman scattering cross sections, and the molecular and Raman depolarization factors of molecular hydrogen as a function of frequency of the incident radiation. The development and method of application of this theoretical technique are presented in detail in the original report (B-5) where it is demonstrated that the calculated parametric values are satisfactory at long wavelengths but unsatisfactory below about 2400Å owing to inadequacies in the representation of the wave function of the undisturbed molecule. By scaling the results to ensure that they tend to

TABLE 2

CALCULATED MOLECULAR SCATTERING CROSS SECTIONS FOR λλ N_2 FOR λλ 10,000-1200Å

Wavelength (Å)	Scattering Cross Section (cm^2)
1200	6.22×10^{-24}
1215.7	5.62
1250	4.53
1300	3.43
1400	2.08
1500	1.43
1600	1.00
1700	7.36×10^{-25}
1800	5.52
1900	4.25
2000	3.34
2500	1.21
3000	5.52×10^{-26}
3500	2.88
4000	1.65
4500	1.02
5000	6.60×10^{-27}
5500	4.47
6000	3.14
7000	1.69
8000	9.80×10^{-28}
9000	6.10
10000	3.99

the zero-frequency limits of Kolos and Wolniewicz [29] one obtains at the laser wavelength 6238Å used by Bridge and Buckingham [30], 0.126 for the molecular anisotropy 0.818Å^3 for the mean polarizability, and 0.309Å^3 for the polarizability anisotropy compared with the corresponding measured values of 0.128, 0.819, and 0.314Å^3, respectively. With appropriate modification, the above theoretical techniques can be employed to calculate the corresponding parameters throughout the VUV spectral region. The resultant data should be significantly more accurate than any available at present.

5. Electron impact excitation of the dayglow. — The fast photoelectrons, produced in the upper atmosphere by the absorption of solar ultraviolet radiation in ionizing transitions, lose energy in collision processes leading to ionization and excitation of the neutral particles and to heating of the electron and ion gases. The excitation processes produce a substantial component of the dayglow luminosity of the upper atmosphere, the observation and the interpretation of which can provide detailed information on the distribution of energy sources in the daytime atmosphere. The prediction of the intensities of the dayglow emission features involves a more detailed description of the individual processes causing the degradation in energy of the photoelectrons but is otherwise similar to studies of photoelectron heating [25,28].

The calculation of the initial energy spectrum of the photoelectrons, which involves a choice of model atmosphere and ionosphere, of absorption and photoionization cross sections, and of solar ultraviolet intensities has been described in detail by Dalgarno, et al. [28]

The photoelectrons lose energy by exciting and ionizing the neutral particle constituents of the atmosphere. Although several processes contribute to the energy degradation, few of the pertinent cross sections are known with precision. In the present study, the roles of atomic O and molecular N_2 were considered. For each case, several relevent experimental cross section data were identified, reviewed, and critically evaluated. Owing to several shortcomings, these experimental data were supplemented by theory to obtain usable cross section estimates. Finally, a new theoretical procedure was developed and applied (B-6) in order to obtain estimates for the contributions to the Earth dayglow owing to the interaction of superthermal electrons with ambient atmospheric atomic oxygen and molecular nitrogen. It was concluded that significant observable airglow contributions can be expected in the following spectral regions: 1302-1306, 1356, 8446, 7774, 1026, and 1152 and 989, 5577 and 6300Å for atomic oxygen; the first positive bands, the second positive bands, the Vegard Kaplan bands and the Lyman-Hopfield bands for N_2; and the first negative bands and the IR Meinel system for N_2^+.

C. Experimental Investigations in the VUV (2000-1000Å) and the EUV (below 1000Å) Spectral Regions

The detailed results of this laboratory phase of the current program are contained in the following publications:

C-1. "Physics of Planetary Atmospheres, VI. Studies of Photoabsorption by Atomic Hydrogen, Oxygen, and Nitrogen," by R. B. Cairns and J. A. R. Samson, GCA Technical Report No. 67-2-N.

C-2. "Photoabsorption Studies of Discharged Hydrogen," by R. B. Cairns and J. A. R. Samson, Proc. Phys. Soc. (London) 90, 879 (1967).

C-3. "Present Status of Ionic Mobility Measurements in the EUV," by P. Warneck and F. F. Marmo, Quarterly Progress Report No. 9, June 1967, pp. 35-39.

C-4. "Measurement of the Ion Mobilities of Selected Planetary Gases in the EUV," by P. Warneck and F. F. Marmo, Quarterly Progress Report No. 11, December 1967, pp. 21-32.

C-5. "Measurement of the Kinetic Energy and Spatial Distribution of Ejected Photoelectrons Due to VUV and EUV Photoionization," by J. A. R. Samson and R. B. Cairns; and Quarterly Progress Reports No. 10, September 1967, pp. 44-47; No. 9, June 1967, pp. 29-35; No. 8, March 1967, pp. 17-24; No. 7, December 1966, pp. 47-70.

C-6. "Vacuum Ultraviolet Research," by J. A. R. Samson, Appl. Opt. 6, 879 (1967), and Quarterly Progress Report No. 7, December 1966, pp. 47-65.

C-7. "Photoelectron Spectroscopy of the Rare Gases," by J. A. R. Samson and R. B. Cairns (submitted for publication to Phys. Rev.) and Quarterly Progress Report No. 12, March 1968, pp. 34-57.

C-8. "The Design, Development and Continuation of New Experimental Devices for VUV and EUV Investigations," by J. A. R. Samson and R. B. Cairns, Quarterly Progress Report No. 10, pp. 46-54.

C-9. "Reflectance and Transmittance of Laser Deposited Iridium in the Vacuum Ultraviolet," by J. A. R. Samson, J. P. Padur and A. Sharma, J. Opt. Soc. Am. 57, 966 (1967, and Quarterly Progress Report No. 8, March 1967, pp. 25-27.

C-10. "The Relative Photoelectric Yield and Transmittance of Aluminum Films," by R. B. Cairns and J. A. R. Samson, J. Opt. Soc. Am. 57, 433 (1967), and Quarterly Progress Report No. 7, December 1966, pp. 65-70.

C-11. "Metal Photocathodes as Secondary Standards for Absolute Intensity Measurements in the Vacuum Ultraviolet," by R. B. Cairns and J. A. R. Samson, J. Opt. Soc. Am. 56, 1568 (1966).

C-12. "The Design, Development and Construction of New Experimental Devices for VUV and EUV Investigations: The Design, Development and Construction of a Suitable EUV Grazing Incidence Monochromator," by J. A. R. Samson, Quarterly Progress Report No. 8, March 1967, pp. 25-27.

C-13. "The Present Status of Grazing Incidence EUV Monochromator," by J. A. R. Samson and R. B. Cairns, Quarterly Progress Report No. 9, June 1967, pp. 35-39.

Brief technical summaries of the laboratory efforts involved are presented below in the following major discussion areas: (1) absorption and photoionization cross section measurements of atomic H, O, and N in the VUV (C-1,C-2), (2) ion mobility measurements in the EUV (C-3,C-4), (3) measurements of kinetic energy distribution of ejected photoelectrons due to VUV and EUV photoionization (C-5,C-6), and (4) design, development and fabrication of new experimental devices for VUV and EUV laboratory investigations (C-8,C-13).

1. Laboratory measurements of the absorption and photoionization cross sections of atomic H, N, and O in the EUV and VUV spectral regions.— It is important to obtain quantitative measurements of the absorption and photoionization cross section of atomic species not only to better understand atomic structure but also because of the unique importance they assume in the upper atmosphere of planets where atomic constituents predominate. Thus, investigations of EUV and VUV photoabsorption processes for atomic H, N, and O were undertaken under the current program. A brief summary of the final results is presented below; the details are available elsewhere (C-1,C-2). For measurements of the photoionization cross sections of atomic H, O, and N, it was necessary to dissociate the parent diatomic gases and to know the resulting partial gas pressures and gas temperatures. Of the several techniques available for this purpose, the afterglow of a CW-electrodeless-rf or microwave discharge was selected since there are no large-scale transient fluctuations of temperature or atom concentration, the gas temperature is essentially room temperature, and there is no sputtering of electrode material resulting in increased atom losses by wall recombination. In an afterglow, the atom concentration is lower than in the discharge itself, but there are fewer unwanted excited atoms and molecules. The relatively complex and varied procedures involved in the production of sufficient concentrations and purities of the atomic species of interest is discussed elsewhere (C-1,C-2) so that no further details are presented here. However, after considerable effort, suitable atom sources were developed and employed in the investigation. A special windowless absorption cell was then designed and attached to the 1/2-meter monochromator exit slit assembly. The required (below 1000Å) monochromator radiation source was obtained from a high voltage condensed spark discharge. The gas in the light source was usually argon since its line spectrum is particularly dense and relatively intense in the required wavelength range. The radiation from the light source was dispersed with a resolution of about 3Å

and then transmitted through the absorption cell and detected using a photodetector (an aluminum plate detector or a windowless photomultiplier). The background pressure in the entire system was about 5×10^{-5} mm Hg. The experimental results of the present investigation were compared to other experimental and theoretical data sources in a systematic critical review. On the basis of the present analytical results and the totality of available data, the presently recommended atomic photoionization data are presented in Figures 14, 15, and 16.

In Figure 14 the theoretical data, $\sigma(H)$, have been plotted on a scale which allows interpolation between the actual datum points. Although the experimental work on atomic hydrogen was not free from systematic error, the results are relatively consistent with theory.

The $\sigma(O)$ data are plotted as a function of wavelength in Figure 15. The theoretical curves of Dalgarno [31], are in fair agreement with experiment but generally indicate lower cross section values. Because of this, the results obtained using the dipole velocity formulation are preferred at wavelengths longer than 732Å. At shorter wavelengths, the dipole length formulation agrees more closely with experiment. The photoionization continuum must be severely distorted, at wavelengths longer than 732Å, by discrete absorption lines many of which are broadened by autoionization. In this spectral region, the experimental cross sections must be regarded as the more reliable data source. However, it should be remembered both that no extrapolation between these datum points is permissible and that the details of the experiment were such that the large cross sections, e.g., at 685Å, probably represent lower limits. The Rydberg series converging to the thresholds at 732 and 665Å can be expected to disguise and effectively remove the step-like features of the theoretical curve.

The preferred data $\sigma(N)$ are shown diagrammatically in Figure 16. The dipole length data of Henry [32] are believed to be more reliable than earlier theoretical results since relatively good agreement exists with the experimental values $1/2\ \sigma(N_2)$ at wavelengths shorter than 367Å.

2. <u>The measurement of ionic mobilities of selected planetary gases in the EUV</u>. – The measurement of ionic mobilities of selected planetary gases is directly applicable to several current planetary aeronomy problems. In general, the overall distribution and localized concentration of ions in planetary atmospheres are governed by several processes which include ion conversion reactions, recombination, ambipolar diffusion, and ion drift velocities. While a relatively large quantity of data has become available recently concerning the first two processes, only scant experimental information is available on ionic diffusion coefficients and drift velocities which are important processes in controlling the redistributions of atmospheric ions in the presence of ionospheric electric fields. In addition, the ambipolar diffusion coefficient values are related directly to the rates involved in controlling the redistribution of

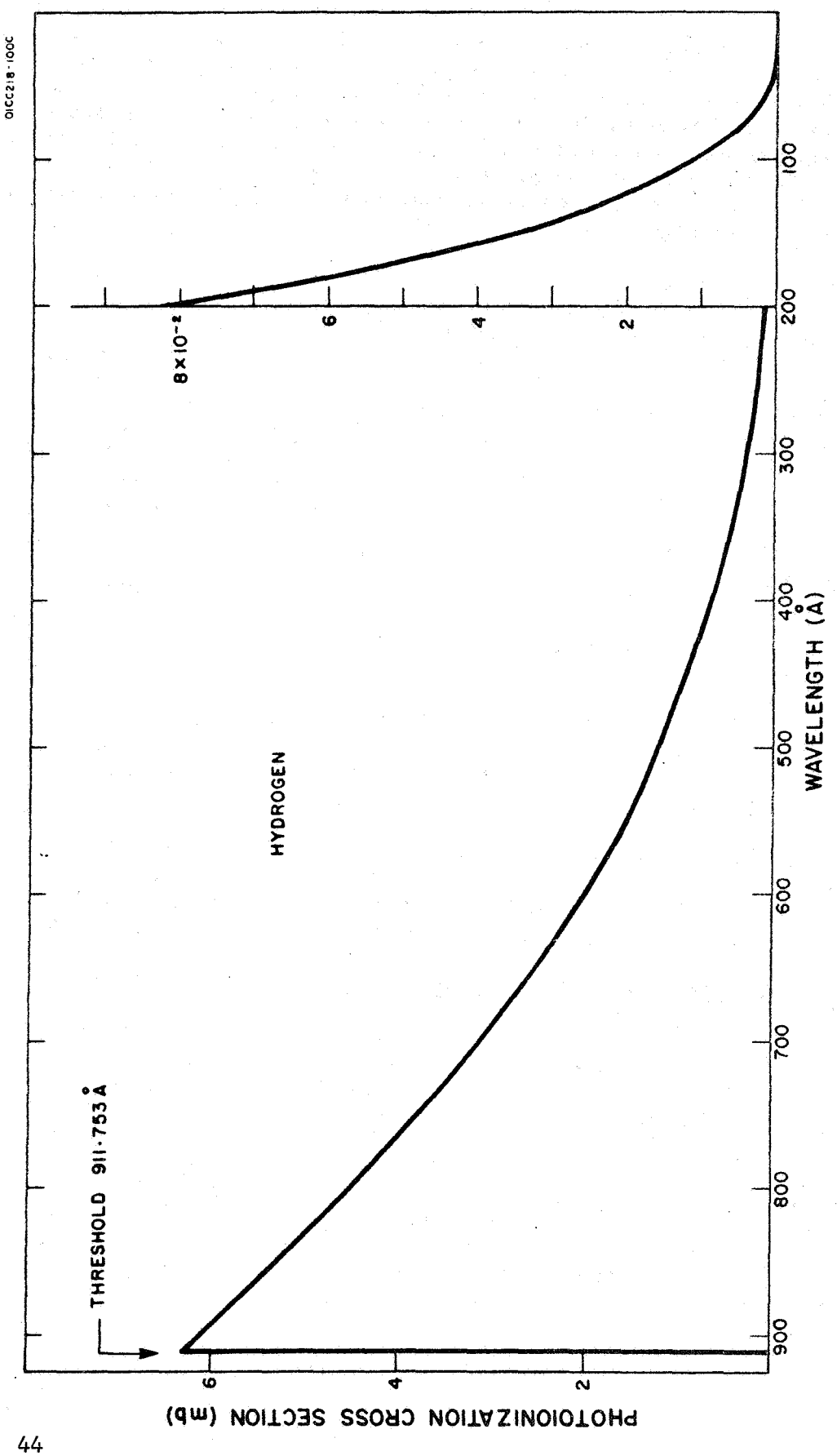

Figure 14. The photoionization cross section of H.

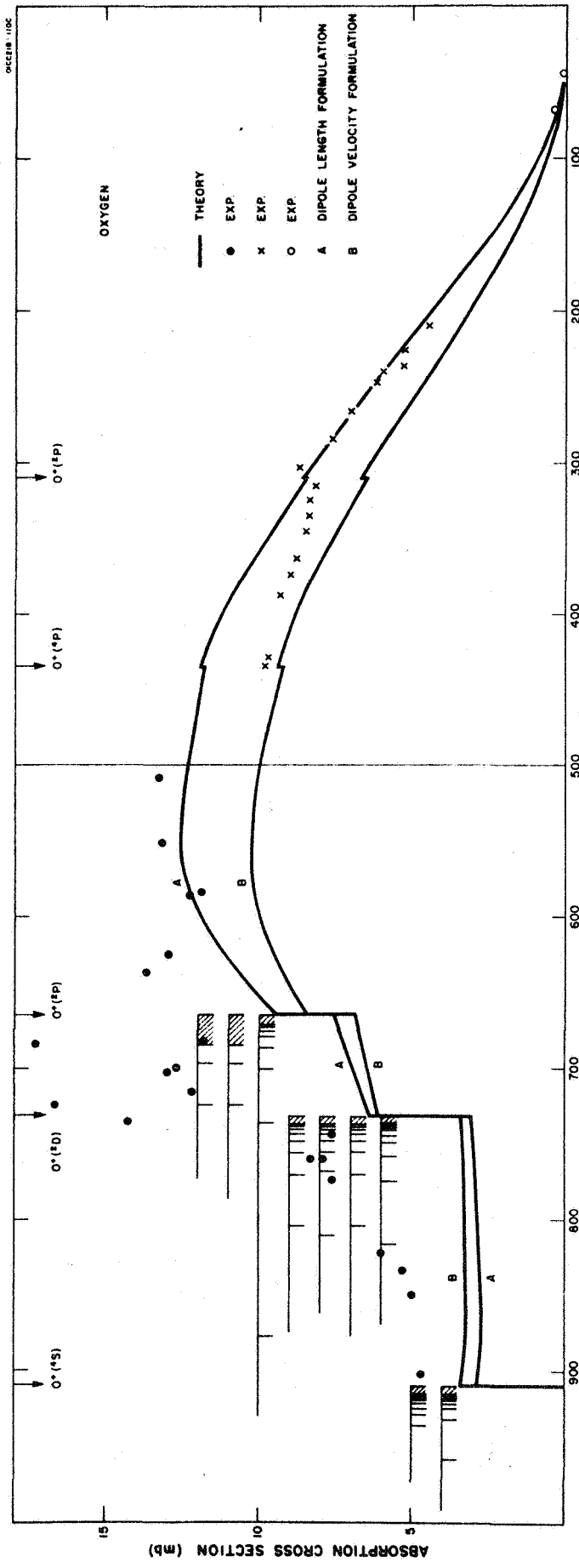

Figure 15. The photoionization cross section of O.

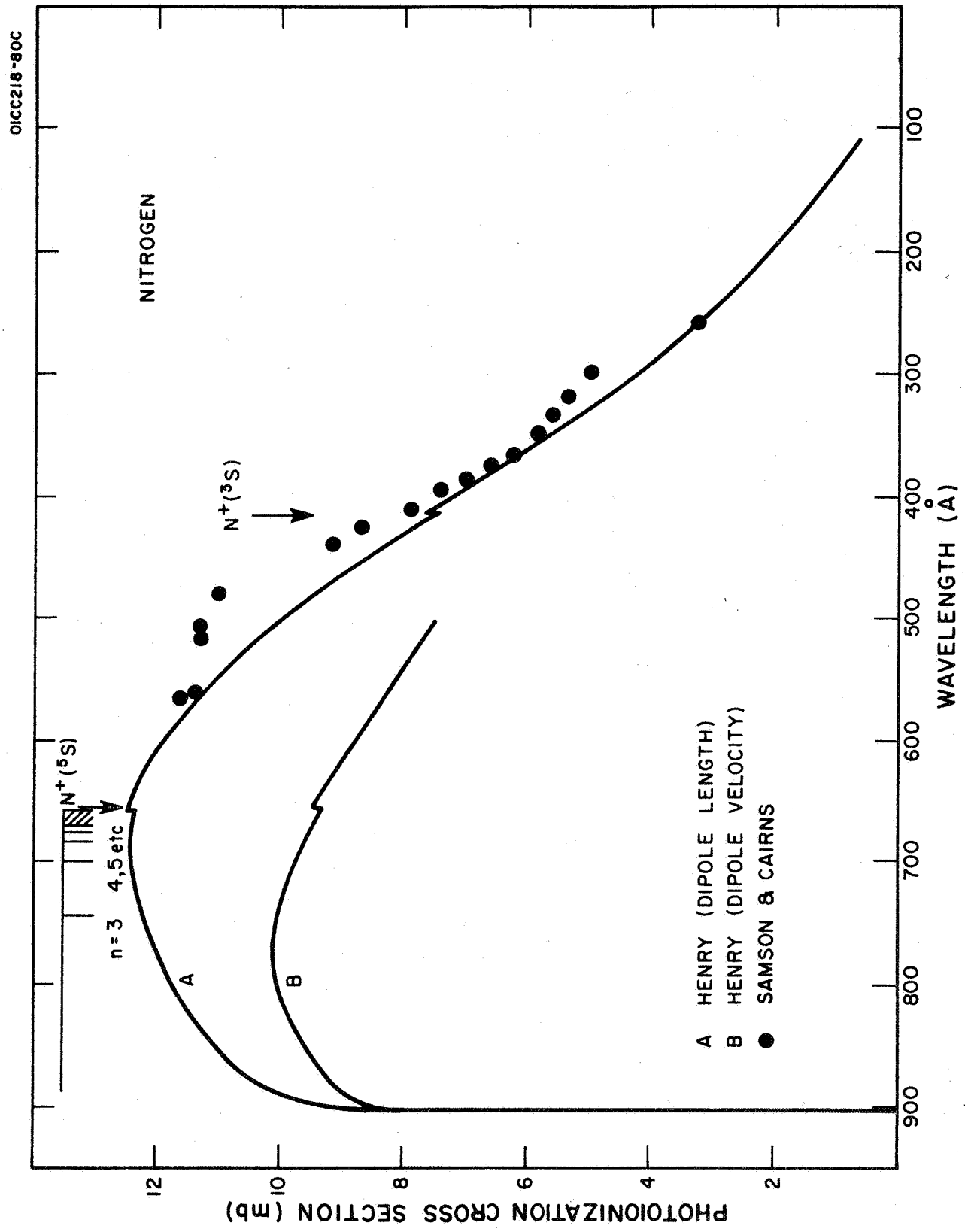

Figure 16. The photoionization cross section of N.

ionization in the presence of concentration gradients. Furthermore, ion mobility values are employed in calculating the rate at which planetary ions cool on collision with neutral ionospheric species. In principle, ion mobilities measured at different values of the applied electric field can be analyzed to yield information on the collision cross sections as a function of energy.

Under the present program, it has been demonstrated that photoionization mass spectrometric techniques can be applied to measure ion-neutral reactions in the VUV and EUV spectral regions [33-36]. During the performance of the above experiments, it became evident that, with proper modification, reliable drift velocity data could be obtained by measuring the residence time of specific ions in the photoionization mass spectrometer ion source chamber. A number of advantages [34] gained by employing this experimental configuration in the performance of ion-neutral reactions are of equivalent importance in the performance of ion mobility measurements. These include: (1) mass identification of the ion, (b) energy selection of the ionizing radiation so that ions can be formed in a well-defined electronic-vibrational state, and (3) use of a pulsed light source of duration sufficiently short to allow observation of the broadening of the ion transient with time. The latter feature makes possible the evaluation of the ionic diffusion coefficients. During the current program, the required experimental apparatus was developed and a number of preliminary measurements were performed on the ionic mobility of N_2^+ in nitrogen.

The feasibility of photoionization-mobility experiments was first demonstrated by Samson and Weissler [37] who employed a conventional shutter technique for measuring ion drift velocities. In the present investigation, this feature was incorporated by employment of the GCA photoionization mass spectrometer which has been used extensively in ion-neutral reaction studies (A-9 to A-12). In this regard, a technique was developed to determine the average residence time of parent ions in the ion source of the instrument involving the time delay experienced by a group of ions between the times of formation and registration on an oscilloscope. This technique can also be applied to measure drift velocities of mass identified ions. However, it should be noted that, whereas the determination of residence time for ion-molecule reactions does not require any knowledge of geometries and field conditions in the ion source, such information is vital to the measurements of drift velocities and mobilities. The detailed instrumentation development and application are described elsewhere (C-4) in detail.

Preliminary measurements employing the photoionization mass-spectrometer configuration have yielded information on the drift velocities of N_2^+ in nitrogen. The experiments were performed using a spectral setting of the monochromator at about 790Å. Energetically, this is about equivalent to the threshold value for the formation of N_2^+ in its ground vibrational and electronic state, so that the N_2^+ ion state is strictly defined which represents a considerable advantage for the present investigation.

It should be noted that N_4^+ formation was observed; however, it amounted to less than 10 percent even at the highest pressure employed. The N_2 gas pressure range was varied between 75 and 200 microns, and the drift velocity measurements were performed at three repeller voltages, i.e., 1.0, 2.0, and 5.0 volts, for which the corresponding field strengths are 1.5, 3.0, and 7.6 volts/cm, respectively. The observed experimental drift velocity values are plotted in Figure 17 as a function of E/P_o, the ratio of field strength, to pressure, P (corrected to 273°K). The results of Keller, et al. [38], are represented by the solid line while the dashed line indicates the data of Saporoschenko [39]. The highly satisfactory agreement among the three sets of data demonstrates that the present technique can be employed with high reliability. It can be seen from the figure that the slope of the present data is slightly less than one, whereas for near thermal ions, a slope of unity would be predicted theoretically. However, since the data of the other experimenters do not follow a slope of unity, it appears that the ions are not sufficiently thermal in the investigated E/P_o range for the theory to be strictly applicable. As a consequence, it is not feasible to derive from these data alone a precise value for the reduced mobility at zero field.

In spite of this limitation an extrapolation of the reduced mobility was performed, the results are shown in Figure 18 where it can be seen that the measured mobility values increase with decreasing E/P_o. The indicated linear extrapolation to $E/P_o = 0$ yields the mobility value $\mu_{oo} = 1.75$, where the second subscript zero indicates zero electric field. Since this value constitutes an upper limit, it is in reasonable agreement with the value $\mu_{oo} = 1.44$ obtained by Keller, et al. [38], and with the theoretical value $\mu_{oo} = 1.5$ derived by Dalgarno [40,41]. Additionally, since theoretically the extrapolation should not be linear but convex, the extrapolated zero field mobility value would be diminished somewhat; thus resulting in better agreement with the μ_{oo}-values deduced by others. Finally, it is likely that for those values of $E/P_o < 10$, the penetration of the accelerating field is no longer negligible so that the measured drift velocities can be too large. This effect must be considered carefully in future applications of the present method.

Nevertheless, from the results presented here, it is apparent that the employed technique yields data in reasonably good agreement with those obtained by entirely different techniques, thereby demonstrating the value of the present new method.

3. Laboratory measurements of the kinetic energy distribution of ejected photoelectrons due to VUV and EUV photoionization. — The role of superthermal or "hot" electrons in the generation of dayglow emissions has been discussed previously in Section B5 of this report where the theoretical studies involved have demonstrated the requirement for new laboratory data on the measurement of kinetic energy (and spatial) distributions of ejected photoelectrons due to photoionization processes

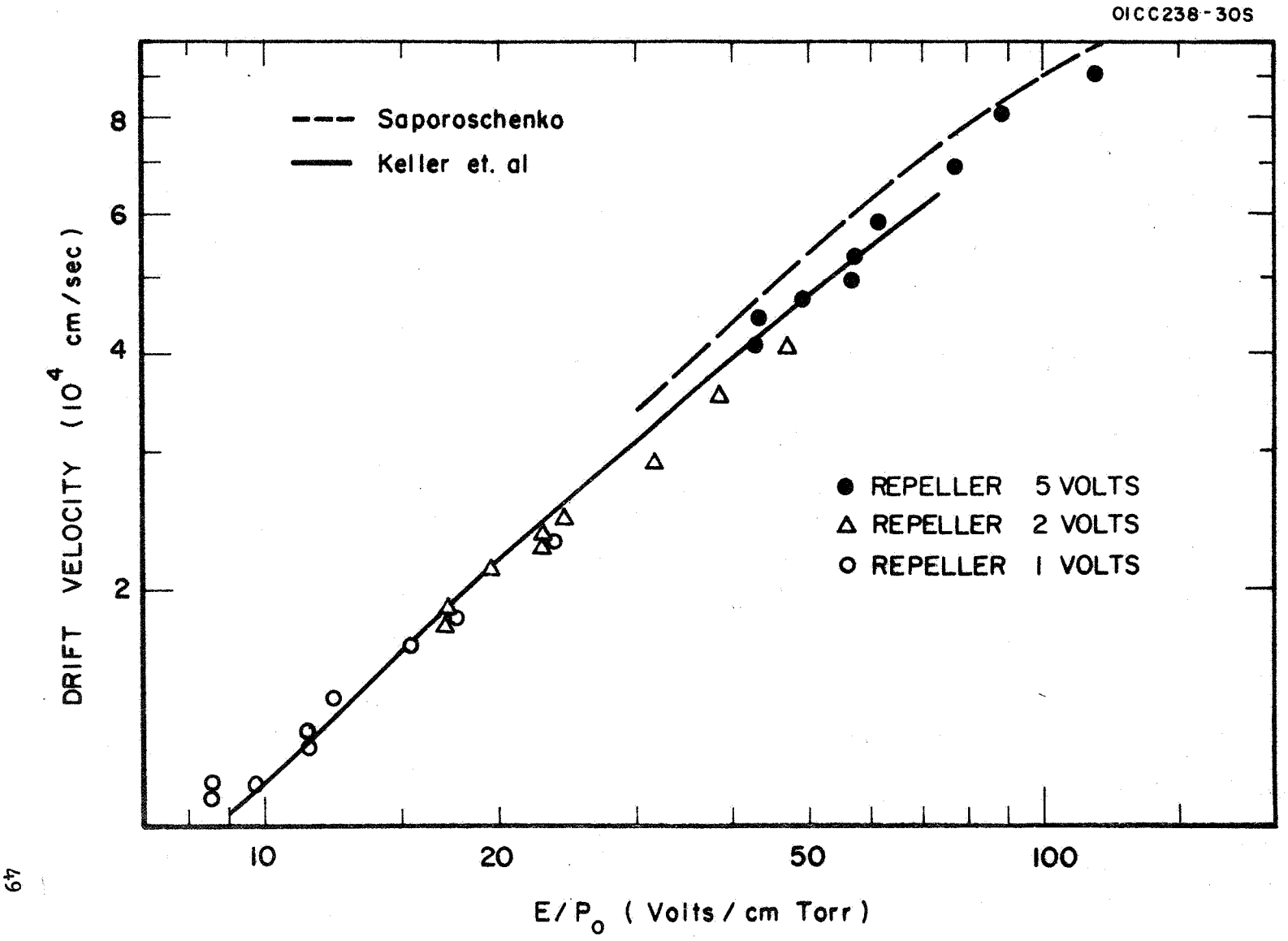

Figure 4. Drift velocities of N_2^+ in nitrogen versus relative field strength. O - neg. potential one volt; △ neg. potential 2 volts, ● np potential 5 volts.

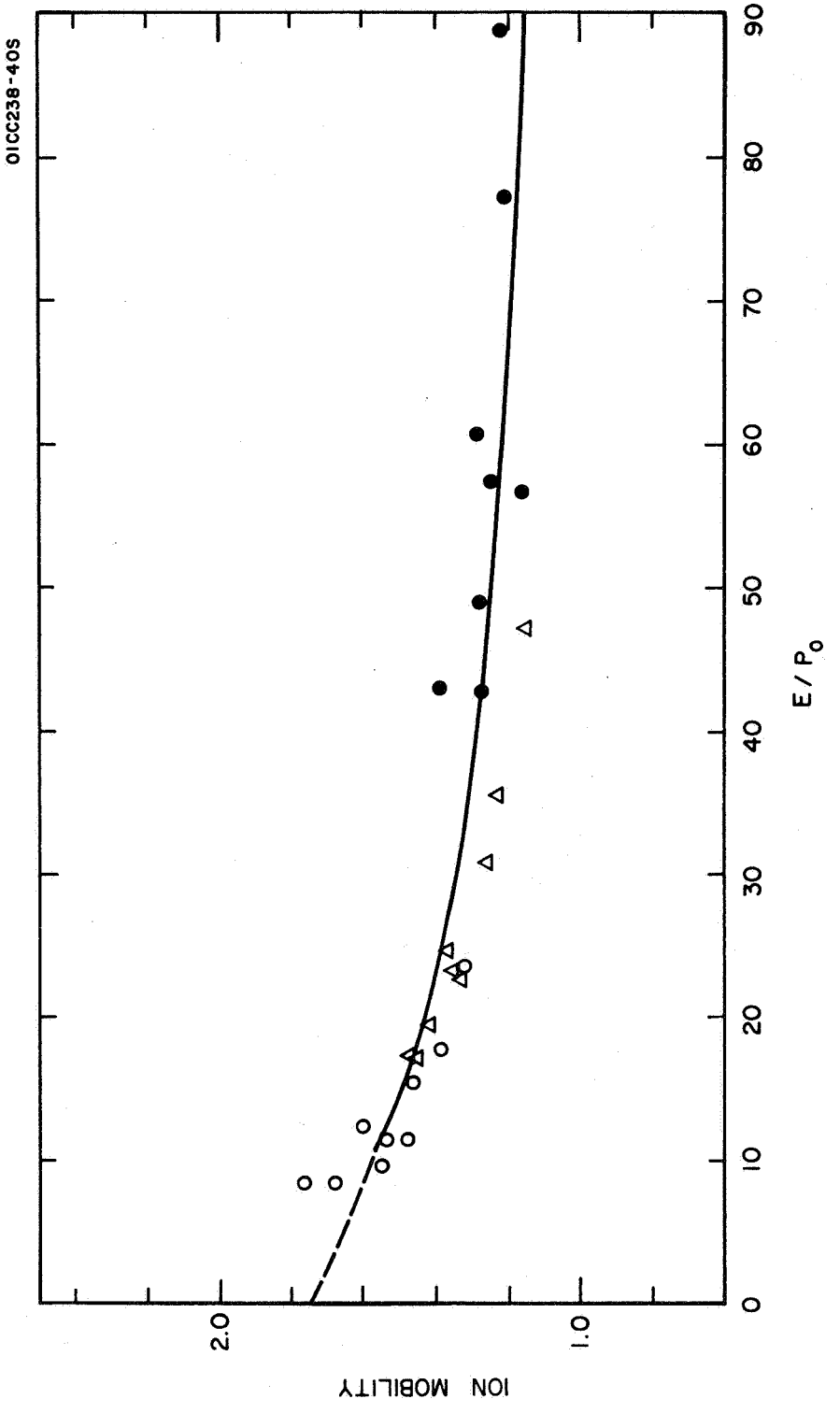

Figure 18. Reduced mobilities of N_2^+ in nitrogen. Symbols are as in preceding figure.

occurring in the Earth's upper atmosphere. In this regard, systematic laboratory investigations have been performed under the current program. The results achieved have been published elsewhere (C-5) so that no detailed account is presented herein. However, a brief summary of the methods involved and the data acquired is included below.

In principle, the laboratory methods involved in VUV and EUV photoelectron spectroscopy are conceptually straightforward. However, in practice, these investigations tend to be relatively complex owing to the large number of experimental difficulties encountered as discussed in the detailed report references (C-5,C-6). The major difficulties generally involve the inadvertent discrimination in the measured electron energy spectrum resulting from the analyzer-monochromator combination. A number of factors are involved including: (1) insufficient signal intensity, (2) the effect of electron-molecule collision in the analyzer, (3) the specific distributions of photoelectrons ejected from different atomic and/or molecular bonding shells, (4) the degree and variation (with EUV wavelength) of the polarization of the exit slit monochromatic radiation, (5) perturbations encountered by low energy electrons which pass through the small holes in the spherical analyzer, and (6) disturbing effects due to the "contact potentials" which exist between the inner and outer spheres of the analyzer. Under the present program these difficulties have been minimized and/or eliminated on the basis of a sustained effort aimed at continuing improvement of the techniques. On the basis of the difficulties enumerated under Items (1), (2), (3), (5), and (6), a relatively complex and sophisticated spherical analyzer was developed, fabricated, calibrated, and employed for the present experimental purpose. With respect to Item (4), new laboratory measurements were performed to obtain the appropriate correction factors. The critical features of the overall technique are shown in Figure 19 which includes a schematic of the photoelectron analysis and the configuration of the setup. The analysis consisted of three spherical grids with a variable retarding potential applied to the middle grid. The diameters of the spheres were 3, 4, and 5 inches. Two hollow metal tubes at the same potential as the inner sphere allowed radiation from the exit slit of a 1/2-meter Seya monochromator to enter the analyzer and release photoelectrons in the small volume element at the center of the spheres. The separation of the two tubes was about 9.5 mm. Baffles in the first tube defined the light path so that radiation did not impinge on the walls of the tubes producing a background of unwanted photoelectrons. The radiation emerging from the tubes was monitored by a photomultiplier sensitized to vacuum UV radiation with a coating of sodium salicylate. The photoelectrons produced at the center of the sphere traveled outwards along radii, i.e., in directions normal to the retarding potential. Electrons produced off center traveled at some angle to a radius and were retarded at a lower voltage. The relative diameters of the volume element and the inner sphere therefore established a limit to the resolving power of the analyzer. For the selected dimensions, electrons of energy E shoud have an energy spread $\Delta E/E = (1.56 \pm 0.1)$ percent. The measured

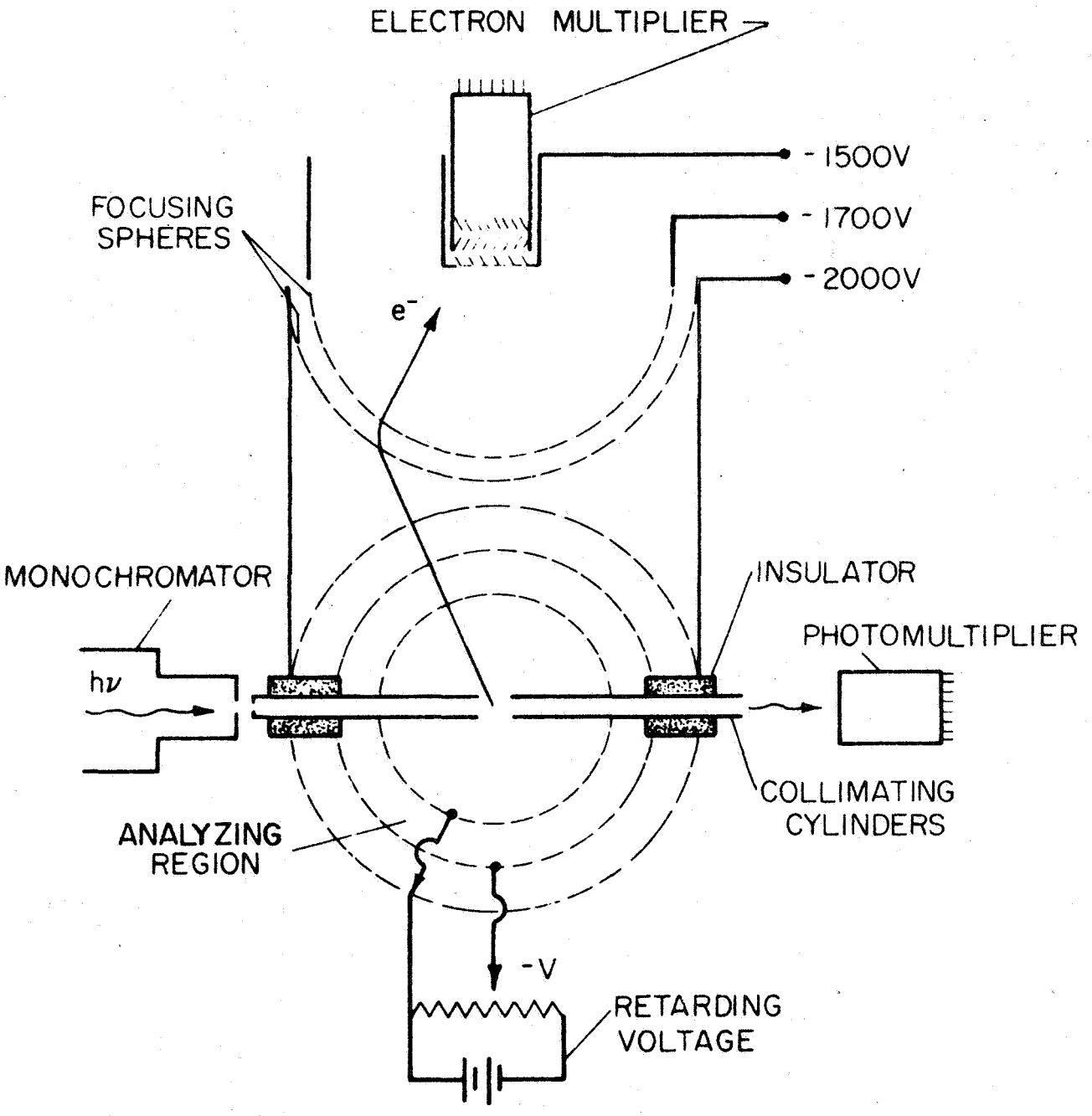

Figure 19. Schematic of the photoelectron energy analyzer.

resolution of the analyzer was 1.65 percent for electron energies in excess of 4 eV. For lower energies the total energy spread tended to a constant value of $\Delta E = 56$ mV. That is, in terms of a full width at half height, structure separated by 28 mV could be observed. However, this resolution could be achieved only when a Helmholtz coil was used to reduce the Earth's magnetic field from 0.5 gauss to about 0.05 gauss. The energy spread ΔE of the analyzer was determined as a function of the electron energy. It was found that the expected energy spread (caused by the finite dimensions of the apparatus) differed from the observed value owing to either (1) the small contact potentials in the field-free region where the electrons were created, or (2) the weak fields penetrating the holes of the mesh. Brass mesh with thirty holes per inch was employed in the fabrication of the spheres.

Electrons which escaped from the analyzer within a cone of 60 degrees centered at right angles to the incident radiation were intercepted by a spherical mesh electrostatic lens [42] and focused onto the first dynode of an electron multiplier. Since the electron multiplier was used in the dc mode, the entire analyzer was maintained at about 2000 volts negative to ground. The gas within the analyzer was maintained at pressures less than 5×10^{-3} torr to prevent high voltage arcing within the electron multiplier.

As the retarding potential of the analyzer was increased, a series of steps in the electron current appeared as each electron energy group was completely retarded. This is illustrated in Figure 20 where the retarding potential curve is shown for neon photoionized by radiation of 543.884Å. At this wavelength, neon can be ionized into either the ground $^2P_{3/2}$ state (I. P. = 21.564 eV) or the excited $^2P_{1/2}$ state (I. P. = 21.661 eV). Thus two groups of electrons should appear separated by 97 mV. The ratio of the numbers of electrons within each group is a measure of the relative transition probabilities for producing these two states of ionized neon. From Figure 20 it can be seen that these two states were clearly resolved with the ground state ion 2.18 times more abundant than the excited ion. The energy spread in the retarding potential steps was 56 mV.

To obtain the specific photoionization cross sections of the rare gases as a function of wavelength, it was only necessary to produce retarding potential curves such as shown in Figure 20 and measure the ratio of the step heights. Thus, applying the pertinent data and making use of the previously measured total photoionization cross sections [43], the specific photoionization cross sections of Ne, Ar, Kr, and Xe were obtained. The results are shown for each gas in Figures 21 through 24, respectively. In the cases of Ar, Kr, and Xe a third group of electrons appeared when the gases were ionized by radiation of wavelengths shorter than the threshold for ejection of an s-electron. The measured kinetic energies of these electrons identified them as s-electrons from the outer subshells of the atoms. Owing to the relatively large energy differences

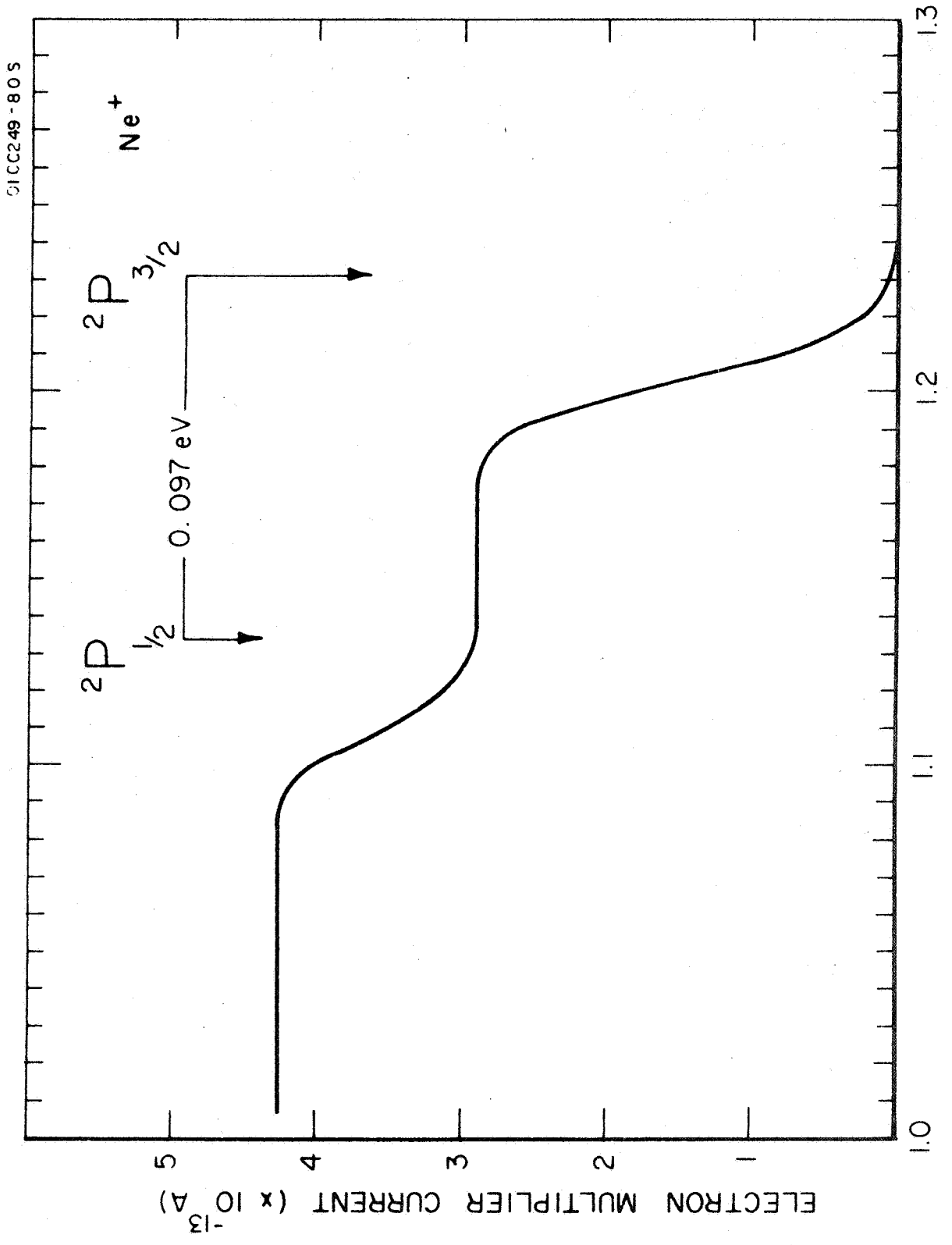

Figure 20. Retarding potential curve for neon photoionized by 543.9Å radiation.

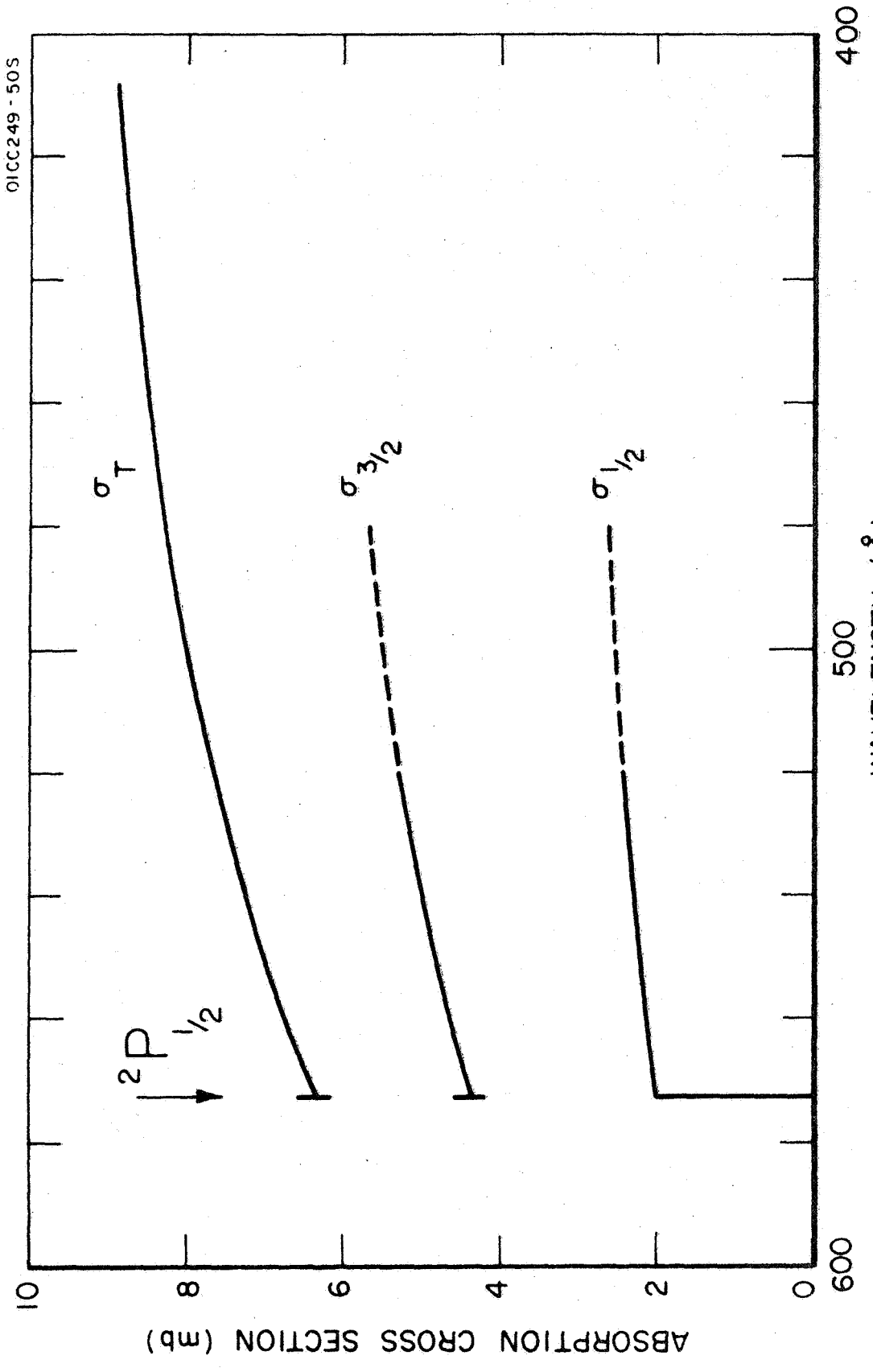

Figure 21. Specific photoionization cross sections for neon for λλ 600-400Å.

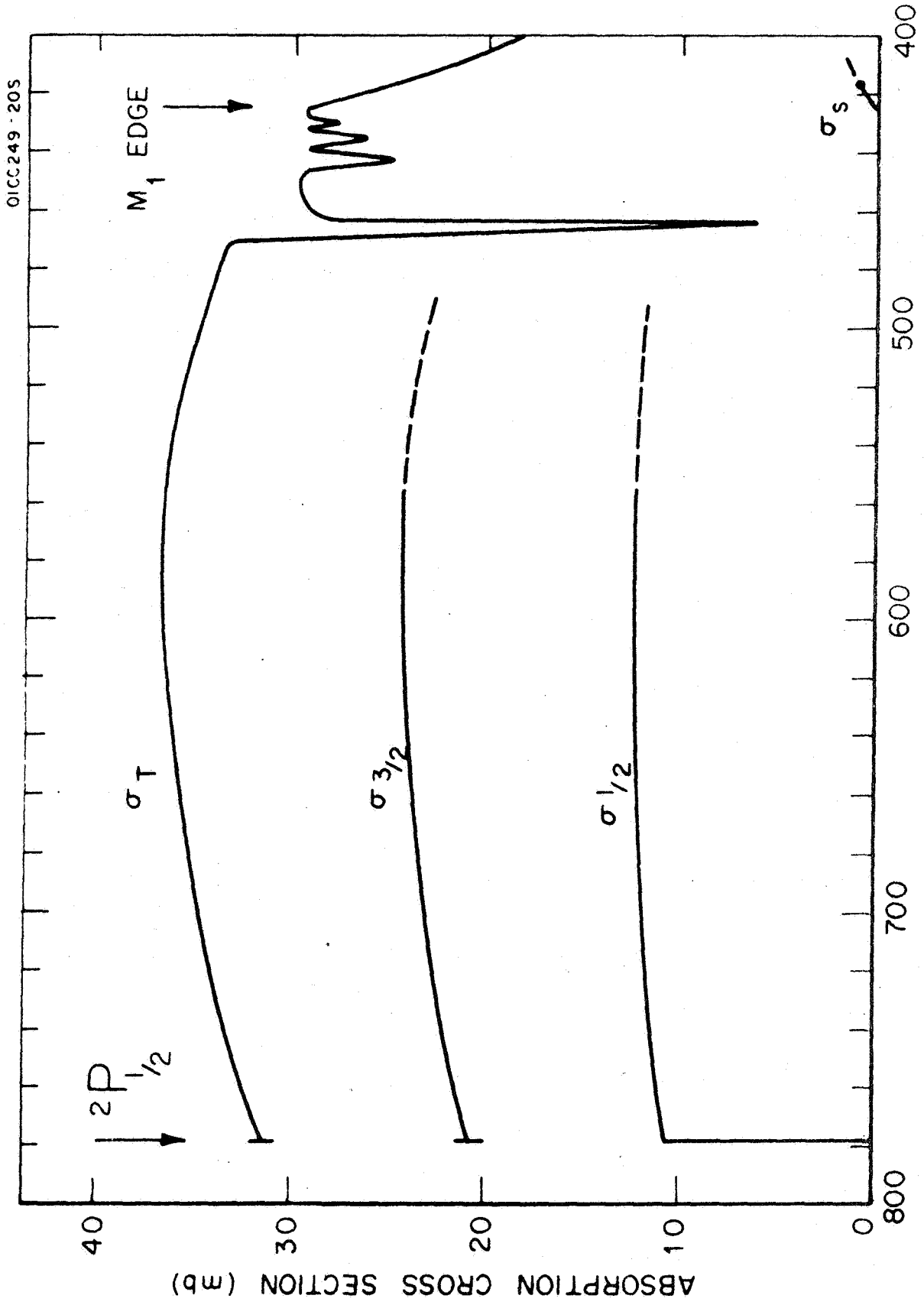

Figure 22. Specific photoionization cross sections for argon for λλ 600-800Å.

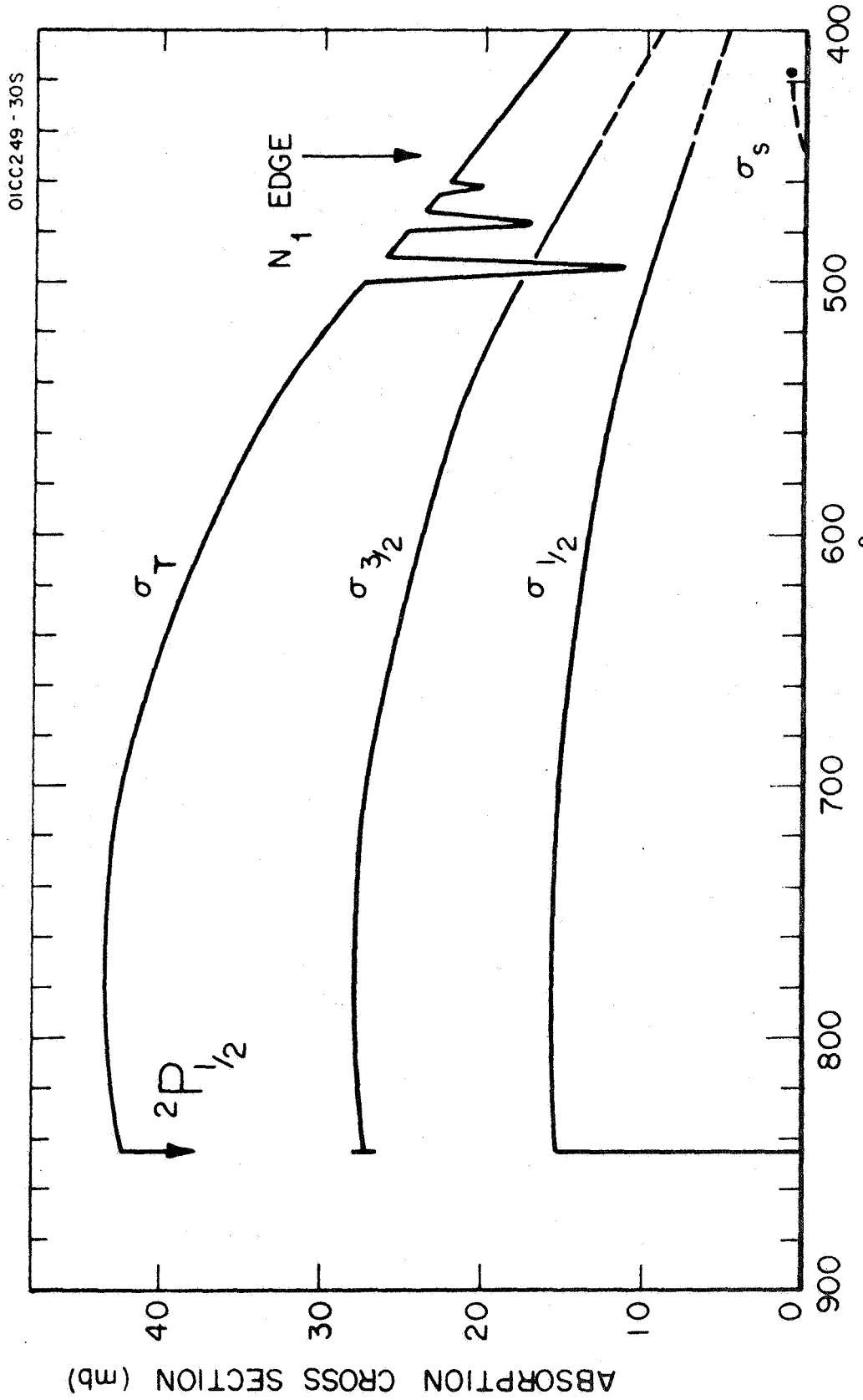

Figure 23. Specific photoionization cross sections for krypton for λλ 400-900Å.

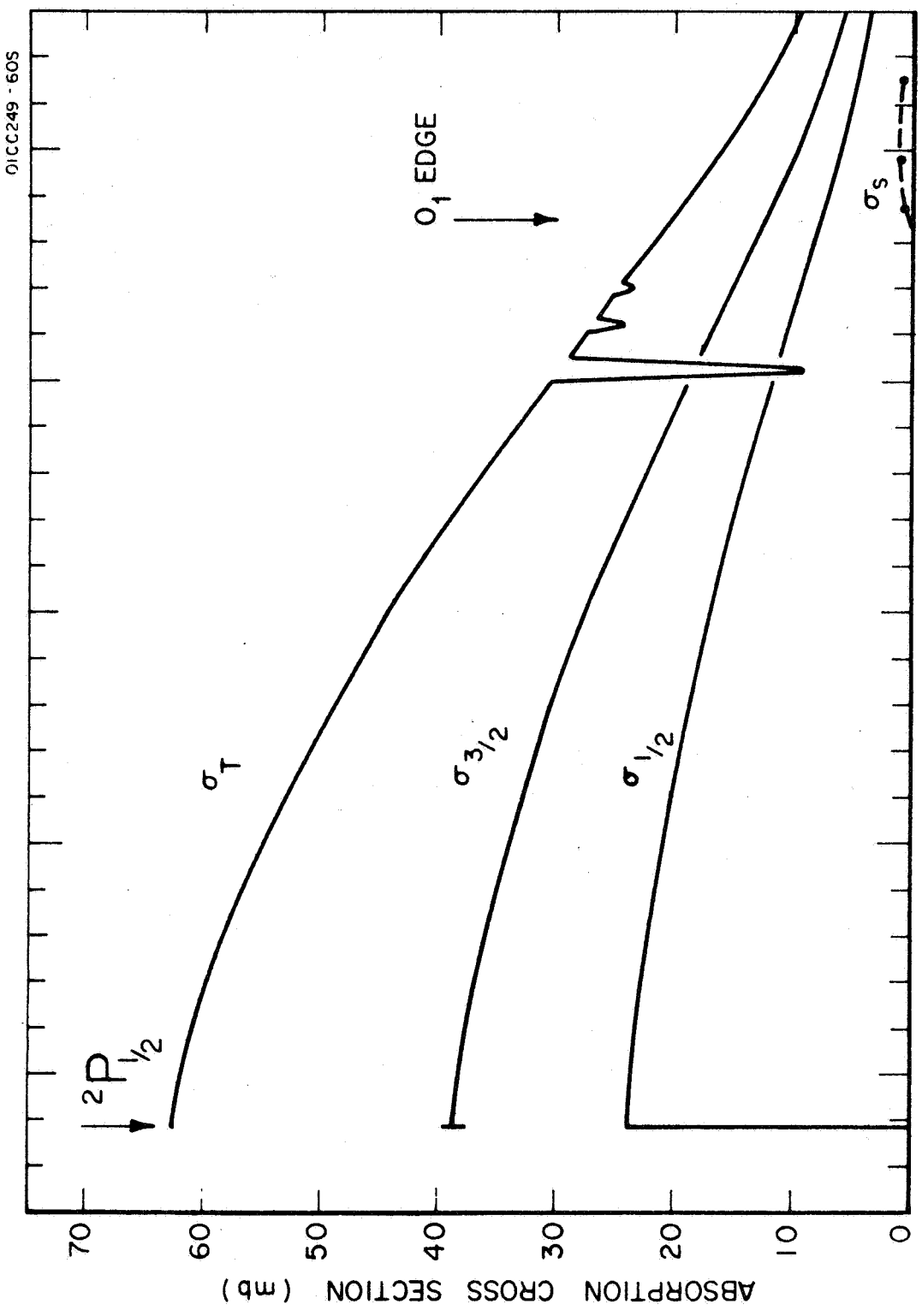

Figure 24. Specific photoionization cross sections for xenon for λλ 425-975Å.

between the s- and p-electrons, corrections for energy discrimination were applied. This yielded the number of produced s-electrons as approximately 4 percent of the total number. The accuracy of this result is probably correct only to within a factor of two owing to the weakness of the signal. On comparison of these data with theoretical results, a number of new experimental and theoretical requirements were identified. Experimentally, it appears appropriate to direct future efforts toward utilizing the present capability to acquire the necessary and corresponding data for several selected planetary atmospheric molecular species, i.e., CO, CO_2, N_2, O_2, etc.

4. The design, development and fabrication of laboratory devices for EUV and VUV investigations. – In order to sustain the required EUV and VUV laboratory capability, it is necessary to design, develop, and fabricate new experimental devices as dictated by specific requirements. In this regard, a number of new applicable investigations were performed in the four following areas: (1) the EUV and VUV optical properties of laser deposited films, (2) photoelectric yield and transmittance of thin films, (3) the use of metal cathodes as absolute secondary standards in the VUV, and (4) the design, development and fabrication of an EUV grazing incidence monochromator. The results of these efforts are summarized briefly below.

a. Reflectance and transmittance of laser-deposited thin films in the vacuum ultraviolet. – During the course of the program, laboratory measurements were performed of the reflectance and transmittance of thin iridium and tungsten films for λλ 237-1600Å. Film thicknesses of the order of 400Å were produced by vacuum evaporation by focusing a single ruby laser beam pulse onto solid rods of iridium and tungsten. Only a brief description of the work is included herein since the material has been published elsewhere (C-9).

Conventional evaporators are limited to the preparation of thin films composed of materials with melting points less than about 1800°C. At higher temperatures, the filaments produce some vapor which results in film contamination. Materials with higher melting points can be evaporated by induction heating techniques [44,45]. The times required to deposit a film of suitable thickness by these processes are of the order of several seconds to minutes. In this regard, evidence indicates that the more rapid the evaporation, the smoother the surface. Furthermore, the highest quality films are produced under high vacuum conditions.

On the basis of these earlier results, it appears that an ideal evaporation source would be a laser device where films of suitable thickness can be produced by a single pulse in a few microseconds. This laser technique has been applied to the evaporation of compounds and elements with melting points less than 1240°C by Smith and Turner [46]. In the following discussion the results obtained in evaporating iridium (M.P. 2454°C) and tungsten (M.P. 3370°C) are described. Additionally, the reflectances of films composed of the above two elements were measured over

the spectral region λλ 350-1600Å, while the transmittance of the iridium film was measured from λλ 237-1600Å. Since the experimental details have been described previously in detail (C-9), these are not repeated herein. Rather, the results are presented along with a brief interpretative discussion.

The reflectance measurements of iridium and tungsten are shown in Figure 25. Unpublished data by Hass, et al. [47], on the reflectance of iridium films produced by electron beam heating techniques are also presented for wavelengths below 600Å. Their longer wavelength results are not shown in Figure 25 owing to the close agreement with the measurements obtained in the present investigation. However, it can be seen that at the shorter wavelengths, their reflectances decrease more rapidly than those obtained for the laser evaporated films.

The relative transmittance measurements for iridium are presented in Figure 26. The variation in the transmittance of iridium as a function of wavelength was obtained, without producing a self-supporting film, by direct evaporation of the material onto one-half of a plastic scintillator (NE 102). The fluorescent radiation produced by the incident vacuum UV radiation was detected by a photomultiplier. Thus, the relative transmittance of the film was obtained [48] by measuring the ratio of the photomultiplier signals for incident radiation on the uncoated portion of the scintillators that form the coated portion. This ratio would represent the true reflectance provided that back-reflected fluorescent radiation from the scintillator-metal interface was not present. However, in all probability, fluorescent reflectance does occur so that the true reflectance of the thin metal film is somewhat lower than the measured relative transmittance. The true transmittance is estimated to be about two-thirds of the relative value shown in Figure 26 for approximately 500Å thick films.

The frequency ν_p at which a metal changes from a reflection to a transmission medium is given by $\nu_p = (ne^2/\pi m)^{1/2}$, where m and e represent the electronic mass and charge, respectively, and n is the number of electrons/cm^3 interacting with the incident radiation. Generally, n is assumed to be the density of the valence electrons. If the electrons in the outermost 6s shell are the only ones operative, the above equation yields a transmission onset of 890Å, while if additionally the seven 5d electrons participate, the predicted onset wavelength is 420Å. These theoretically determined onset wavelengths are indicated in Figure 26 by the vertical arrows. Alternatively, the experimental data indicate that the transmission onset occurs at about 650Å. Critical absorption edges in iridium are expected to occur at 263Å (O III edge), 221Å (N VII edge), and 207Å (O II edge) [50]. The sudden decrease in the transmittance at 260Å in Figure 26 can be correlated with the O III absorption edge.

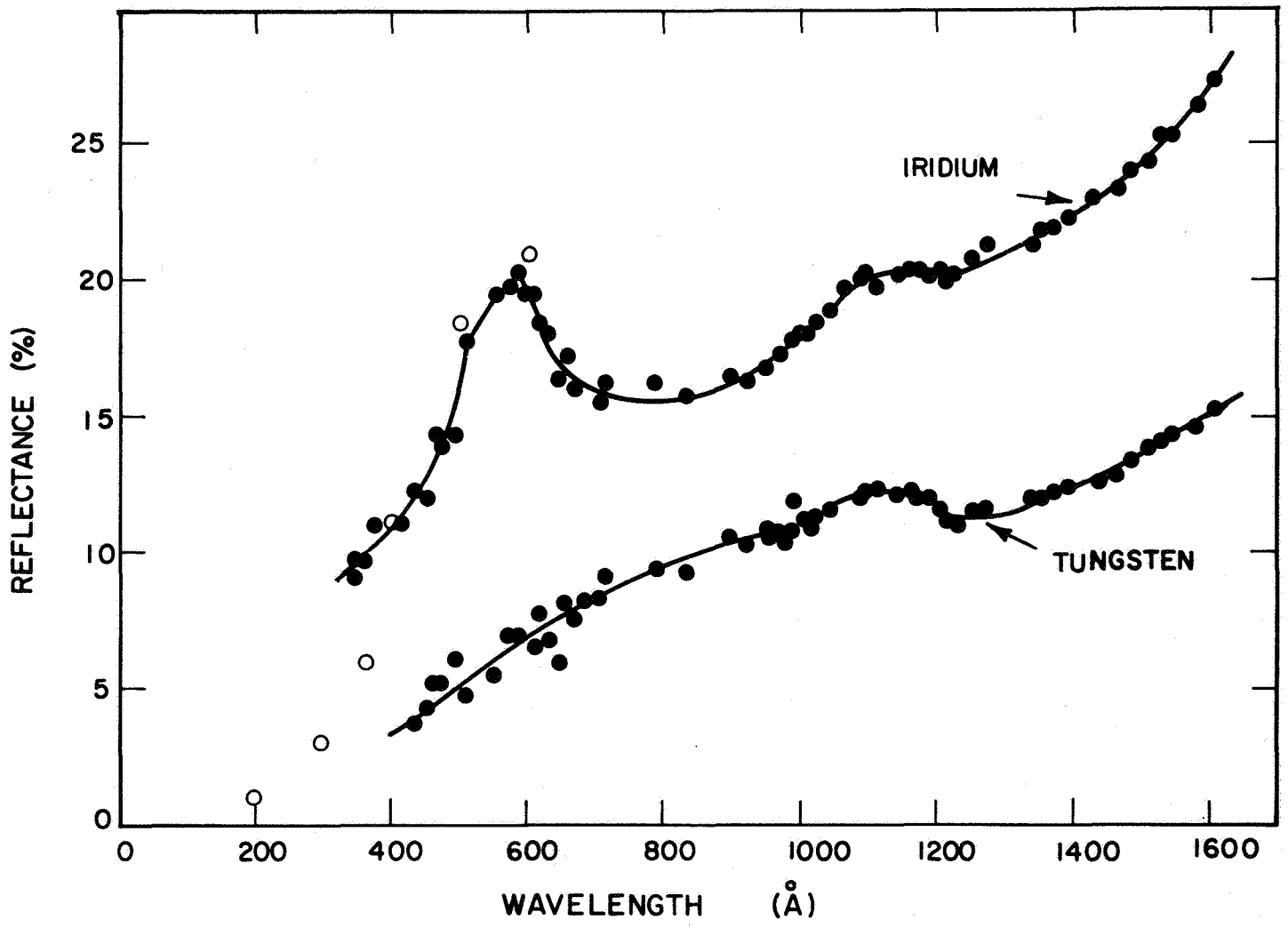

Figure 25. Reflectance of iridium and tungsten between 350 and 1600Å. The open circles represent reflectance data of iridium obtained by Hass et al. [47].

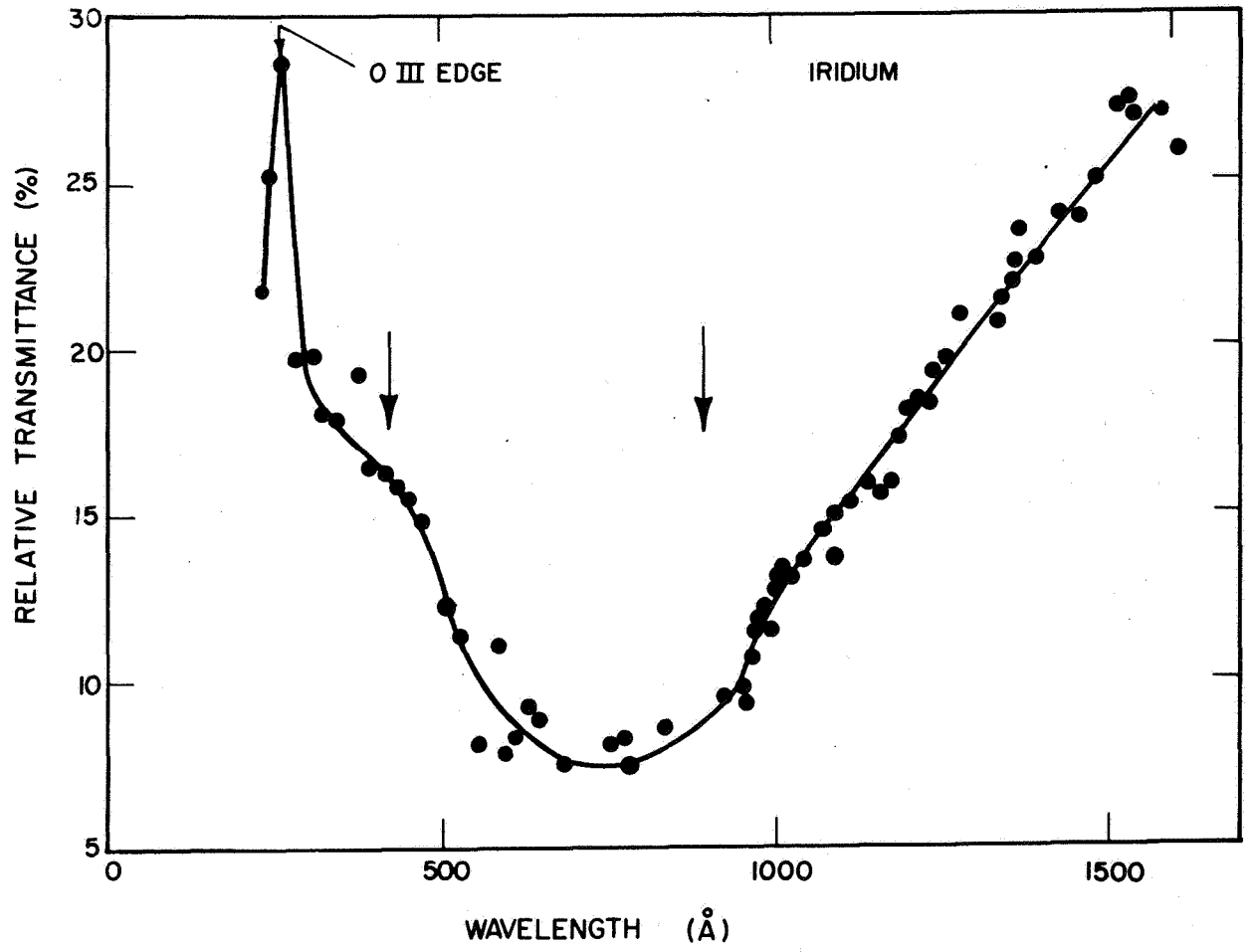

Figure 26. Transmittance of iridium between 237 and 1600Å. The vertical arrows at 890 and 420Å represent the plasma frequencies assuming the number of active electrons to be two or nine, respectively.

The employment of a laser in the production of thin films for optical studies in the vacuum UV has several advantages over film generation by conventional evaporation techniques including the higher deposition speed, the simplicity of evaporating films in an ultra-high vacuum system, the lack of contamination from hot filaments or crucibles, and the ability to evaporate materials with high melting points.

b. The relative photoelectric yield and transmittance of aluminum films. – Under the current program, measurements have been performed of the transmittances and the photoelectric emissions from both the front and back faces of two unsupported thin aluminum films, 1380 and 470Å thick. The ultimate objective of the work is two-fold. First, the magnitude of the photoelectric emission from the back face is a parameter of interest in the design of certain photon detectors, e.g., ionization chambers, which might utilize thin metal films as selective filters. Second, the combined transmittance-photoemission data might contribute to an increased understanding of the processes of photon absorption and electron excitation and ejection from metals.

In Figure 27 are shown the transmittances of the two films in the spectral region 720-400Å. The transmittances do not increase monotonically toward shorter wavelengths, but have structure similar to that reported by Hunter [51] and by Rustgi [52]. The transmittance data could not be accounted for quantitatively if the two films were assumed to be of pure aluminum since, at any given wavelength, different values of the absorption coefficient $\mu_{A\ell}$ were obtained. It is known that evaporated aluminum films exposed to air at atmospheric pressure rapidly form $A\ell_2O_3$ surface layers which have a terminal thickness [53]. Either interference effects due to reflections at the air-$A\ell_2O_3$ and $A\ell_2O_3$-$A\ell$ boundaries or suitably varying absorption coefficients $\mu_{A\ell}$ and $\mu_{A\ell_2O_3}$ could then give rise to the periodic structure in the transmission curves and could account for the dependence of this structure on the film thickness. While the photoelectric emission measurements described in the following paragraph, support the contention of Hunter [52] that the structure is due to interference effects, it is worth noting that if boundary reflections are small and can be ignored, the coefficient $\mu_{A\ell}$ can be calculated from the data given in Figure 27 since

$$\mu_{A\ell} = \frac{1}{(1380 - 470)10^{-8}} \ell n \frac{I_o}{I_{1380}} - \ell n \frac{I_o}{I_{470}} \quad cm^{-1} \qquad (2)$$

where I_o is the intensity of radiation incident upon the films and I_{1380} and I_{470} are the intensities of radiation transmitted through the 1380Å and 470Å thick films, respectively. To obtain this expression, all the oxide surface layers were assumed to have the same thickness. Values of $\mu_{A\ell}$ calculated at all the measured wavelengths were within the range 9 to 2 x 10^4 cm^{-1}. These values are to be compared with published values of about 7 x 10^4 cm^{-1} at 720Å which decreases to about 4 x 10^4 cm^{-1} at 400Å [54].

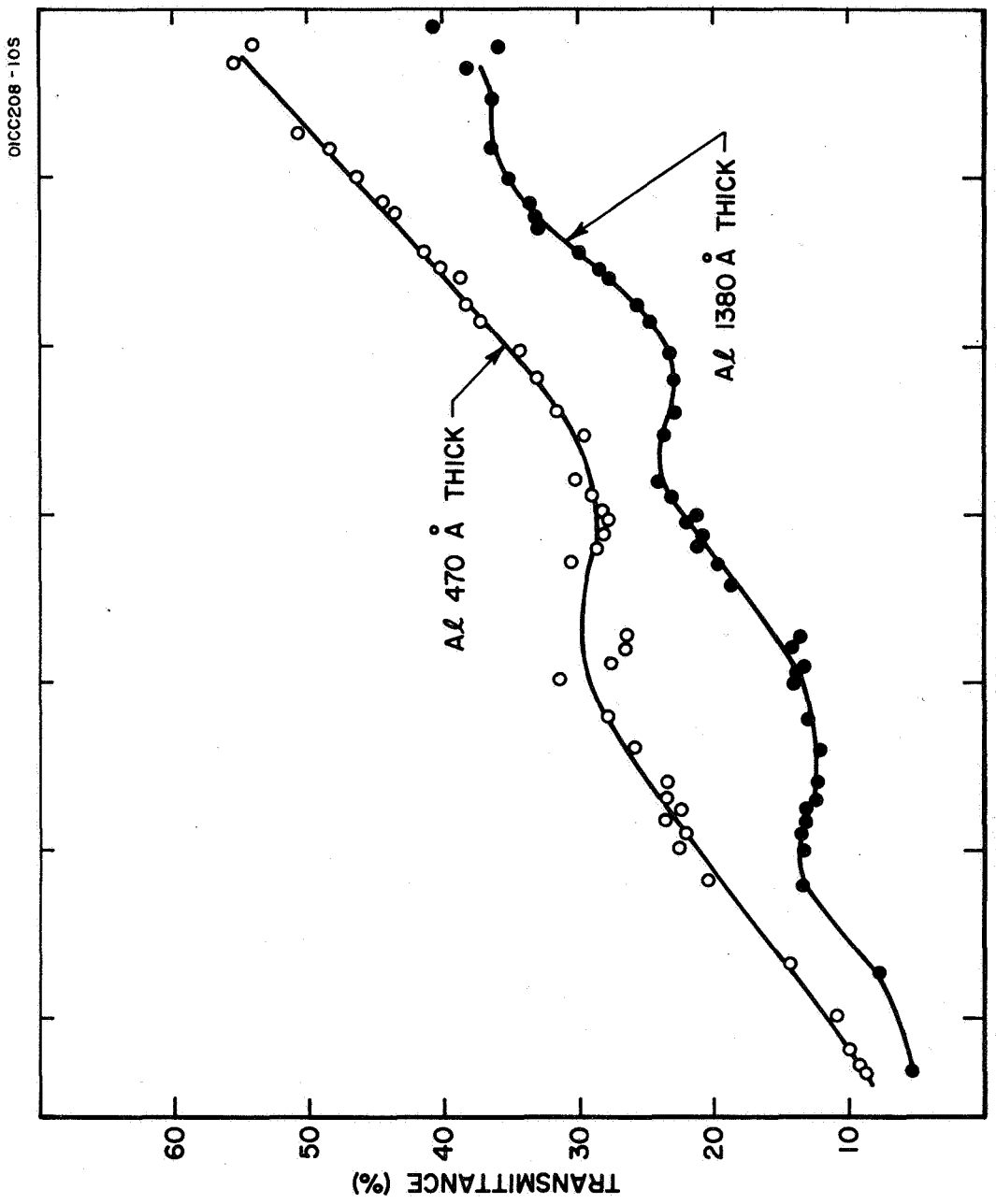

Figure 27. The transmittance of thin unsupported Aℓ films.

Relative values of the photoelectric yields are shown in Figures 28 and 29 as a function of wavelength from both the front and back faces of the thin aluminum films. As expected, the yield from the front face attained maximum values and from the back face minimum values at wavelengths where the transmittance was minimal. If the observed variations in transmittance and, hence, in yield were due to changes in the effective absorption coefficient of the $A\ell$-$A\ell_2O_3$ film, the photoelectric yield of a thick opaque $A\ell_2O_3$ surface $A\ell$ photocathode should also vary periodically with wavelength. However, if the periodic variation in yield of the thin films is due to interference effects, no similar variations would be expected for a thick opaque photocathode. An absence of such fine structure has been reported for $A\ell$ photocathodes [55] which supports the fact that interference effects account for the detailed shape of both the yield and transmission curves of the thin films.

c. Metal photocathodes as secondary standards for absolute intensity measurements in the vacuum ultraviolet. – Frequently, experiments performed in the vacuum ultraviolet spectral region require measurements of absolute intensity. Various techniques have been devised which employ thermocouples, ionization chambers, etc. to perform this function. These techniques, although accurate, cannot be incorporated conveniently into certain experimental designs. Thus, there the requirement exists for the development of a secondary standard with the following characteristics: operationally simple, size compactness, relatively compatible to introduction into laboratory apparatus without radical modifications.

Metal photocathodes which have been employed on occasion as vacuum ultraviolet radiation detectors, are relatively attractive since they are comparatively insensitive to stray visible light. However, there have been reports of large variations in the photo-yields of metals which have been either exposed to different gases or to heat. Thus, since a metal photocathode can be employed to detect radiant energy, the feasibility of its use in the measurement of absolute intensities has been examined in the laboratory investigation described briefly below and in greater detail elsewhere (C-11). The photoelectric yields of a large number of selected photocathode materials (T, Ni, $A\ell$, Zn, Cu, Be, Fe, Ti, Ta, In, Pt, Sn, Mo, Ag, Av and Pb) have been measured under a variety of conditions (heat treatment, surface contamination, polishing, etc.) over a broad spectral range (1216-200Å). For this purpose, a suitable photoelectric ion chamber was devised (C-11) and attached to the exit slit of the 1/2-meter Seya monochromator. Both a high voltage repetitive spark discharge and a hydrogen dc-glow discharge were employed as light sources. In order to determine the photoelectric yield for a given metal, both the number of electrons emitted from the illuminated (monochromatic) surface was measured as well as the absolute incident flux. Plots of photoelectric yield as a function of λ were obtained for the sixteen metals. Where possible, the results were compared with previously published data to evaluate the extent of reproducibility of the yields. Additionally, the data were interpreted in terms of their utility for the calibration of photocathods as secondary radiation standards in the VUV and EUV.

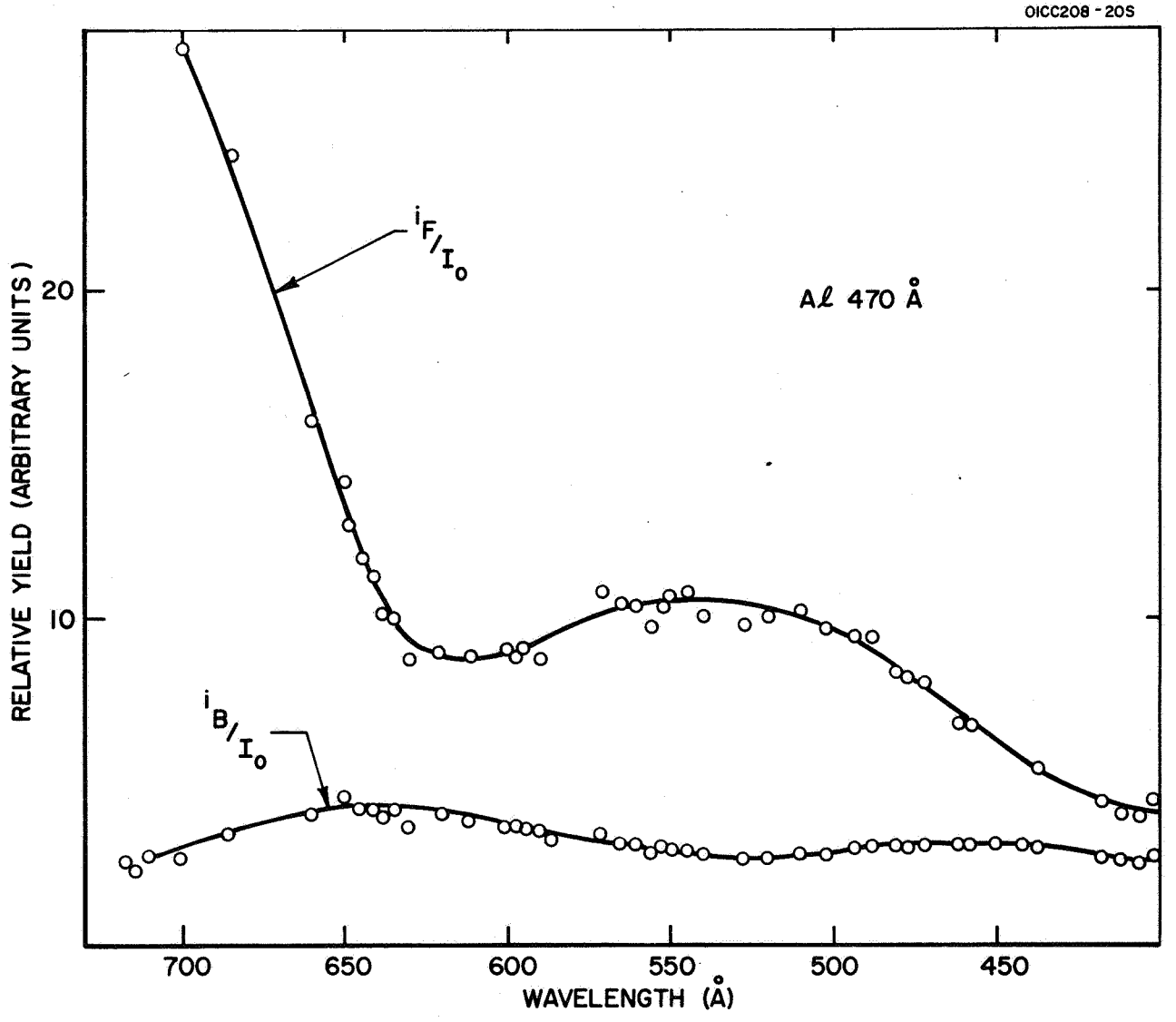

Figure 28. The relative photoelectric yield from the front face (i_F/I_o) and from the back face (i_B/I_o) of a 470Å thick Aℓ film.

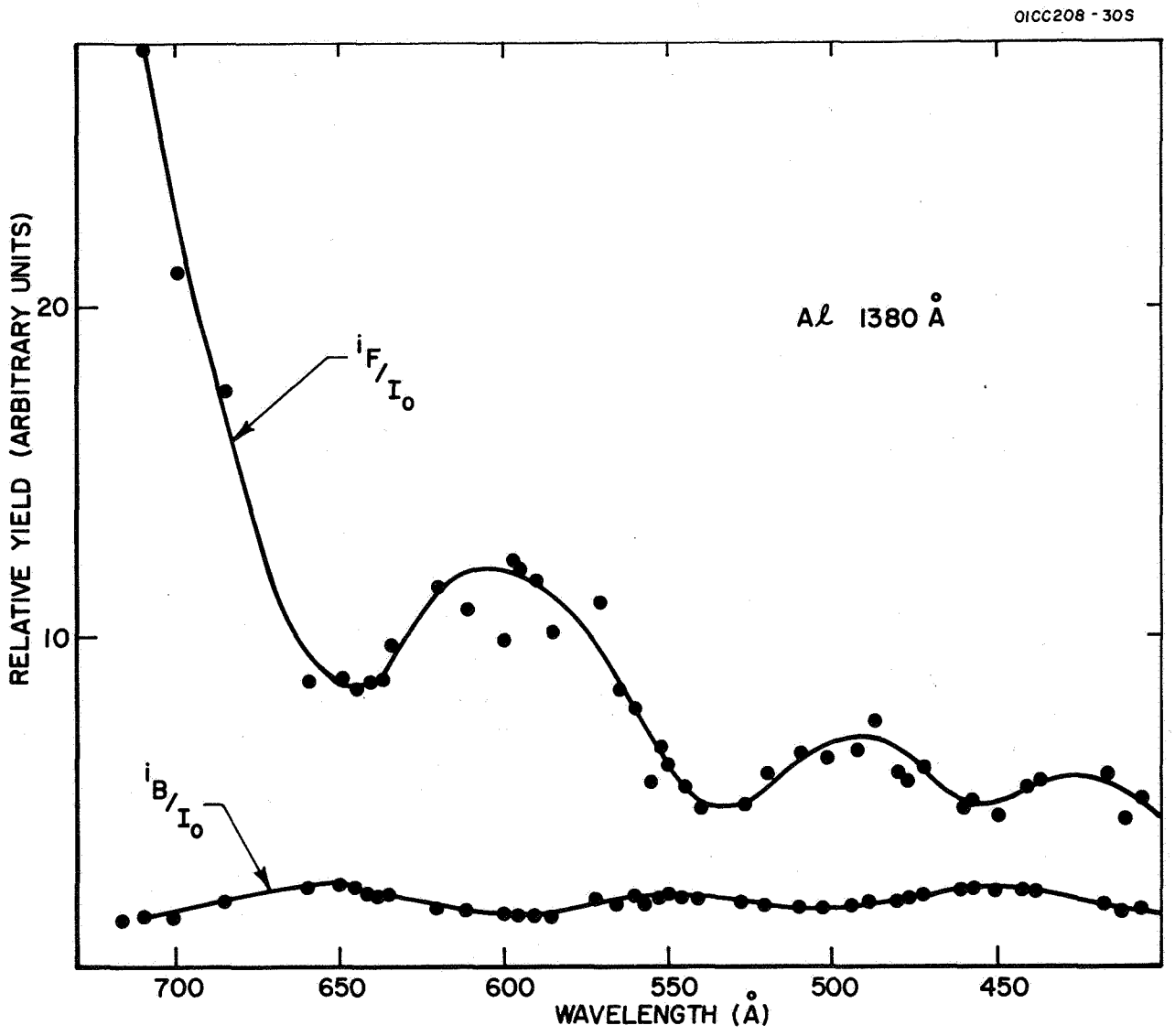

Figure 29. The relative photoelectric yield from the front face (i_F/I_o) and from the back face (i_B/I_o) of a 1380Å thick Aℓ film.

d. Grazing incidence monochromator. — With grazing incidence monochromators it is necessary to maintain the entrance slit, exit slit, and the grating on the Rowland circle at all times. Any slight deviation from the Rowland circle results in intolerable defocusing of the image with a subsequent loss of radiant energy. Thus, all designs are predicated basically on resultant monochromatic radiation while maintaining the optical elements on the Rowland circle. Since, in most applications, monochromatic radiation is required to enter relatively massive experimental chambers it is desirable to fix the exit slit in space and move one or more of the remaining elements. A suitable design for laboratory construction was developed wherein both the grating and entrance slit are caused to move along on the Rowland circle. The operational principles are described below.

With the fixed exit slit, both the grating and entrance slit maintain their relative positions on the Rowland circle as shown in Figure 30. The entrance slit (S_1) is fixed rigidly to the grating (G) thereby fixing the distance, GS_1. When the spectrum is scanned, S_1 and G are constrained to move along the straight line paths, S_1S_2 and GS_2, respectively. From the above geometry, since the angle $S_1S_2G = \alpha$ remains constant and the distance S_1G is fixed, it follows that the points S_1, G, and S_2 will always lie on the Rowland circle of diameter R given by $GS_1 = R \cos \alpha$, so that the instrument maintains perfect focus throughout the spectral scan.

To translate this principle into a working unit, the problem of building a vacuum housing around moving parts (entrance slit and grating) had to be solved. As described in Quarterly Progress Report No. 9, telescoping extension tubes were designed for use between the grating and the exit slit. However, experience indicated that this approach involved difficulties in providing smooth motion and a vacuum-tight seal. As a consequence, the design was altered to accommodate special flexible bellows capable of extending over an abnormal range. It was found that Bell-Metrics Corporation, San Fernando, California produced flexible bellows with a maximum change in length of 17 inches. This represented the design criterion required to accommodate a spectral span of 0 to 650Å. An angle of incidence of 84 degrees was selected with a 2.217 M gold coated replica grating ruled with 600 lines/mm. The spectral span is from -11 to 640Å, i.e., it includes the central image. A 22-inch long precision lead screw driven by a variable speed motor was employed in the wavelength scan mechanism. A linear scale was used to measure the distance moved by the grating relative to the fixed exit slit. This motion is related to wavelength by the following formula:

$$\lambda = d[\sin \alpha - (1 - L^2/R^2)^{1/2}]$$

$$= [1.6575 - 1.6667 \ (1 - L^2/R^2)^{1/2}] \times 10^4 \text{ Å} \quad (3)$$

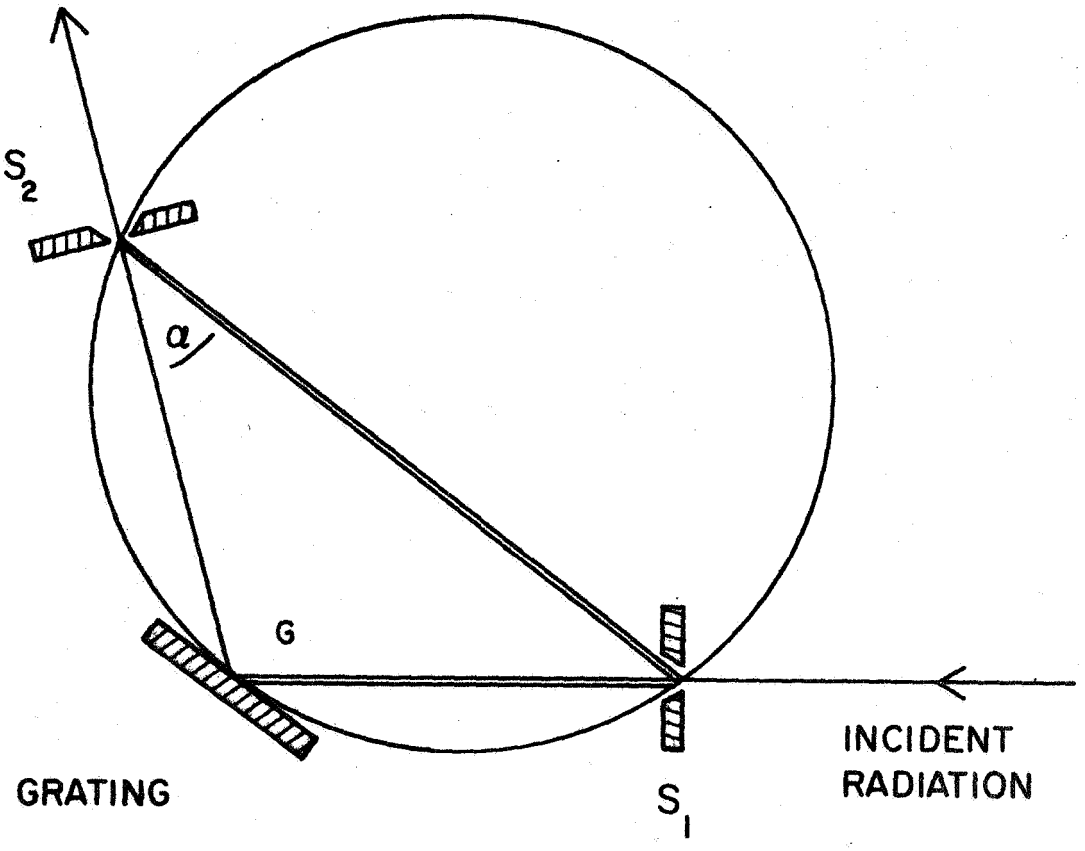

Figure 30. Grazing incidence monochromator.

where d is the grating constant (600 lines/mm), α is the angle of incidence (84 degrees), R is the radius of the grating (221.7 cm), and L is the distance from the grating center to the exit slit (= 23.17 + x cms, where x is the distance traveled from the central image to a wavelength λ). A clutch is employed to disengage the motor to allow manual wavelength selections and adjustments.

Photographs showing the overall instrument are presented in Figures 31 and 32. The long bellows seen in the photograph extends from the grating housing to the fixed exit slit. The manual scanning lever is shown at the extreme right of the photograph.

In order to satisfy the design specifications, it was necessary to construct a straight-through vacuum valve which also acted as the main pump manifold and as the housing for the exit slit (see Figure 32). This provided a very rigid exit slit for mounting the experimental equipment. A close-up view of the grating housing, the short entrance bellows, and the long exit bellows are shown in Figure 31. The precision lead screw is represented by GS_2 in Figure 30, while the stainless steel guide tracks shown in the photographs represent S_1S_2.

Although detailed accounts of the individual component functions or operations are not presented herein, it should be noted that the various mechanical specifications have been fulfilled so that the corresponding required capability has been achieved. A remaining task involves the completion of a detailed evaluation of the optical performance of the monochromator with a view toward achieving the laboratory measurements associated with pertinent current EUV associated aeronomy problems.

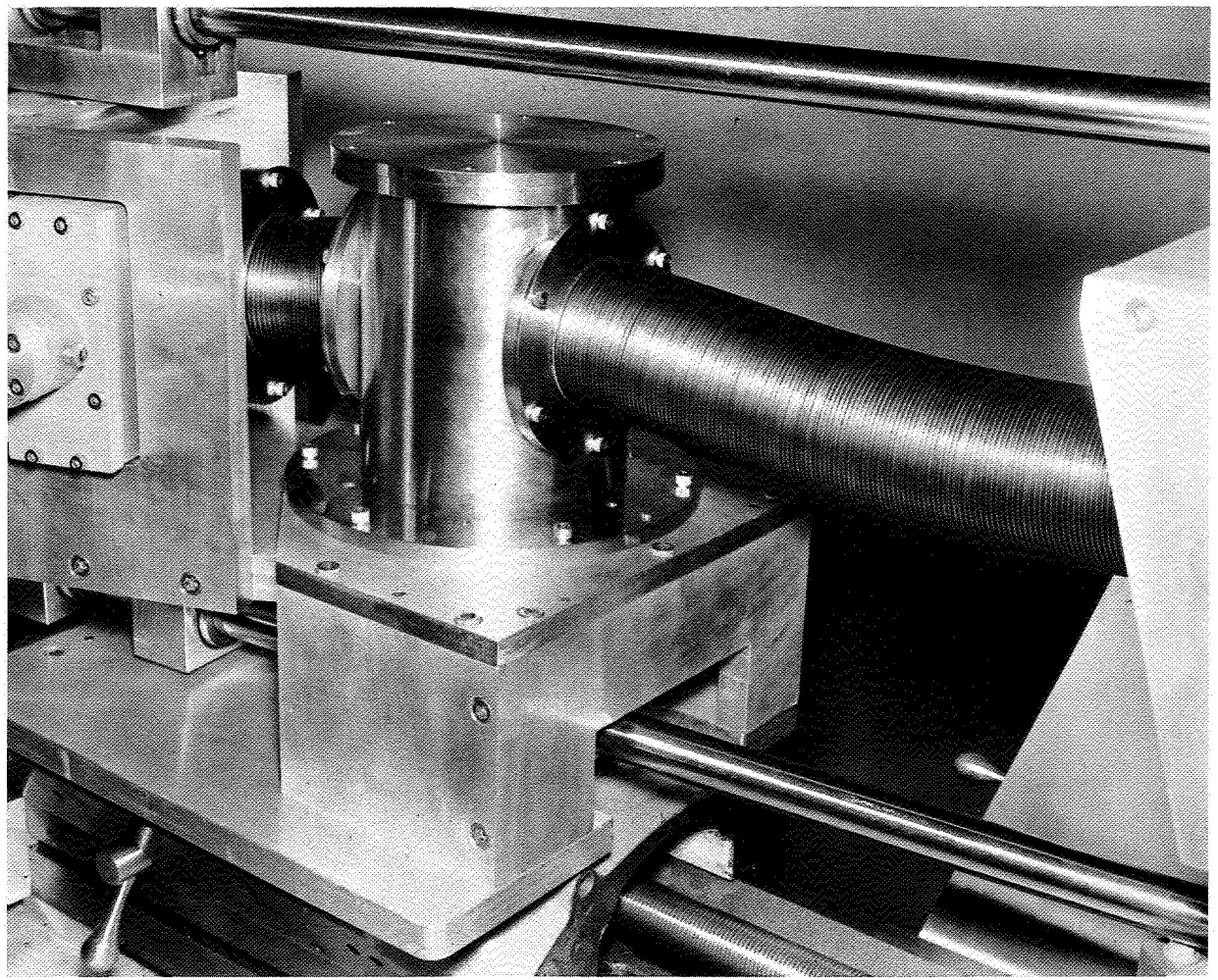

Figure 31. Photograph of assembled grazing incidence EUV monochromator. The long bellows shown extends from the grating housing to the fixed exit slit (see text).

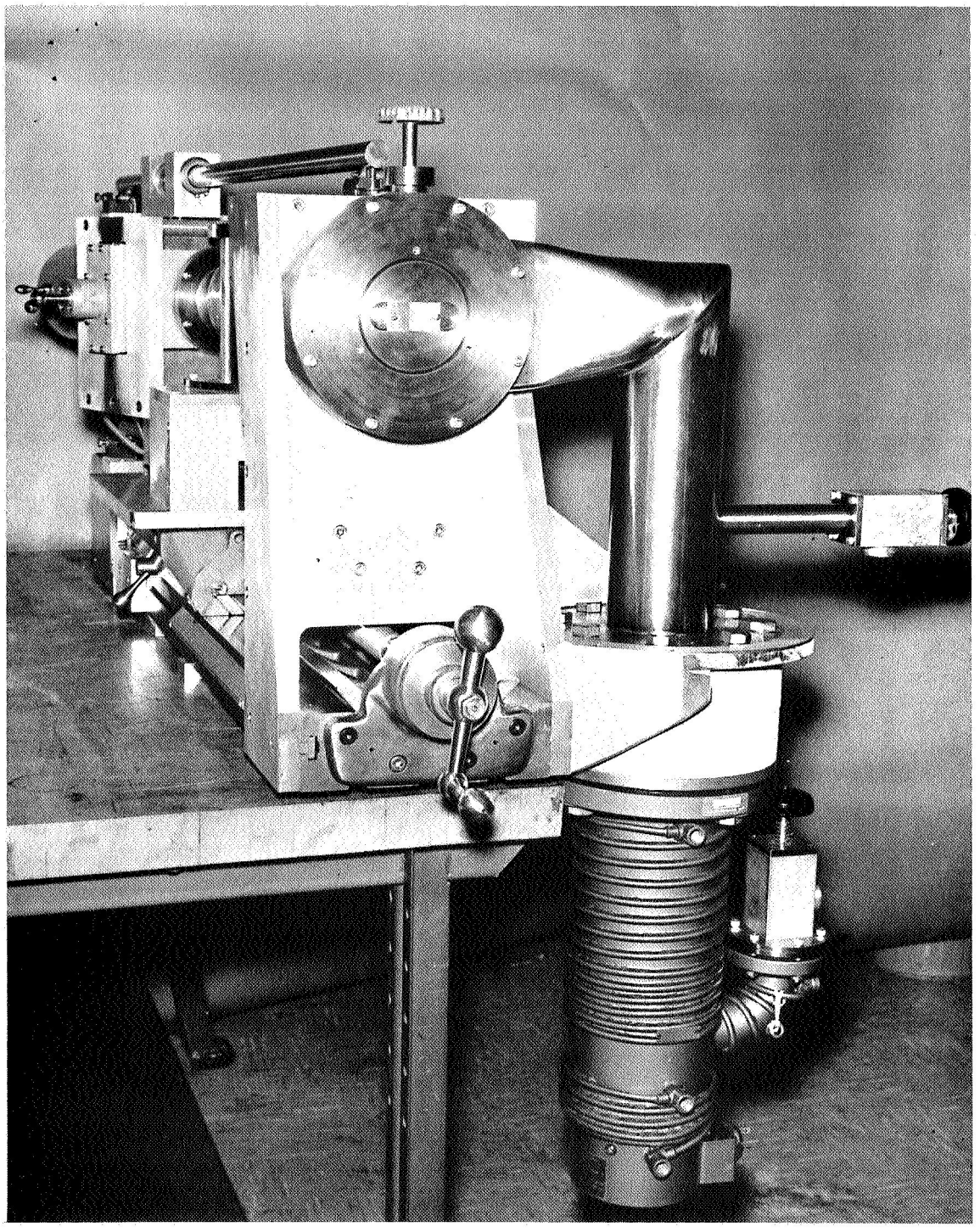

Figure 32. End-on photographic view of the entrance slit-pumping facility housing of the EUV monochromator.

D. Theoretical and Experimental Planetary Aeronomy

The work performed under this phase of the program has been reported in the following publications:

Theoretical Aeronomy

D-1. "On the Observation of Noctilucent Clouds in Planetary Atmospheres," by F. F. Marmo, A. Engelman, and H. Miranda, Quarterly Progress Report No. 7, December 1966, pp 70-109.

D-2. "Feasibility of Observing Noctilucent Clouds in Planetary Atmospheres: Photographic Observation of Noctilucent Clouds in the Earth Atmosphere from a Synchronous Satellite," by F. F. Marmo, A. Engelman and H. Miranda, Quarterly Progress Report No. 8, March 1967, pp 33-48.

D-3. "Theoretical Model of the Atmosphere of Mars and Venus," by F. F. Marmo and B. Schultz, Quarterly Progress Report No. 8, March 1967, pp 48-49 and Quarterly Progress Report No. 9, June 1967, pp 48-65.

D-4. "The VUV (1200-2000Å) Albedo of the Solar Illuminated Atmospheres of Mars and Venus," by F. F. Marmo, T. Degges, and A. Engelman, Quarterly Progress Report No. 10, September 1967, pp 70-81.

D-5. "The VUV Fluorescence Due to Solar Illuminated CO in the Atmospheres of Mars and Venus," by F. F. Marmo and T. Degges, Quarterly Progress Report No. 11, December 1967, pp 33-58.

Experimental Aeronomy

D-6. "Electron Impact Studies on Selected Planetary Gases," by F. F. Marmo and T. Wentink, Quarterly Progress Report No. 7, December 1966, pp 109-112.

D-7. "Measurement of the Relative Photon Scattering Cross Section of Selected Planetary Gases in the UV and VUV Spectral Regions," by Shardanand, F. F. Marmo and Y. Mikawa, Quarterly Progress Report No. 8, March 1967, pp 50-59 and Quarterly Progress Report No. 9, June 1967, pp 39-48.

D-8. "Measurement of the Efficiency of Visible, UV, and VUV Fluorescence Due to the Interaction of Electron Impact with Selected Planetary Gases," by A. Sharma and F. F. Marmo, Quarterly Progress Report No. 8, March 1967, pp 59-62 and Quarterly Progress Report No. 12, March 1968, pp 80-85.

D-9. "Laboratory Investigation on the Measurement of Depolarization Factors for Planetary Atmospheric Gases," by F. F. Marmo, Quarterly Progress Report No. 11, March 1968, pp 58-72.

D-10. "Photon Scattering Cross Sections at Lyman-α (1215.7Å) for Ar and Ne," by Shardanand and Y. Mikawa, J. Quant. Spectrosc. Radiative Transfer 7, 605-609 (1967).

D-11. "Experimental Evidence for Xe_2 Molecules," by Shardanand, Phys. Rev. 160(1), 67-71 (1967) and Quarterly Progress Report No. 10, September 1967, pp 55-70.

D-12. "The Scattering Cross Sections of Argon and Krypton in the VUV," by R. B. Cairns, F. F. Marmo, and J.A.R. Samson (submitted to JOSA, April 1968) and Quarterly Progress Report No. 12, March 1968, pp 74-79.

D-13. "Laboratory Investigation on the Selective Scattering by CO in the VUV," by F. F. Marmo, R. B. Cairns, Quarterly Progress Report No. 12, March 1968, pp 62-74.

The major subject matter contained in these publications can be briefly summarized in the following five categories: (1) satellite UV observations of noctilucent clouds, (2) theoretical model atmospheres of Mars and Venus, (3) the VUV day airglow in planetary atmospheres, (4) VUV fluorescence due to electron impact excitation of air, and (5) laboratory measurements of VUV photon scattering cross sections for selected planetary atmospheric gases.

1. Satellite UV observations of noctilucent clouds. — In a recent paper, Marmo, et al [56] have demonstrated the feasibility of performing global observations of solar illuminated noctilucent clouds using a satellite-borne photometer operating in the VUV spectral region (i.e. around 1800 Å). Additionally, it was demonstrated that photographic (or other imaging techniques) could also be employed throughout the VUV and UV regions wherein the optimum operating wavelength was defined by the observing geometry. Following this investigation, an opportunity became available to participate in the Gemini XII program. Specifically, Dr. Karl G. Henize of Northwestern University was the principal investigator in a program involving stellar photography in the spectral region 2250-2450Å during nightside orbits only. On this basis, the UV camera equipment was available for dayside orbit observations under a number of specific operational constraints. Thus, a feasibility study was initiated in order to define both the role of the astronaut and the system operational parameters. On the basis of the study results, an operational plan was defined and employed in the Gemini XII program. In addition, the feasibility study was extended to include the possibility of utilizing a synchronous satellite platform for observing noctilucent clouds on a global basis (D-2).

The experimental constraints which were imposed in the Gemini XII program can be summarized as follows:

(1) The fixed Gemini XII orbital geometry could not be modified.
(2) The available UV imaging instrumentation must be employed with no modification.

(3) Neither additional astronaut training nor significant astronaut effort would be available.

The feasibility study summarized herein was performed with the above constraints in mind.

Constraint (1) [along with the UV screening altitude of 60 km established by atmospheric ozone] dictated that the highest northern latitude during the autumn (November) which is sunlit at 80 km (the resident altitude of noctilucent clouds) is about 76 degrees, while at the South Pole this altitude is solar-illuminated. For the specific Gemini XII orbit, which was constrained in latitude between 28.9°N to 28.9°S, the highest observable latitude for which an 80-km altitude tangency could be achieved was 43.6 degrees.

Constraint (2) established the available optical characteristics as follows: (a) the UV camera was equipped with an f 3.3 LiF quartz lens of 73 mm focal length capable of transmitting down to $\lambda \approx 2000$ Å, (b) the film format dimensions were 70 mm x 48 mm, (c) only Kodak IO film was available in a magazine which accommodated five exposures, and (d) a UV interference filter was employed (in front of the viewing lens) which transmitted $\lambda\lambda \approx 2250\text{-}2450$ Å with about 3-percent transmission. The required parametric calibration values were made available by Dr. K. Henize on the basis of laboratory results and previous Gemini stellar photographic experiments.

The detailed analyses which are described elsewhere (D-1) produced the results shown in Figure 33 where the solid curve refers to the expected signal intensity from a solar-illuminated, fully-developed (i.e. assumed 50 particles cm^{-3} with a 2-km thickness located at 80 km) noctilucent cloud as a function of viewing angle and film formate, while the dotted curve represents the background intensity. The results indicate that it would be possible to detect a signal intensity of only about 1.3×10^{10} photons cm^{-2} sec^{-1} (10 percent of the background intensity) at the 80-km level. Since the expected signal amounts to 2.4×10^{12} photons cm^{-2} sec^{-1}, it was concluded that the photographic system would be capable of imaging significantly under-developed noctilucent clouds to the extent wherein the minimum required local number particle density can beless than 1 cm^{-3}. Another feature demonstrated by the results in the figure is that a fully-developed noctilucent cloud would appear as the brightest feature on the entire film format. It should also be noted that the above cloud can be detected photographically for viewing angles as low as -18° from center line-of-sight. The latter angle is below the real Earth horizon which, is incidentally indistinquishable due to absorption by atmospheric ozone. All the above factors indicate that fully-developed noctilucent clouds would be readily detectable on the full film format display. Additionally, further information on the physical characteristics, geographical extent, inhomogeneities, wave structure, etc. of noctilucent clouds can be derived against the near ideal, homogeneous, constant background level. Coupled with this capability is the requirement of utilizing relatively-short exposure times (less than 10 seconds) to minimize distortion due to movements of the astronaut and the satellite.

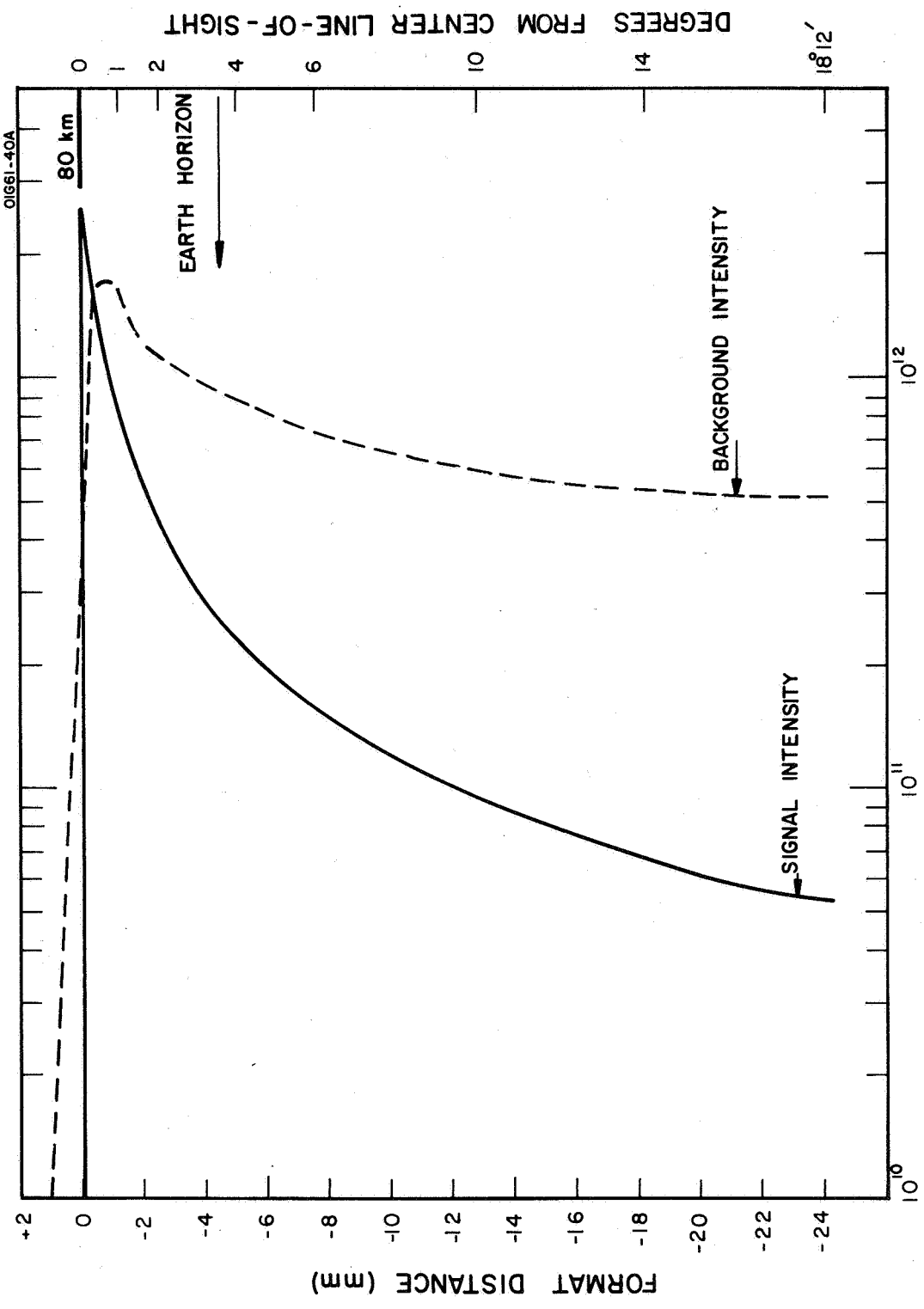

Figure 33. Calculated UV emission rates for background and signal intensities as a function of format distance and degree from center line-of-sight.

Detailed calculations (D-2) resulted in a recommended exposure-time range between about 0.1 second to 100 seconds. The final time range selection is predicated on the scientific goals of the experiment. For example, for low-altitude observations of fully-developed noctilucent clouds, the employment of relatively-short exposure times between a few seconds and about 0.1 second is indicated. On the other hand, to achieve optimum sensitivity as required at higher altitudes, longer exposure times would be required. Thus, if the major scientific objective is to photograph tenuous high-altitude dust such as reported by Fiocco, et al [57] are implied by the data of Mikorov [58], it would be experimental requirement to employ relatively long exposures since the local number densities are expected to be of the order of 1 cm^{-3} or less. Accordingly, even to establish meaningful upper-limit particulate-matter densities, the indicated exposures would be required in spite of the fact that a corresponding degradation of imaging capability would necessarily result.

It is appropriate to note here that a detailed comparison (D-1) of the UV capability with the achievable in the visible spectral region has demonstrated that in the visible region, the noctilucent cloud image on the film format would result in a relatively-narrow line (i.e., 2 mm in height) containing essentially no other information concerning the extent, dimensions, structure, or other characteristics of the clouds, whereas in the ultraviolet, where the cloud image covers the entire bottom portion of the film format, the above characteristic cloud data would be easily obtained. Furthermore, it should be noted that a significant degradation in experimental capability in the visible region can be expected due to relatively high instrumental scattered light. As such, it is concluded that photographic observation of noctilucent clouds is performed more efficiently in the spectral region under investigation, i.e., 2250 to 2450Å, albeit not optimum as discussed below. Finally, for this spectral region, it has been shown that radiation due to such other sources as fluorescence, scattering, airglow, etc., associated with solar-illuminated atomic and molecular atmospheric constituents does not constitute a serious interference problem since these emissions are generally weak and confined to relatively narrow wavelength intervals compared to the experimental spectral bandpass.

Prior to the Gemini XII flight, it was decided on the basis of the results of the preceding investigation that a more appropriate trade-off experiment would involve atmospheric dust observations at sunrise. In the overhead sun situation, although the entire film format would contain useful data as defined by the 10-percent contrast criterion, it was felt that higher contrast information could be obtained during sunrise conditions. The results of a representative sunrise calculation, shown in Figure 34 for a solar depression angle of 4°, can be compared to the overhead sun results in Figure 33. Although the total amount of information is cearly more limited during sunrise, the extensive contrast for the tangent ray altitude region between about 60 and 80 km is apparent. Since the Gemini XII orbit is confined to relatively-low latitudes as discussed previously, it was felt that an initial yes-no determination on the

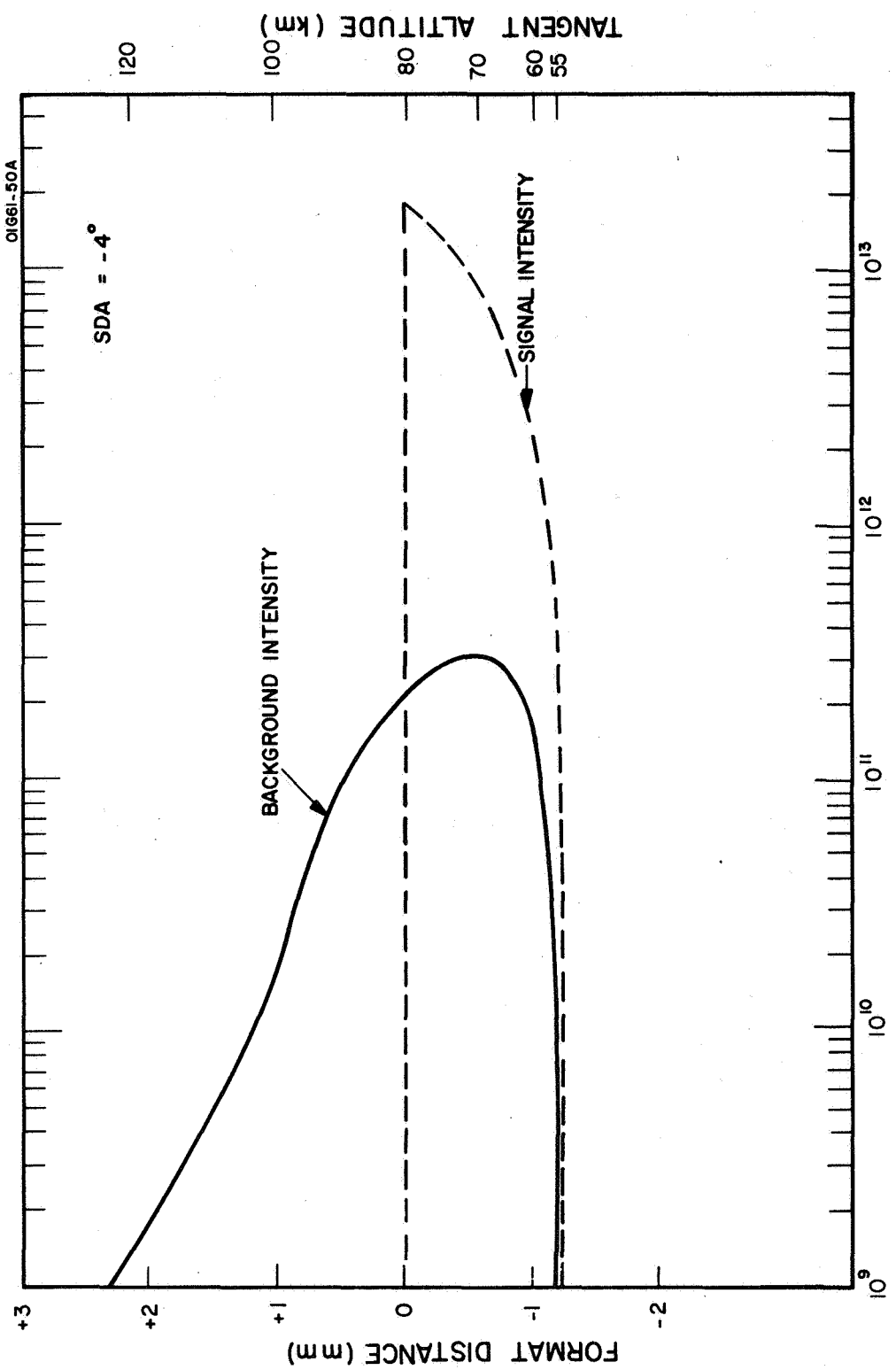

Figure 34. Calculated UV emission rates for background and signal intensities as a function of format distance and tangent altitude.

presence of dust in the Earth's atmosphere in the vicinity of 80 km would be more appropriate. The sunrise results also indicate strongly decreasing signal and background intensities below a tangent ray altitude of about 60 km due to the predominance of ozone absorption. Clearly, with the contrast indicated in Figure 34, the presence of noctilucent clouds at relatively-low latitudes could be detected at a relatively high sensitivity not available heretofore.

The Gemini XII sunrise experiment was performed in accordance with the analytical results discussed above. Unfortunately, the camera malfunctioned so that no useful photographic data were acquired. However, the feasibility of the experiment has been demonstrated on a technical basis as well as an on operational basis.

The results and techniques derived from the feasibility studies described above are applicable to the general problem of observing noctilucent (or other Mei scattering) clouds in planetary atmospheres. Thus, the feasibility of performing similar experiments using a satellite-borne sensor which is located remotely from the planetary atmosphere is examined herein. Specifically, the present investigation is concerned with the photographic observation of noctilucent clouds in the Earth's atmosphere from a synchronous satellite. As such, the derived results are applicable to any remote orbital configuration (i.e., from Earth orbit or during transit to Mars), with appropriate modification.

The present study is predicated on the realistic instrumentation capability employed in the Gemini XII program except that a spectral region centered around 2500Å is examined, whereby an interference filter is employed which transmits the λλ 2450-2650Å region. The physical-mathematical models employed in the Gemini XII study were modified appropriately and the detailed calculations were performed (D-2) to obtain the signal and background curves shown in Figures 35 and 36 which obtain for a back and side illuminated planet (Earth), respectively. For the side-illuminated Earth, noctilucent clouds are observable on a global basis (i.e. over the entire film format) from the center of the Earth to an altitude of 80 km above the Earth's horizon. This capability is reduced somewhat for the back-illuminated case since successful detection is only expected down to about -1500 km from the limb of the Earth. These conclusions are predicated on the criterion that an observable signal level must amount to about 10 percent of background emission level. Finally, a lower limit value for the number of particles in a cm^2-column can be established as follows. For a noctilucent cloud with 10^7 particles cm^2-column, the maximum signal obtains at 80 km and amounts to about 3×10^{12} photons cm^{-2} sec^{-1} in both illumination configurations, whereas the corresponding background emission amounts to about 3×10^{11} photons cm^{-2} sec^{-1}. Accordingly, application of the 10 percent criterion indicates that a signal level of only 3×10^{10} photons cm^{-2} sec^{-1} would be detectable and this emission rate corresponds to a cm^2-column count of only 10^5 particles. Thus, it can be concluded that for a 2-km thick noctilucent cloud of uniform number density, a detection

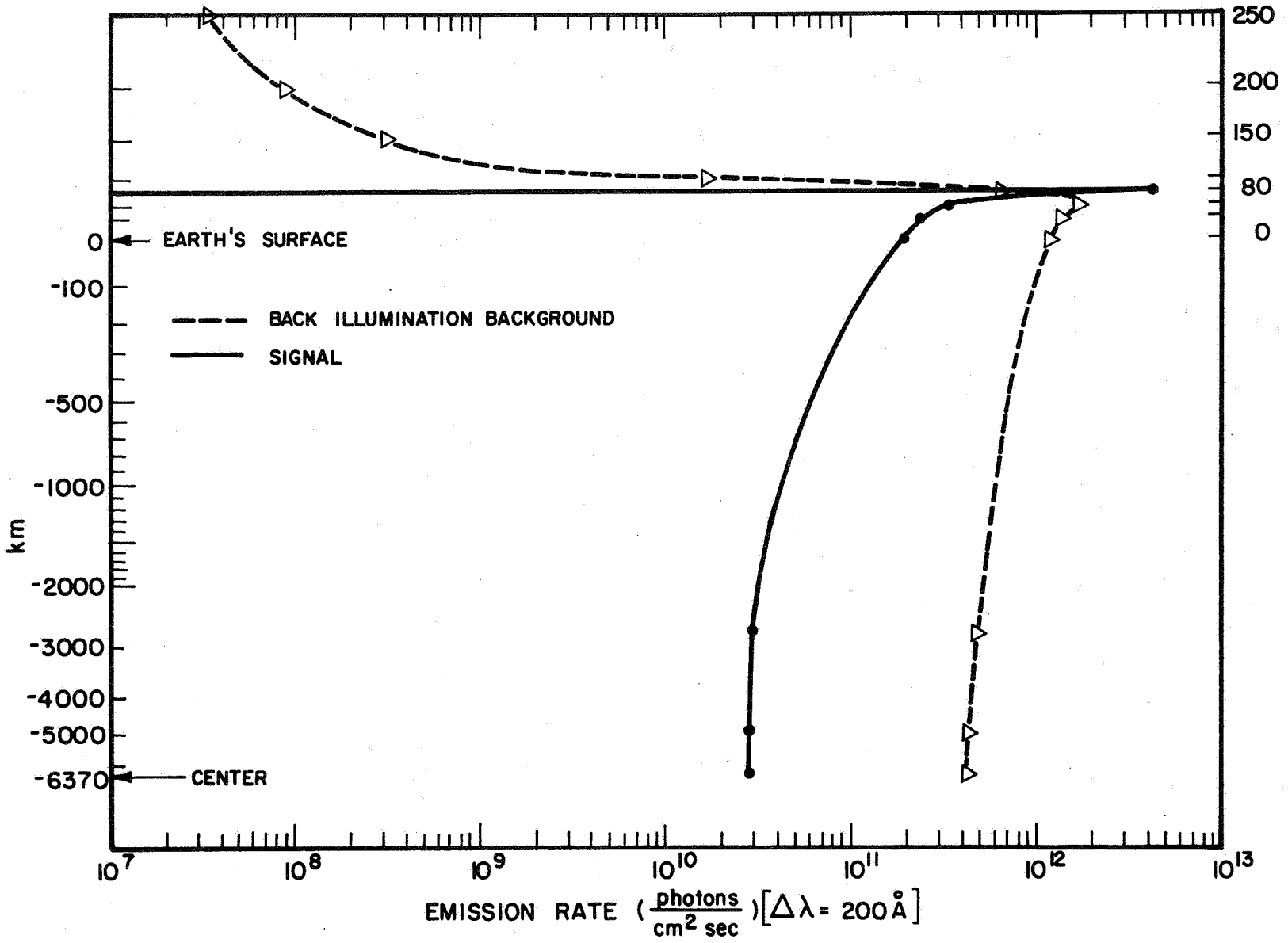

Figure 35. Computed signal and background emission rates for the case of back illumination.

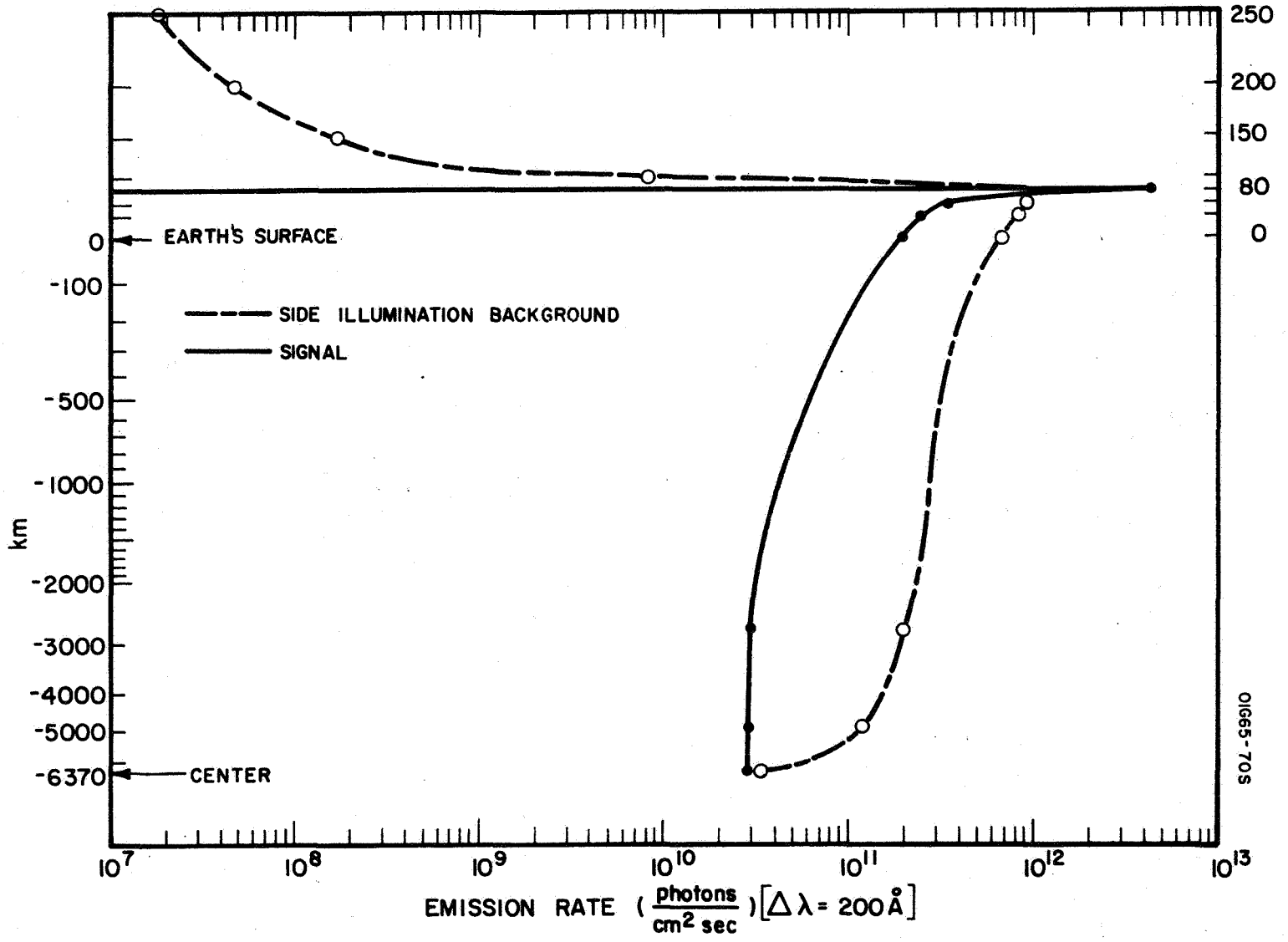

Figure 36. Computed signal and background emission rates for the case of side illumination.

capability is available for observing less than 1 particle cm^{-3}. On the basis of these studies, it becomes evident that a powerful detection capability is now available for the UV observation of Mei scattering particles resident in planetary atmospheres.

2. Theoretical models of the atmospheres of Mars and Venus. — A number of current scientific investigations require a model atmosphere for definition of specific parameters. For this reason, considerable effort has been directed toward obtaining reliable models for the atmospheres of Mars and Venus (D-3). At the present time, more definitive data are available concerning the planet Mars so that the major portion of the study involves this planet. In fact, the data concerning Venus are so sparce that for some applications it appears safe to regard its upper atmosphere as essentially the same as the upper atmosphere of Mars. On this basis, then, a detailed analysis was performed in order to derive a usable model atmosphere on Mars which was considered to be directly applicable to Venus.

The major aim of the study was to define realistic models consisting of temperature and composition altitude profiles. The first step in accomplishing this task was to establish reliable estimates for lower atmospheric parameters which were then coupled to the upper atmosphere treatment in order to establish a limited range of values for the number-density altitude profiles for the several constituents involved.

Concerning the best estimates for lower atmospheric parameters the following comments apply. Recent work by House, et al [59] involved a critical review and evaluation of available observational and theoretical material on the Martian lower atmosphere in order to establish best estimates of pressure, temperature, and atmospheric composition from the surface to the tropopause (up to about 30 km). The body of the most reliable recent observational data is summarized in Table 3 where a number of generally accepted values of CO_2 abundances are presented in addition to their individual corresponding surface pressure estimate. In addition to these data, House, et al [59] re-evaluated the published radio occultation data (obtained by the Mariner IV fly-by of Mars in 1965) by employing an inversion technique wherein an arbitrary structure, atmospheric composition, and surface pressure was employed. A computer program was established involving a variable temperature profile and an arbitrary CO_2 abundance as basic input parameters. The temperature profile inputs were based on theoretical calculations for the time-of-entry and time-of-exit occultations; the CO_2 abundance estimates were taken from the experimental values in Table 3. A number of trial surface pressures were fed into the program which contains a loop to select the specific surface pressure which provided the most acceptable solution. On this basis, a best fit surface pressure was selected from which the corresponding best fit composition was computed from combining the CO_2 abundance with varying amounts of N_2. From the over-all experimental evidence, it appears that the spectroscopic data suggest a surface pressure of about 6 mbar whereas the re-evaluation of the Mariner IV measurements suggests a value of about 8 mbar. For the present purpose, a compromise value of 7 mbar is representative of the preferred model surface pressure of Mars.

TABLE 3

TOTAL CO_2 ABUNDANCE AND SURFACE PRESSURE ESTIMATES

Observer(s)	Opposition	CO_2 Abundance, w (m-atm) STP = 200°K	Surface Pressure, P_o (mbar)		
			Low	Preferred	High
Kaplan[a]	1963	50 ± 20	10	25	40
Belton and Hunten[b]	1965	68 ± 26	5	6	13
Owen[c]	1965	65 ± 20	5	9	20
Spinrad[d]	1965	90 ± 27	5	10	20
Belton[e]	1967	73 ± 7	5	6	8

(a) Kaplan, L. D., G. Munch, and H. Spinrad, Astrophys. J., 139, 1-15 (1964).

(b) Belton, M., and D. Hunten, "The Abundance and Temperature of CO_2 in the Martian Atmosphere," Astrophys. J., 145, 454-467 (1966).

(c) Owen, T. C., "The Composition and Surface Pressure of the Martian Atmosphere: Result from the 1965 Opposition," Astrophys. J., 146, 257-270 (1966).

(d) Spinrad, H., R. A. Schorn, R. Moore, L. P. Giver, and H. J. Smith, "High-Dispersion Spectroscopic Observations of Mars. I. The CO_2 Content and Surface Pressure," Astrophys. J., 146, 331-338 (1966).

(e) Belton, M., private communication, 1967.

This value, coupled with a CO_2 abundance of 70 m-atm, leads to the preferred choice of model atmosphere to be employed in the present study. House, et al [59] selected corresponding upper and lower limit model atmospheres on the bases of the uncertainty in the spectroscopic measurements. The three resultant model atmospheres are summarized in Table 4 which gives selected surface pressure and composition models for the lower atmosphere of Mars.

A key parameter in extending these models to the upper atmosphere is the temperature altitude profile. In fact, the proper choice of this parameter is intemately involved with the interpretation of the Mariner IV observations of a Martian ionosphere with a peak charged particle number density of 9×10^4 cm^{-3} (at an altitude of about 125 km above the surface) and a plasma scale height of about 20 to 25 km. It appears that the E-region model proposed by McElroy [60] utilizes a realistic temperature profile. On this basis, then, a number of Martian upper atmospheric models were derived by coupling the lower atmospheric models discussed previously to a temperature profile calculated in accordance with a scheme suggested by McElroy [60]. For this purpose, three different compositions were assumed at the ground level in accordance with the data of Table 4. Additionally, in the present models two alternate turpopause altitudes were employed; namely, 80 km and 120 km. Finally, all the models pertinent to solar minimum conditions have been calculated. For illustrative purposes, only those of the preferred model atmosphere are presented in Figures 37 through 42 where the specific parametric values are defined so that they need not be repeated here. These models have been employed as required for the performance of a number of tasks under the current program, which bears witness to their utility for the present purposes.

3. The VUV day airglow in planetary atmospheres. – The VUV day airglow in the atmospheres of Mars and Venus can be produced by a variety of processes involving the interaction between several energy sources and atmospheric constituents. The resultant emissions must be observed against background radiation due to VUV molecular scattering by the solar-illuminated constituents. Thus, one of the tasks performed under the current program involved theoretical calculations of the VUV albedo of the solar-illuminated atmospheres of Mars and Venus. In addition, a specific signature airglow emission was investigated, i.e., the VUV fluorescence due to CO in the atmospheres of Mars and Venus. The progress achieved in these two areas is summarized below.

a. The VUV (1200-2000Å) albedo of the solar-illuminated atmospheres of Mars and Venus. – The physical-mathematical models and general theoretical techniques involved in calculating the VUV albedos of planetary atmospheres have been given by Marmo and Degges [61], who obtained results for the Earth's atmosphere. At that time, similar calculations for the Martian atmosphere were not performed due to the lack of a suitable model for application to the problem. However, as noted in the previous section, a relatively detailed analysis has now been performed for the expressed

TABLE 4

SELECTED SURFACE PRESSURE AND COMPOSITION MODELS
FOR THE LOWER ATMOSPHERE OF MARS

Selection	Surface Pressure (mbar)	Composition by Volume		CO_2 Abundance (m-atm)	Mean Molecular Weight
		CO_2	N_2		
Lower Limit	5	100%	---	67	44
Preferred Choice	7	64%	36%	70	38.3
Upper Limit	14	21%	79%	55	31.3

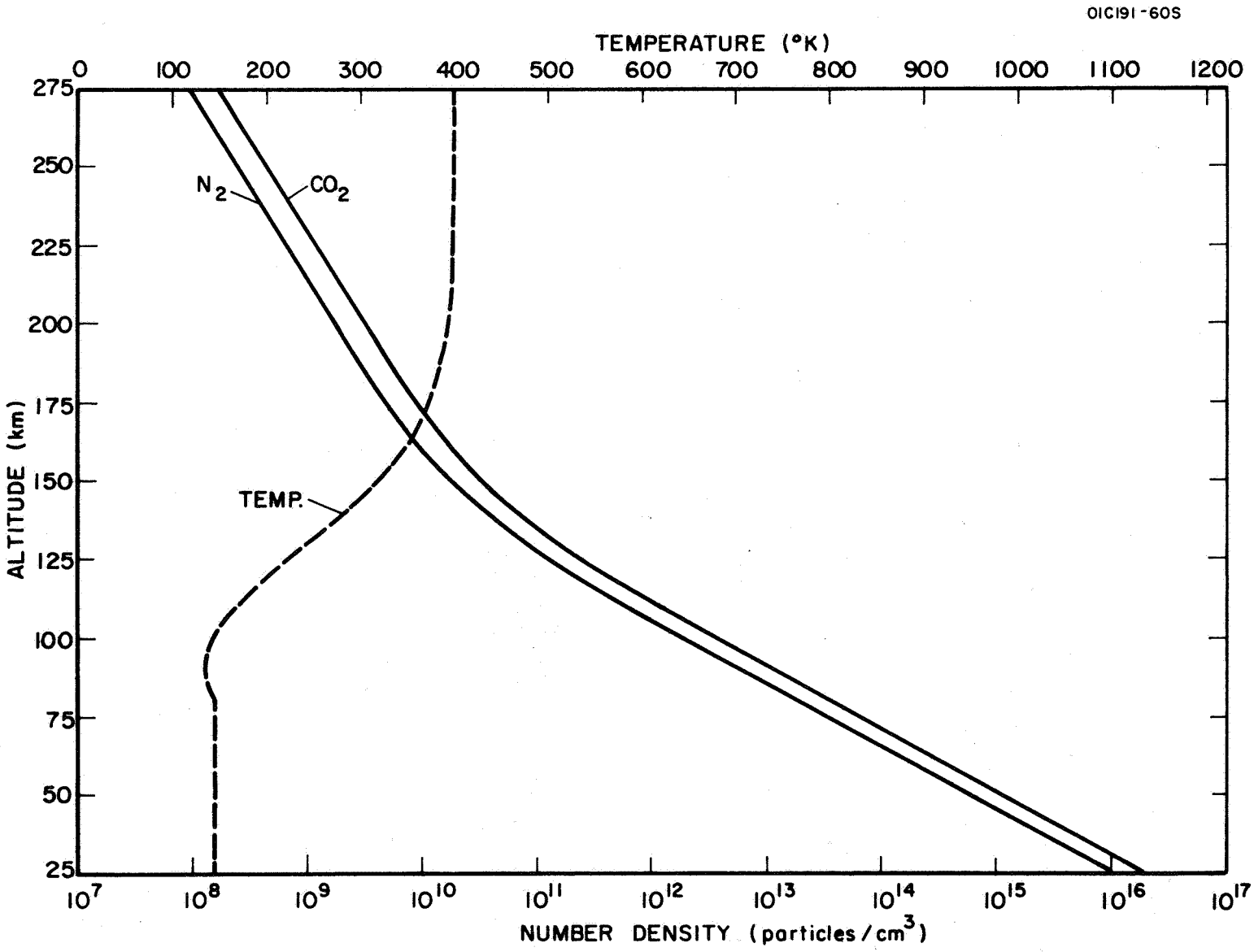

Figure 37. Calculated model atmosphere of Mars based on the minimum temperature model with no CO_2 dissociation or turbopause. Surface pressure is taken to be 7 mbar with a composition of 64 percent CO_2 and 36 percent N_2.

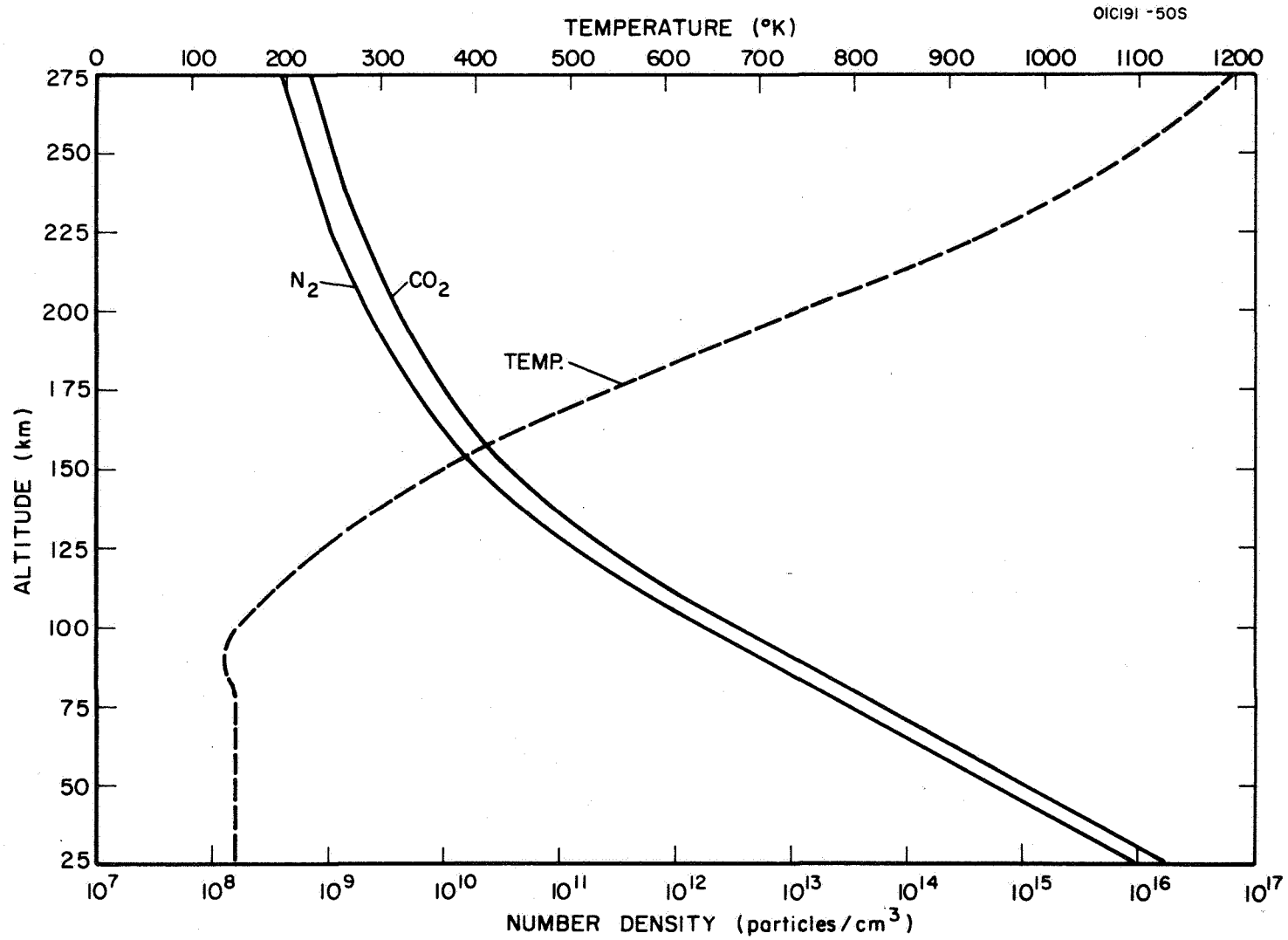

Figure 38. Calculated model atmosphere of Mars based on the maximum temperature model with no CO_2 dissociation or turbopause. Surface pressure is taken to be 7 mbar with a composition of 64 percent CO_2 and 36 percent N_2.

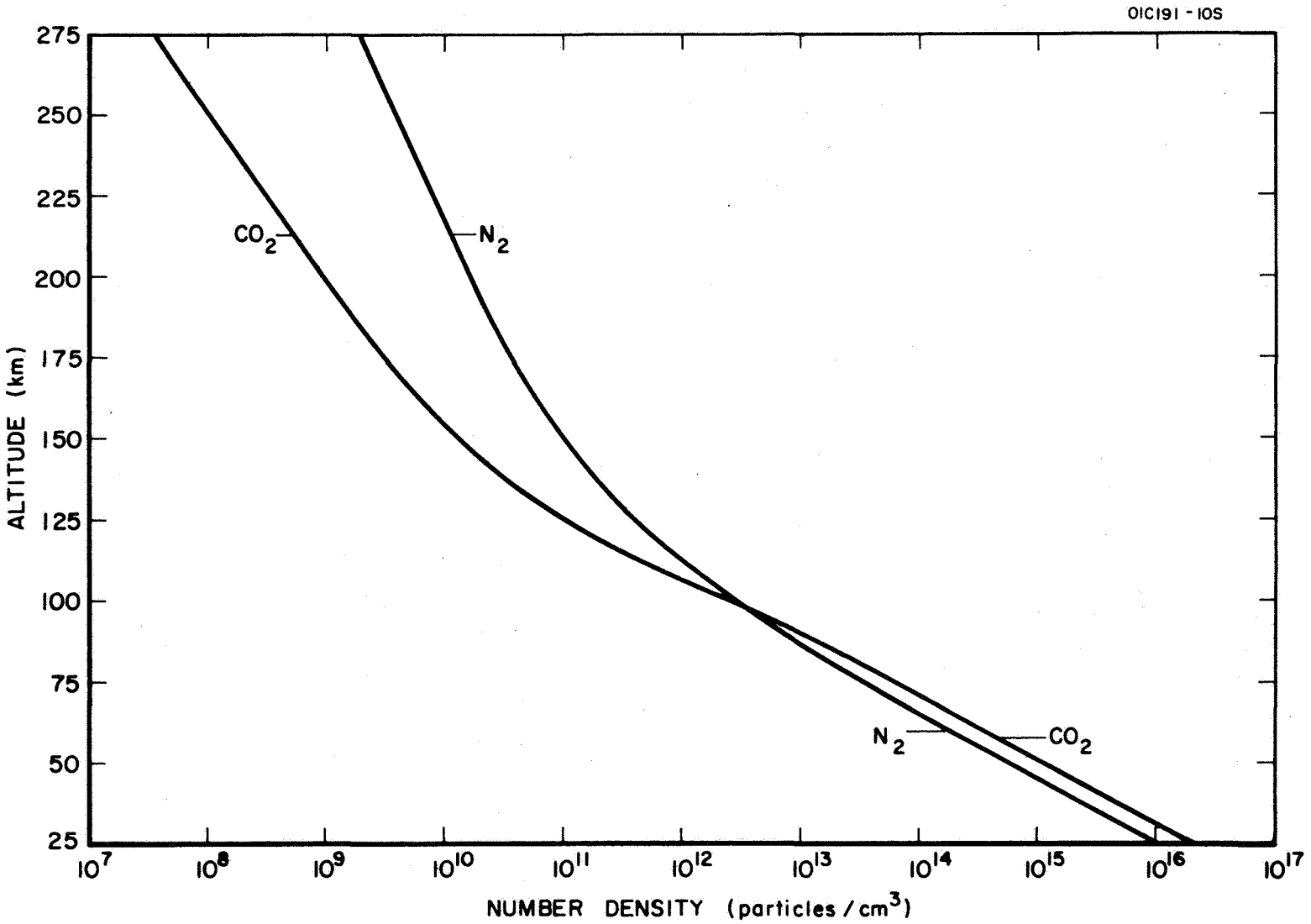

Figure 39. Calculated model atmosphere of Mars based on the minimum temperature model with no CO_2 dissociation but with 80 km turbopause. Surface pressure is taken to be 7 mbar with a composition of 64 percent CO_2 and 36 percent N_2.

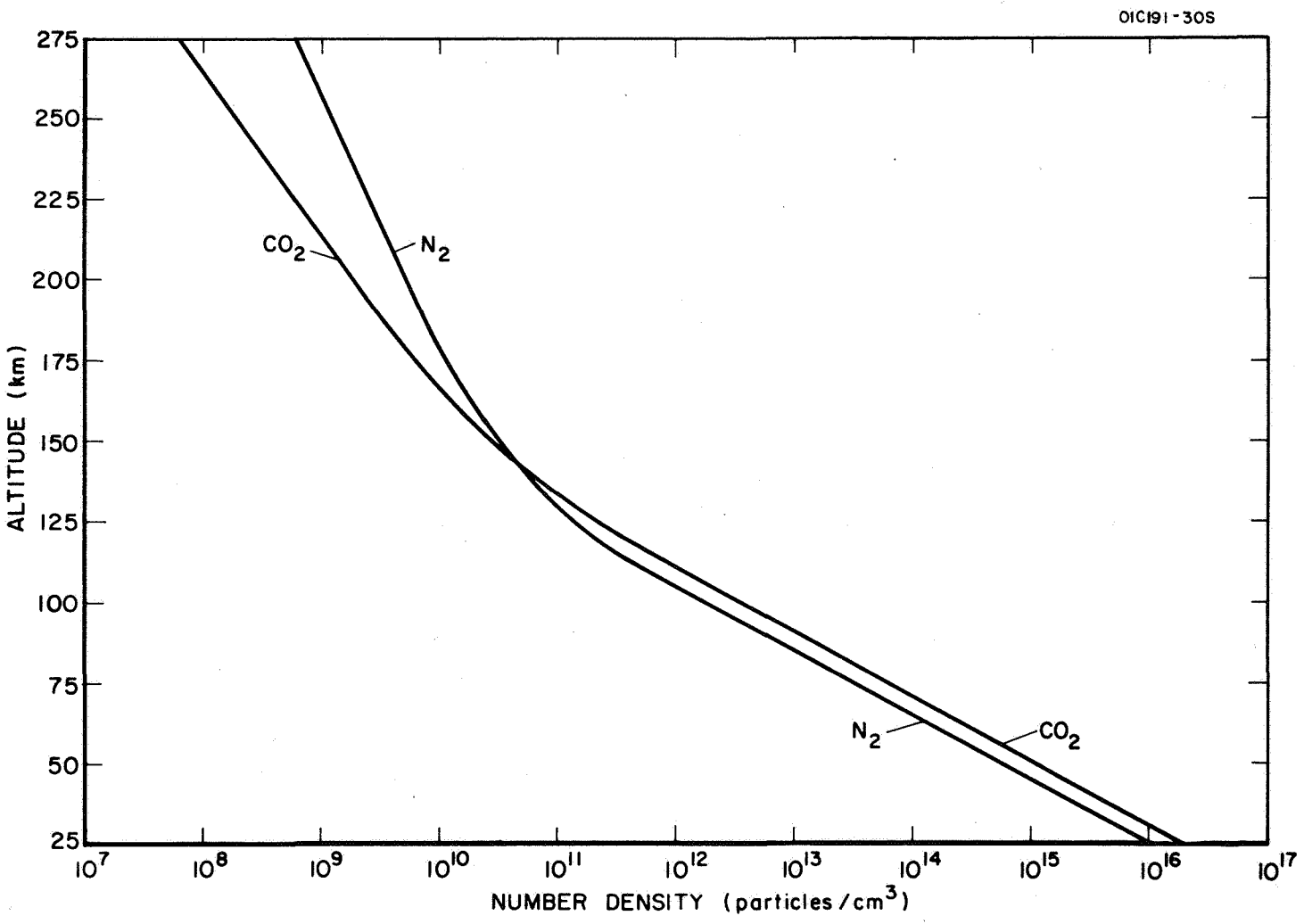

Figure 40. Calculated model atmosphere of Mars based on the minimum temperature model with no CO_2 dissociation but with 120 km turbopause. Surface pressure is taken to be 7 mbar with a composition of 64 percent CO_2 and 36 percent N_2.

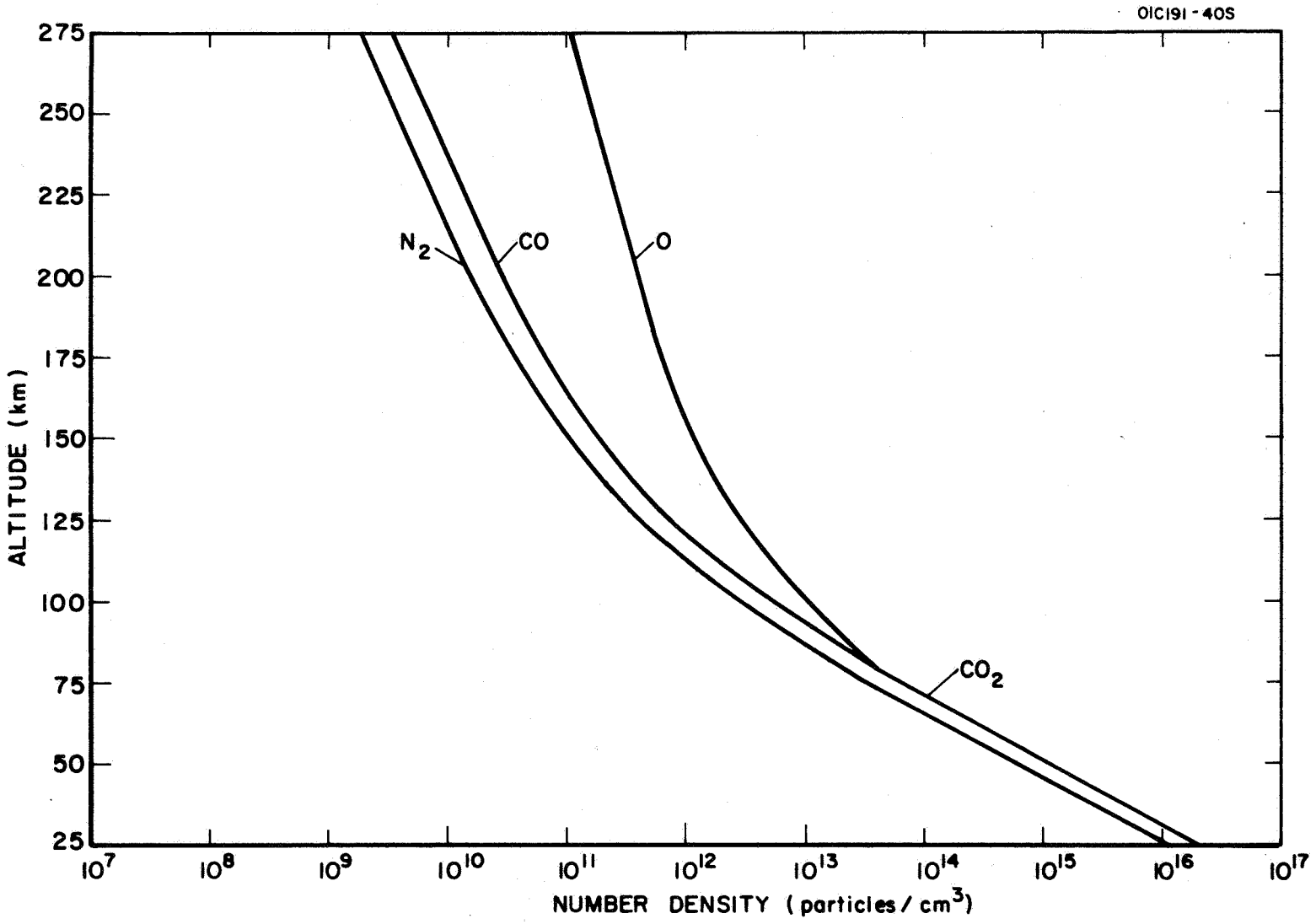

Figure 41. Calculated model atmosphere of Mars based on the minimum temperature model with complete CO_2 dissociation and 80 km turbopause. Surface pressure is taken to be 7 mbar with a composition of 64 percent CO_2 and 36 percent N_2.

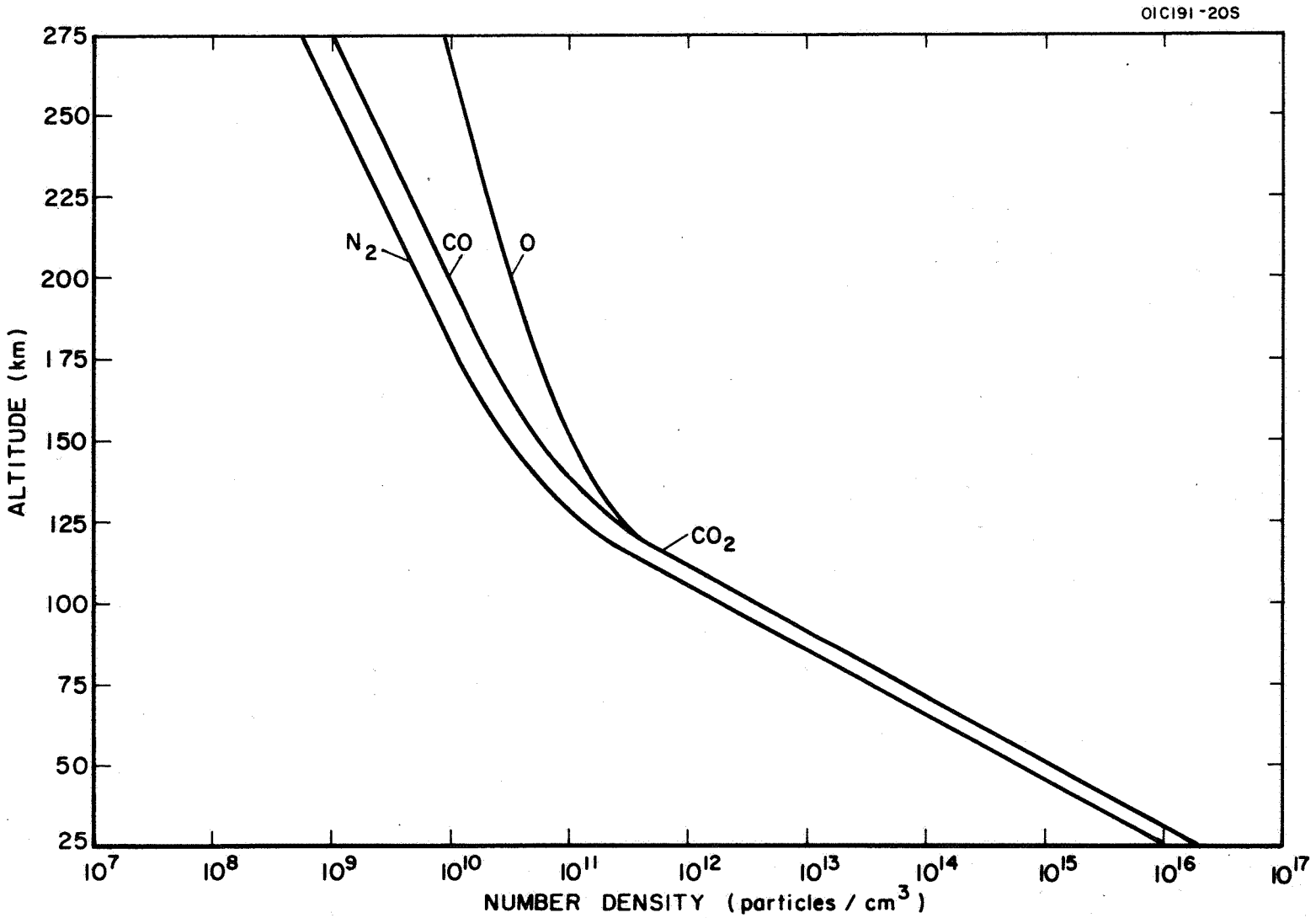

Figure 42. Calculated model atmosphere of Mars based on the minimum temperature model with complete CO_2 dissociation and 120 km turbopause. Surface pressure is taken to be 7 mbar with a composition of 64 percent CO_2 and 36 percent N_2.

purpose of obtaining reliable Martian atmospheric models based primarily of selected ground observations as well as the Mariner IV occultation data. For the present application, the selected model atmosphere involves a surface pressure of 7 mbar, a CO_2 abundance of 70 m-atm, and an atmospheric composition of 64 percent CO_2 and 36 percent N_2 (see Preferred Choice, Table 4) with corresponding number density-altitude and temperature-altitude profiles shown in Figure 37. Although other models have been suggested, it can be shown that computed diffusely-reflected solar flux intensities are rather insensitive to this factor so that utilization of other reasonable alternate models would not result in data significantly different than those derived in the present study. Finally, it can also be argued that, within theoretical uncertainties, this model applies equally to the Cytherian upper atmosphere so that the present albedo values are appropriate to Venus by modification of the incident solar flux.

It has been shown [61] that only single scattering need be considered since the atmospheres of Mars and Venus are optically thick to solar radiation throughout the VUV region owing to absorption by CO_2. Furthermore, since the relative concentrations of N_2 and CO_2 do not vary with altitude, the albedo for single scattering ω, can be considered constant with altitude for a given wavelength. The pertinent parameters involved in the calculation of the required ω-values are $\sigma_s(N_2)$, $\sigma_s(CO_2)$, and $\sigma_a(CO_2)$, which are the cross sections for the molecular scattering by N_2, the molecular scattering by CO_2, and absorption due to CO_2, respectively. Both theoretical (B-4) and experimental [62] $\sigma_s(N_2)$-values were employed on the basis of work performed un the current program. the $\sigma_a(CO_2)$-values were obtained from two sources. For $\lambda\lambda$ 1200-1750Å, the data of Watanabe, et al[63] were employed, whereas for $\lambda\lambda$ 1750-1950Å, the data were taken from Thompson, et al[64]. Since the required $\sigma_s(CO_2)$-values were unavailable in the literature, a theoretical procedure was developed and employed to calculate approximate values for $\lambda\lambda$ 1000-2000Å (D-4). Finally the incident VUV solar flux values were taken directly from GCA-TR-62-14-N.

The required calculations were then performed to produce the VUV albedo curves shown in Figures 43 and 44 for Mars and Venus, respectively. The results apply to an overhead sun and the resultant vertically reflected flux for the spectral region 1200-2000Å. These data are directly applicable to problems associated with satellite and/or rocket observation of VUV dayglow in the atmospheres of Mars and Venus. This point is made evident in the following discussion where CO fluorescent signals are compared to the VUV albedos derived herein.

b. VUV fluorescence due to solar illuminated CO in the atmospheres of Mars and Venus. — The previously discussed VUV albedo values represent practical lower limit values since they involve only the contributions due to molecular scattering from solar illuminated planetary atmospheric constituents. In practice, a number of additional contributing factors must be considered in determining the final VUV albedo of these atmospheres. For example, major contributions can be expected from specific signature

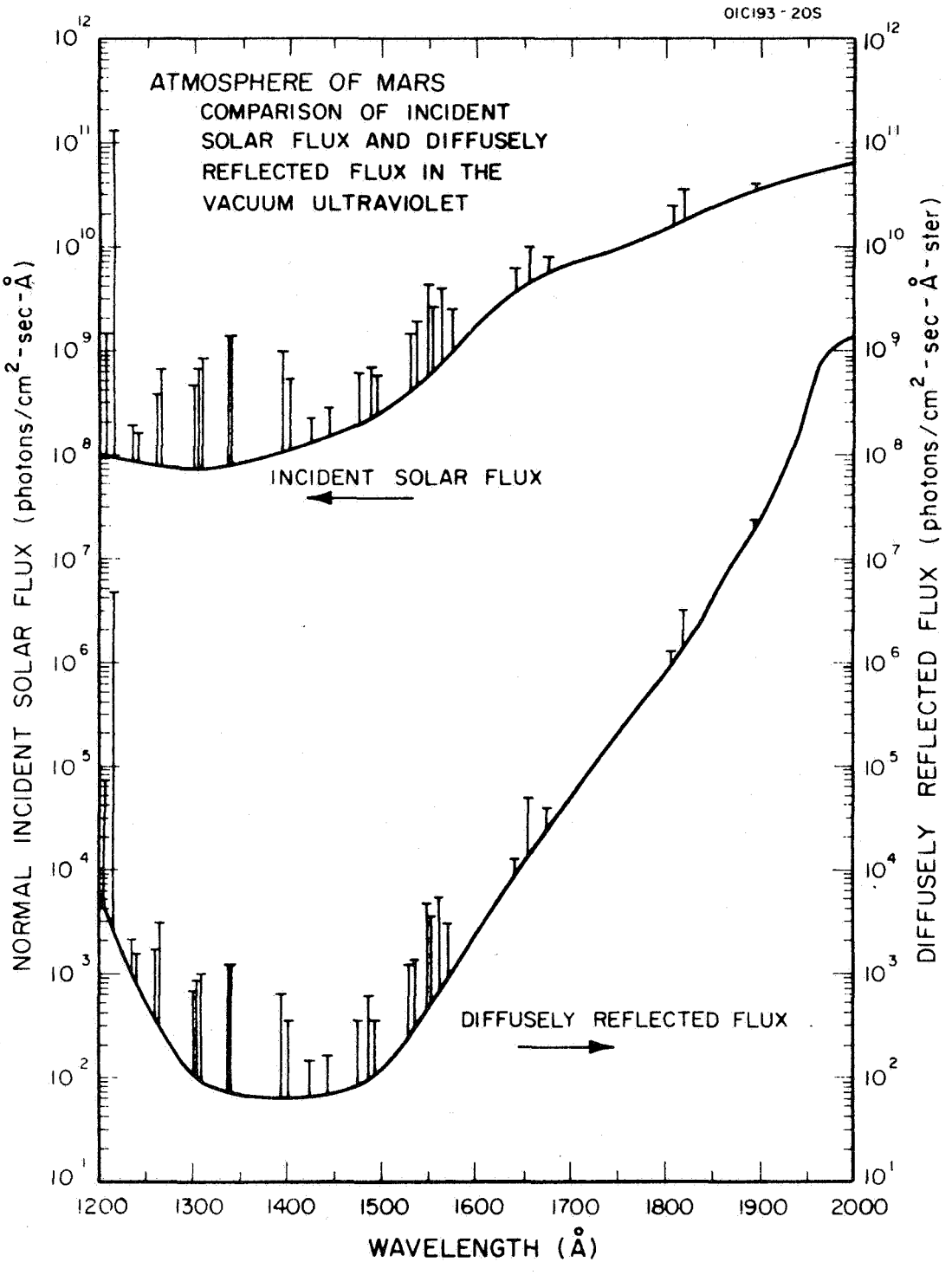

Figure 43. VUV albedo of Mars for solar zenith and look angles of zero degrees.

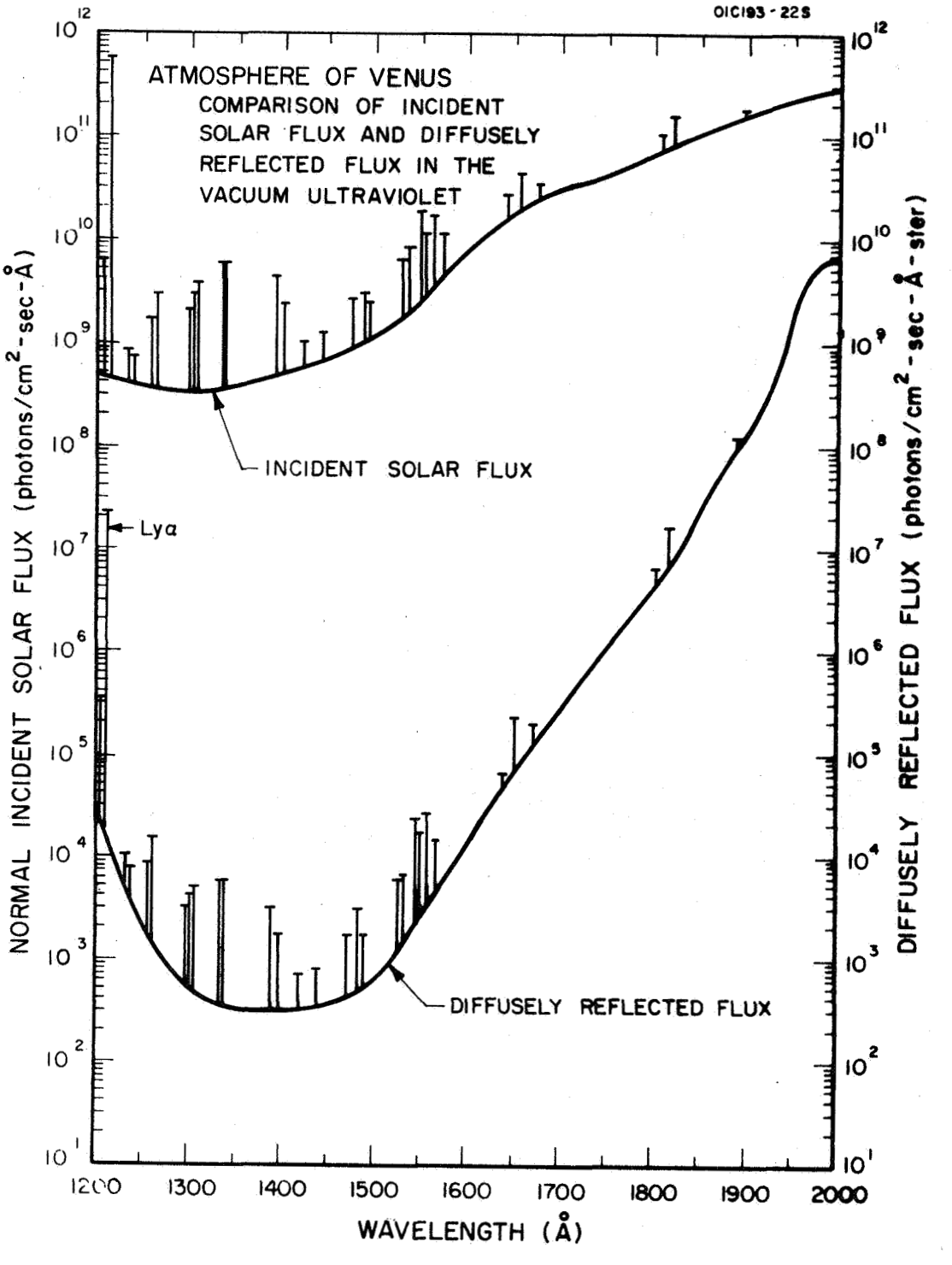

Figure 44. VUV albedo of Venus for solar zenith and look angles of zero degrees.

radiations associated with the resonance lines of solar-illuminated atomic atmospheric species such as H(Lyman-α, 1216Å), O(1304 and 1310Å), C(1560Å), etc. In addition, other specific airglow emissions can be anticipated owing to the interaction between atmospheric constituents and the superthermal photoelectrons which are produced by the EUV ($\lambda\lambda$ < 800Å) photoionization of ambient species. Furthermore, in some spectral regions, the dominant contribution to the VUV albedo can result from the resonance-fluorescence signals from solar-illuminated molecular species such as CO, CO_2, N_2, O_2, etc. Of these species, there is particular interest in evaluating the role of CO since its inventory is intimately related to the degree of photodissociation that prevails in the upper atmospheres of these planets. Accordingly, a significant effort was directed toward obtaining reliable estimates of the VUV background contribution owing to the resonance-fluorescence from solar illuminated CO in the upper atmospheres of Mars and Venus. A brief description is presented below of the procedure employed and the final results (D-5).

In this investigation, an initial task involved the determination of an upper limit estimate of the CO content in the upper atmospheres of these planets. This limit prevails for the case wherein solar photodissociation equilibrium prevails. An appropriate technique which applies under equilibrium conditions has been described previously so that it is not repeated here. The technique was applied to the updated Martian model atmosphere shown in Figure 37 and the resultant cm^2-column count for the several photodissociation species involved are shown in Figure 45 as a function of altitude. Similar curves obtain for the upper atmosphere of Venus except that, in this case, the altitude scale cannot be established with confidence. However, if both planetary atmospheres are optically thick in CO, the altitude scale is of no consequence since the total VUV albedo intensity is not affected significantly. Thus, the data can be applied equally to the problem of investigating the resonance-fluorescence emission from CO in both the atmospheres of Mars and Venus. It appears that optical thickness prevails since a representative cross section for CO absorption = 10^{-16} cm^2 whereas the data in Figure 45 indicate that a cm^2-column count as high as 2×10^{18} cm apply. This important fact also indicates that even if only 1 percent of the model CO content prevails, the atmospheres would still be "optically thick."

The fluorescent efficiency of optically thin, solar-illuminated CO has been estimated by others [65]. However, for the present requirement, it is necessary to determine the variation of fluorescent efficiency with optical thickness for each of the bands involved in the fourth positive system. Although no details are presented here, the typical result shown in Figure 46 indicates that a significant variation exists and must be considered in any realistic assessment of the over-all problem of VUV dayglow in the atmospheres of Mars and Venus.

An appropriate physical-mathematical model was developed which incorporated the input data shown in Figures 45 and 46. The calculated dayglow

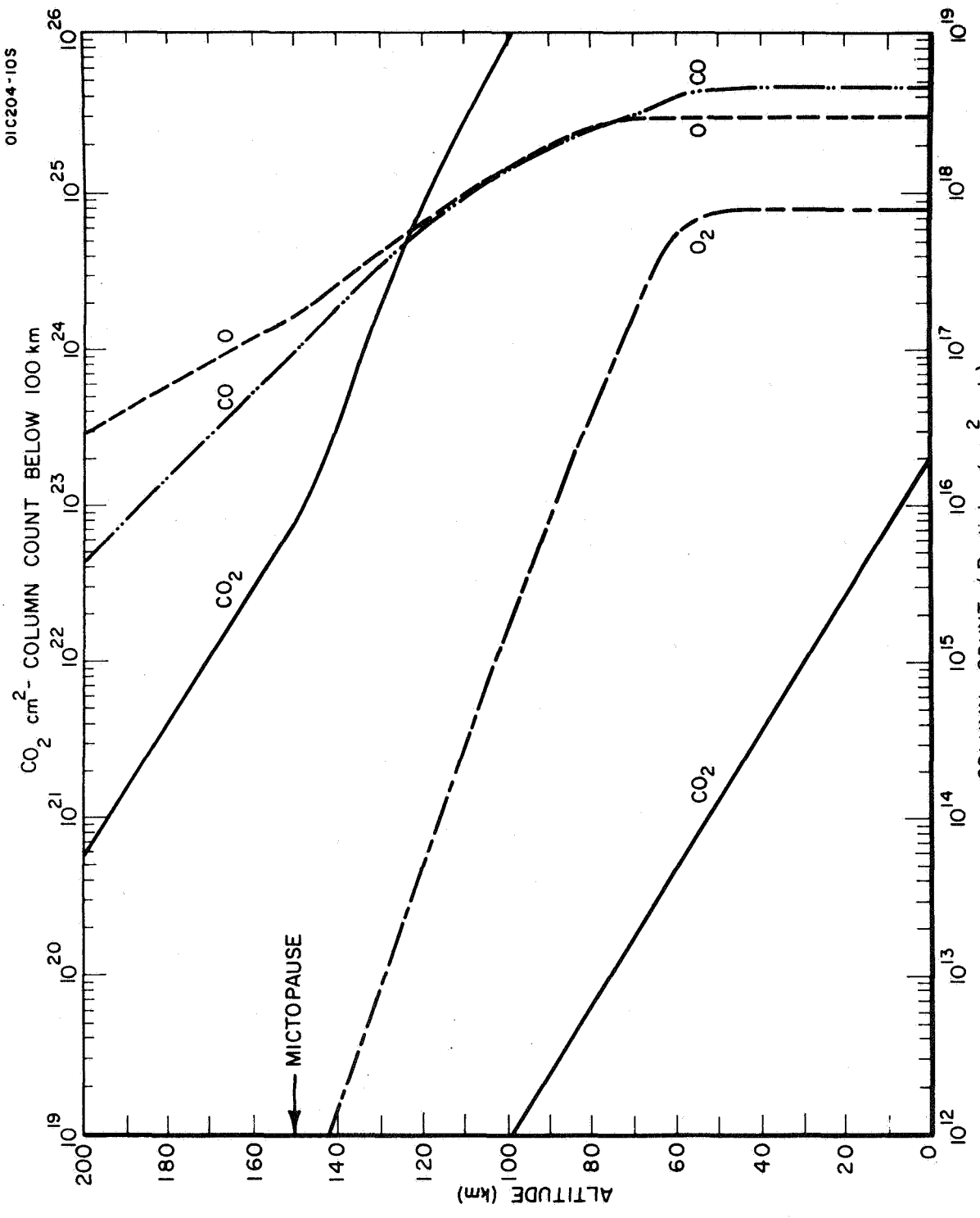

Figure 45. Curves showing the cm^2-column count of photodissociation species in the Martian and Venus atmosphere.

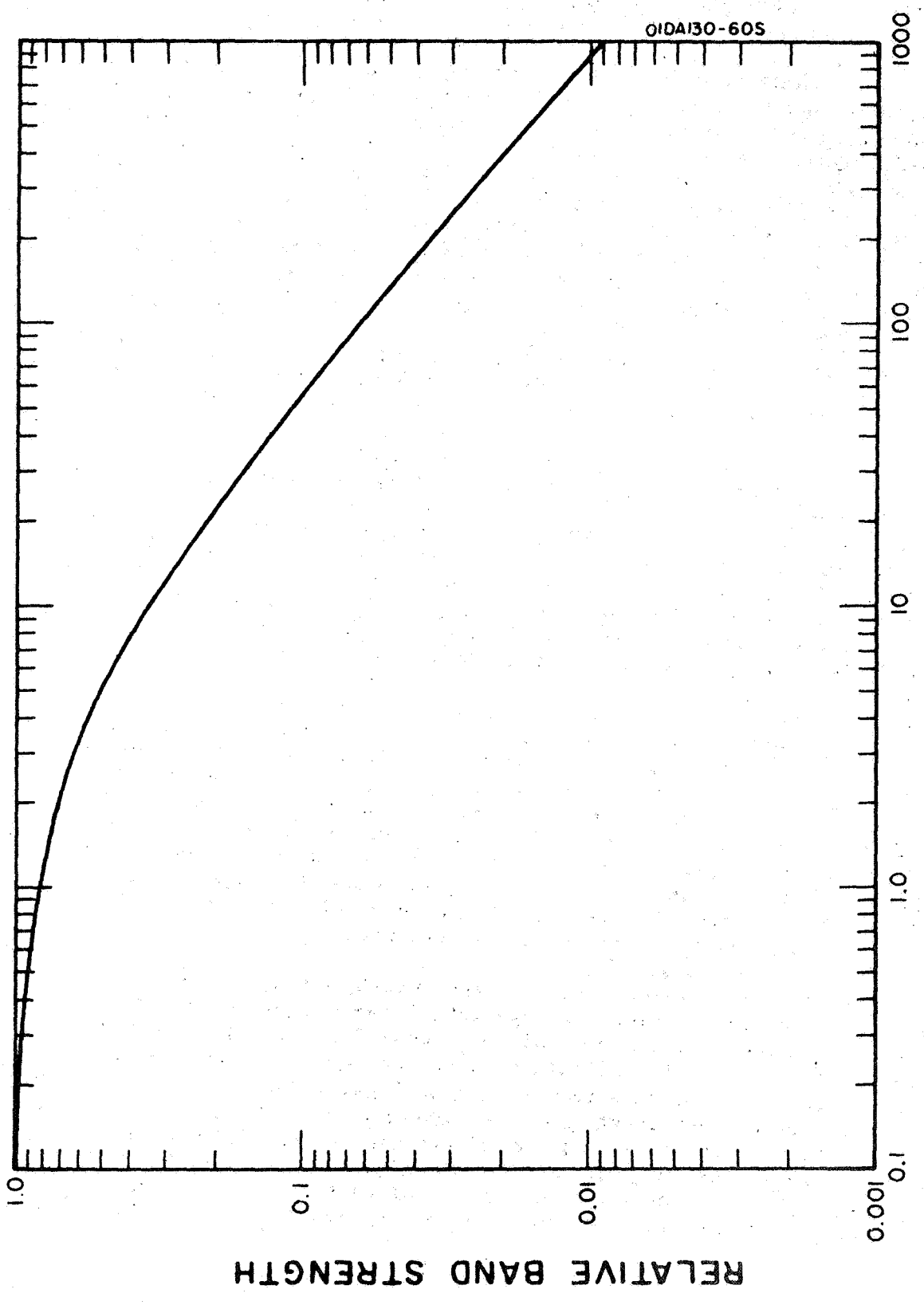

Figure 46. Optical Thickness, T_o, at center of strongest line vs relative line strength.

intensities (for selected fourth positive bands) due to solar-illuminated CO in the upper atmospheres of Mars (and Venus) are listed in Table 5.

Inspection of the tabulated results indicates that, for the 3Å-bandwidths employed, there is considerable overlap of the emission distribution of the individual bands. If a larger effective bandwidth were applied, the over-all intensities in the individual bands would not decrease by more than a factor of 2 or 3 owing to the large optical thickness for CO in the planetary atmosphere. Thus, it appears that treatment of the fluorescence emission as a continuum is justified since, in practice, it can be expected that VUV planetary probe data will be obtained with relatively poor resolution (say $\gtrsim$ 10Å). Evidently, the "continuum" dayglow will be superposed on the molecular scattering continuum as shown in Figures 11 and 12. Thus, the resultant VUV albedos for the atmospheres of Mars and Venus shown in Figures 47 and 48, respectively, include the contributions due to molecular scattering and resonance-fluorescence from solar-illuminated CI in the upper atmospheres of the planets.

4. Laboratory measurements of the VUV fluorescence of air due to electron impact excitation. – Fluorescence radiation excited by the electron bombardment of planetary gases depends on the transfer of energy from the incident electron to the target molecule and the ensuing radiative transition. Therefore, an understanding of this phenomenon requires pertinent information regarding excitation cross sections of the different states of the molecules by electron impact and the relevant transition probabilities (e.g., electronic, vibrational). In order to develop a useful methodology in the current program, a critical review of previous work was performed. This preliminary literature survey revealed that nitrogen represents an extensively studied molecule for which the necessary structural and spectroscopic information is also available. Review of the question of excitation of the nitrogen spectrum by electron bombardment has revealed that experimental cross section and excitation functions are available for only a few of the states of N_2 molecule. Applicability of the Franck-Condon principle to the excitation of diatomic molecules by electron impact has been tested by high resolution study of the electron impact spectrum in the visible region. Corresponding spectra for VUV fluorescence are not available in the literature.

Considering the present state of the development of the theory of inelastic scattering of electrons by diatomic molecules, it is not feasible to perform rigorous quantum mechanical calculations for the low energy ionization and electronic excitation cross sections of molecules containing several electrons. For this reason, a more empirical approach was employed wherein some of the pertinent cross sections can be acquired by laboratory experimentation. The specific progress achieved has been discussed elsewhere (D-7, D-9) wherein several preliminary investigations have been described in which an early design electron impact chamber configuration was employed. On the basis of this preliminary measurement program and an

TABLE 5

TOP OF ATMOSPHERE OF MARS
INTENSITY OF RESONANCE-FLUORESCENT RADIATION IN
SELECTED CARBON MONOXIDE FOURTH POSITIVE BANDS
ZERO SOLAR ZENITH AND LOOK ANGLES

λ (Å)	Band (v'v")	Intensity*
1246	16,2	6.3 (3)†
1261	15,2	1.2 (4)
1263	13,1	9.0 (3)
1269	16,3	2.8 (4)
1278	14,2	2.6 (4)
1280	12,1	1.9 (4)
1296	15,3	4.2 (4)
1297	13,2	5.1 (4)
1299	11,1	3.9 (4)
1300	17,4	3.6 (4)
1311	14,3	8.1 (4)
1317	12,2	9.3 (4)
1318	10,1	8.4 (4)
1322	8,0	4.8 (4)
1330	15,4	7.8 (4)
1332	13,3	1.3 (5)
1333	11,2	1.6 (5)
1339	9,1	1.5 (5)
1344	7,0	1.1 (5)
1348	14,4	1.1 (5)
1354	12,3	1.8 (5)
1356	10,2	2.5 (5)

*Photons/cm^2-sec-ster

†Number in parentheses is power to which 10 is raised.

TABLE 5 (continued)

λ (Å)	Band (v'v")	Intensity*
1361	8,1	2.8 (5)†
1368	6,0	2.6 (5)
1374	11,3	2.2 (5)
1378	9,2	3.3 (5)
1384	7,1	4.8 (5)
1392	5,0	5.4 (5)
1396	10,3	2.2 (5)
1401	8,2	3.9 (5)
1409	6,1	7.5 (5)
1419	4,0	1.1 (6)
1426	7,2	3.6 (5)
1435	5,1	9.0 (5)
1447	3,0	2.1 (6)
1464	4,1	7.5 (5)
1478	2,0	3.3 (6)
1481	10,5	1.3 (5)
1487	8,4	1.6 (5)
1494	3,1	2.2 (5)
1497	6,3	2.2 (5)
1506	9,5	1.8 (5)
1510	1,0	4.2 (6)
1510	4,2	2.8 (6)
1516	7,4	3.0 (5)
1528	5,3	5.4 (5)
1542	3,2	1.1 (6)
1545	0,0	3.0 (6)
1560	1,1	2.7 (6)

*Photons/cm^2-sec-ster

†Number in parentheses is power to which 10 is raised.

TABLE 5 (continued)

λ(Å)	Band (v′v″)	Intensity*
1577	2,2	1.0 (6)†
1582	8,6	9.0 (4)
1597	0,1	6.6 (6)
1603	9,7	1.4 (5)
1611	4,9	4.2 (5)
1615	7,6	2.4 (5)
1630	2,3	1.2 (6)
1634	8,7	8.4 (4)
1648	3,4	6.9 (5)
1653	0,2	6.3 (6)
1670	1,3	1.1 (6)
1689	8,8	1.1 (5)
1705	3,5	6.0 (5)
1712	0,3	3.9 (6)
1724	4,6	5.1 (5)
1729	1,4	2.4 (6)
1747	2,5	4.8 (5)
1775	0,4	1.7 (6)
1792	1,5	2.1 (6)

*Photons/cm^2-sec-ster

†Number in parentheses is power to which 10 is raised.

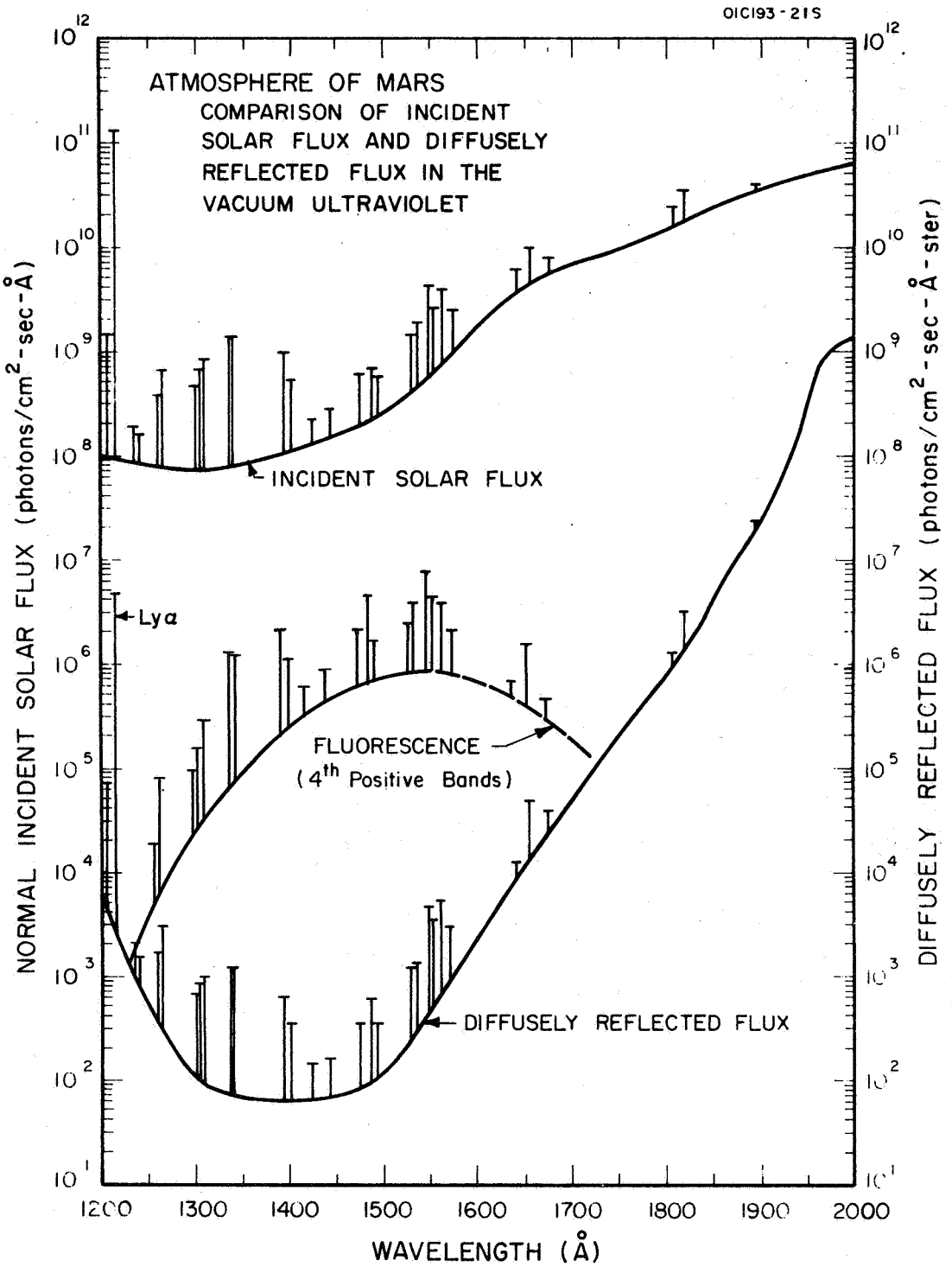

Figure 47. Diffusely reflected and fluorescence scattering contribution to the VUV albedo of Mars for solar zenith and look angles of zero degrees.

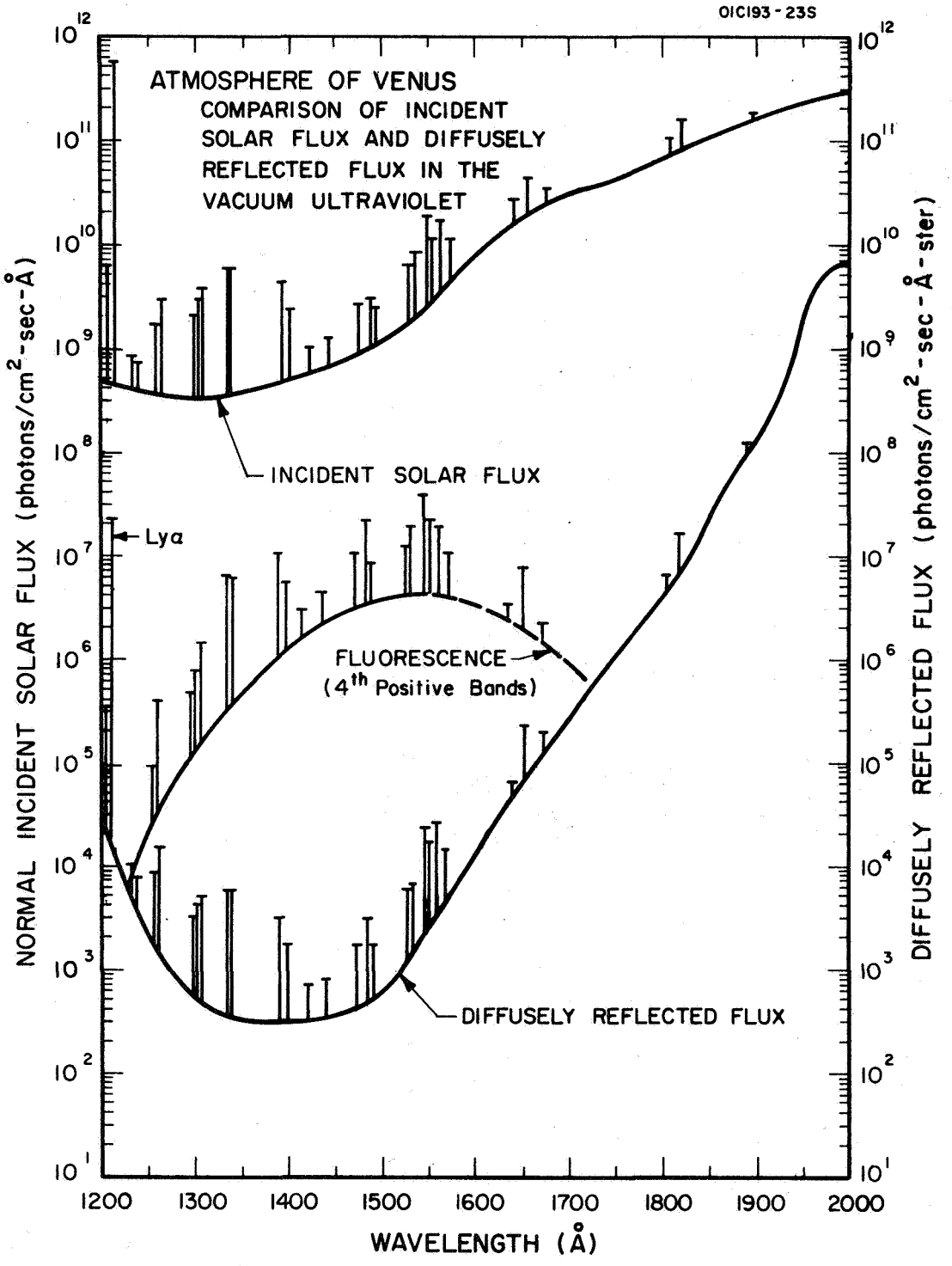

Figure 48. Diffusely reflected and fluorescence scattering contribution to the VUV albedo of Venus for solar zenith and look angles of zero degrees.

evaluation of the several experimental parameters involved, the electron impact sample chamber was subsequently modified appropriately to the new configuration shown schematically in Figure 49. Specifically, this chamber was designed to measure the intensity and spectral character of the fluorescent radiation due to the electron impact interaction with atmospheric gases.

The electron gun is available commercially from Veeco Instruments, Inc. The vacuum housing enclosing the gun portion requires a highly efficient and rapid pumping rate to sustain the lower pressure ($\approx 10^{-4}$ mm Hg) in the reaction chamber when sample gas is leaked in. Otherwise, the high pressure buildup will cause intolerable high absorption in the monochromator-reaction chamber system. The mounting flange of the chamber is compatible to direct coupling to the 2.2-meter monochromator (wherein photographic spectra can be obtained). The end window permits either direct viewing of the visible radiation or the use of a suitable PM tube.

The sequence of experiments performed with the above system configuration is described briefly below. First, evacuation of the entire system to a pressure of about 10^{-7} mm Hg was achieved and sustained without dynamic pumping. The electron gun was tested under this vacuum condition and observed to operate satisfactorily. Its general performance was verified visually as follows. Under this high vacuum, the electron beam impact upon the viewing LiF window results in the generation of a visible blue fluorescent light spot which permits a simple check on the alignment of the exciting beam. For example, the beam position could be adjusted to pass through the center (or any other desirable path) of the reaction chamber. This capability represents a considerable advantage in the alignment procedure in the coupled chamber-monochromator configuration. Additionally, since details of the beam geometry (i.e., the divergence) could be ascertained using the above procedure, the derived information would be of considerable value in obtaining absolute data values. In practice, the beam divergence resulted in about a 1.0" diameter spot at the LiF viewing window. The next procedural step involved slow filling of the reaction chamber with an ordinary air sample. The pressure was then allowed to increase in time and the following behavior was noted. At the initial low pressures, a relatively weak pink glow occurred directly within the geometric confines of the electron beam. At higher pressures, the flow intensity was observed to increase. Thereafter, at even higher pressures, an effective "quenching" of the electron impact radiation was observed. This general behavior is expected in terms of increased collision frequency at the elevated chamber pressures. On this basis, it was also noted that at increasing pressures, the maximum intensity approached the electron gun filament. Thus, the results of the above procedure indicated the optimum pressure range for obtaining the maximum visible glow along the excitation beam path was between 1-10 mm Hg. For the present purpose, it was felt that the spread in this pressure range permitted the preliminary extrapolation of the results to the case of VUV radiation due to electron impact. Recent laboratory data [66] obtained under the present program involving

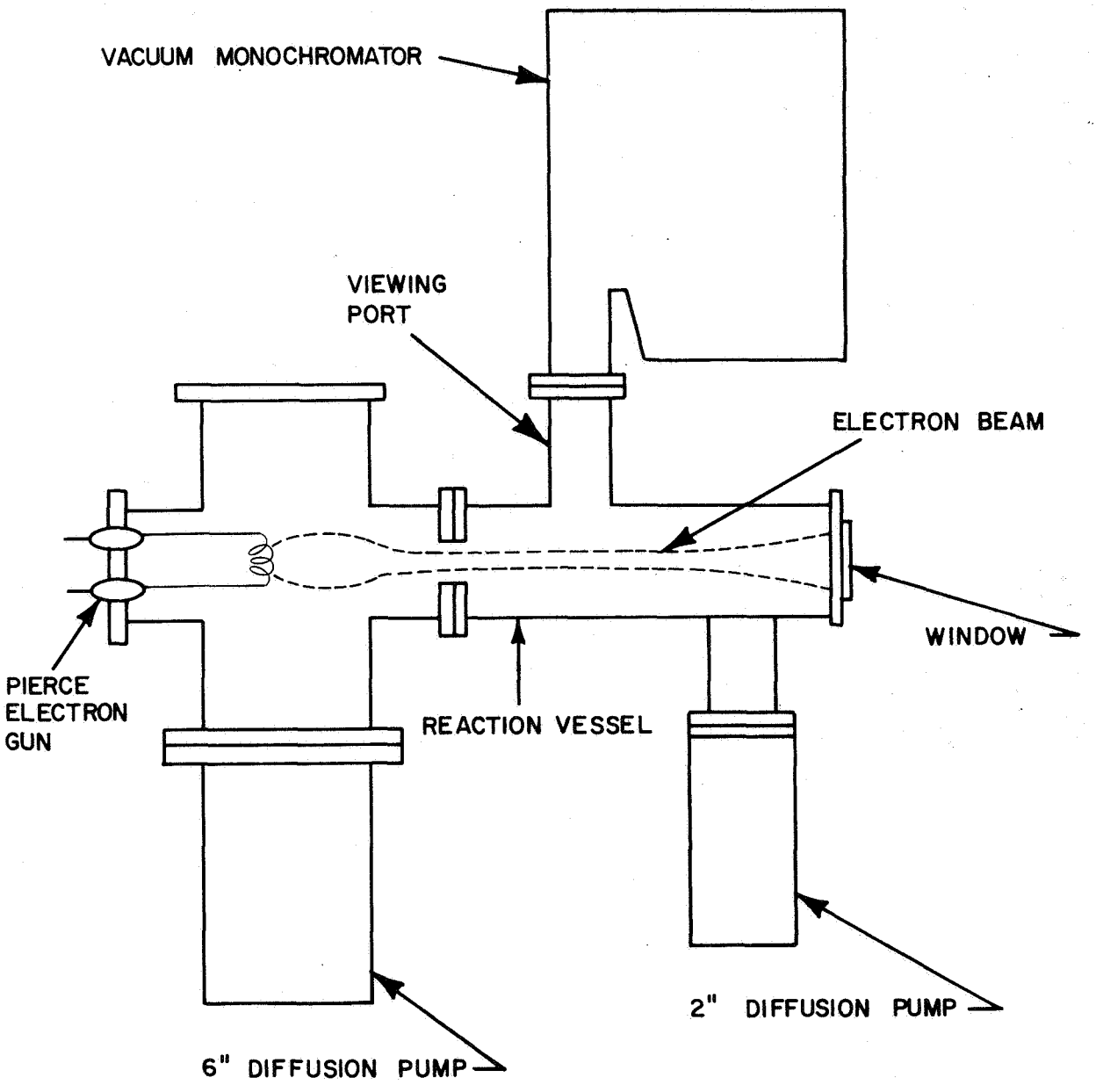

Figure 49. Electron impact reaction chamber.

unresolved VUV fluorescent radiation due to electron impact, demonstrate the necessity of obtaining relatively high resolution spectra of these radiations. Although the detailed analytical reasoning is not repeated herein, observation of the VUV spectrum (with 5Å resolution) due to electron impact produced in the reaction chamber was attempted.

The chamber was attached to the monochromator as shown in Figure 49. Since relatively weak intensity visible radiation was observed in the trial runs, it was decided to perform the preliminary measurements photographically, since considerable time integration could be invoked. It was planned subsequently to obtain quantitative photoelectric spectra if the observed photographic intensities were sufficiently high to warrant such action.

Eighty photographic exposures were obtained for the experimental configuration illustrated in Figure 49. The chamber pressure was varied between 1 and 10 mm as follows: 1.2, 3.0, 6.2, and 9.7 mm. Twenty exposures were obtained at each pressure using variable exposure times between one to twenty minutes. In spite of this tedious, time-consuming observational program, no useful VUV photographic spectra were obtained owing to the relatively low electron impact fluorescence radiation intensity. On the basis of these results, it is clear both that the f22 spectrograph is too slow for the present purposes and that a more sensitive radiation detection scheme must be developed. However, this latter requirement was considered to lie beyond the scope of the current program. Finally, the observed limitations on the present experimental capability has demonstrated that the system could not be employed successfully for observing VUV fluorescence due to the interaction between alpha particles and atmospheric gases. Accordingly, no further effort was directed toward this entire area of investigation.

5. Laboratory measurements of VUV photon scattering cross sections for selected atmospheric gases. – The efficiency with which planetary atmospheric constituents scatter incident solar VUV radiation represents an important input parameter in establishing VUV albedo and/or day airglow emission intensities. To date, theoretical techniques are not available to perform the calculations except for the case of simple atoms. Thus, for molecular constituents, the requirement for experimental data is evident. However, only limited experimental programs have been performed to obtain these required data. For example, relative photon scattering cross-section measurements at Lyman-α were first obtained by Gill and Heddle [67] for Ar, H_2, N_2, Xe, and Kn. In a subsequent investigation performed under the current program, Marmo [68], Shardanand (D-11), and Shardanand and Mikawa (D-10) employed an improved experimental procedure to measure the comparatively low (relative) cross sections of Ne and He (as well as Ar, H_2, N_2, Xe and Kr). The He determinations were of particular significance since Chan and Dalgarno [69] calculated an accurate absolute value for He at Lyman-α of 3.5×10^{-26} cm^2 which could then be employed to place the experimentally-measured relative values on an

absolute basis. For the cases of Ar, H_2, and N_2, the cross section values of both Marmo, et al. [68] and Gill and Heddle [67] were in good agreement. However, for the cases of Xe and Kr, a significant disagreement was observed which Marmo [68] ascribed to the formation of Xe_2 and Kr_2 molecules which was not recognized by Gill and Heddle [67]. To test this hypothesis, a series of additional experiments were devised and performed where the Xe and Kr cross sections were measured (at Lyman-α) at various temperatures and pressures (D-11) wherein it was observed that the apparent cross section increased linearly with pressure (i.e., did not obey Beer's law) and decreased with temperature. This behavior was ascribed to the formation of Xe_2 and Kr_2 molecules. An analysis of the data yielded (1) the equilibrium constant for the atom-molecule reaction, (2) the absorption cross sections for Xe_2 and Kr_2, and (3) the heats of dissociation for Xe_2 and Kr_2. Following this investigation, a considerable experimental improvement was achieved by utilizing monochromatic radiation by attaching a newly designed scattering chamber to the exit slit of the 2-meter McPherson VUV monochromator. This increased laboratory capability facilitated the performance of a number of new experiments including two of specific importance. The first involved the measurement of the absolute scattering cross section values for Ar and Kr over the spectral region $\lambda\lambda$ 1080-1700Å (D-12). On this basis, these gases are now available as secondary standards against which other gases can be calibrated. In the second investigation, preliminary measurements were performed on the efficiency of selective scattering by CO in the fourth positive band system (D-13).

a. The absolute scattering cross section values of argon and krypton for $\lambda\lambda$ 1080-1700Å. – The systematic laboratory investigation of VUV scattering requires the establishment of a secondary standard whereby all relative measurements can be placed on an absolute basis. This standard gas should be chemically nonreactive, possess spherical symmetry (zero depolarization factor) and be amenable to relatively simple handling and preparation. The rare gases qualify in all regards. Thus, new laboratory measurements were performed for the express purpose of obtaining the absolute scattering cross section values for two of the rare gases, i.e., argon and krypton over the spectral region $\lambda\lambda$ 1080-1700Å.

The photon scattering cross section of an atom can be calculated from its measured refractive index. Precise measurements in the visible and ultraviolet spectral regions have been reported for argon [70] and krypton [71,72]. An empirical extrapolation can be made to shorter wavelengths using dispersion formulae fitted to such data [73]. Recently there have been reports, both theoretical and experimental, of scattering cross sections in the vacuum ultraviolet [74-80]. The theoretical data indicate that the choice of discrete oscillator strengths is critical. For example, this is true for argon even at 1216Å, i.e., 150Å from the first resonance line [80]. The experiments have been performed with nondispersed radiation, a procedure which is somewhat inadequate in close proximity to the resonance lines where the cross sections exhibit rapid variations. In such

regions, dispersed radiation must be employed with the concomitant reduction in intensity. In the present investigation, the incident radiation (from a hydrogen source) was dispersed by a 1/2-meter Seya monochromator with an MgF_2 coated aluminized grating blazed at 1500Å with a spectral bandpass of 3Å. Monochromatic radiation entered the scattering cell through an LiF window and its transmitted intensity was monitored with an EMI 0514S phototube coated with sodium salicylate. Radiation scattered through 90 degrees was detected with an EMR541H-08-10 phototube. It has been shown that relative scattering cross sections can be obtained using this technique with much greater accuracy than absolute scattering cross sections since neither the scattering volume nor the detector geometry influence the results [76]. Cross sections measured relative to those of helium can be rendered absolute since the helium cross sections have been calculated reliably [69]. It was therefore planned to measure the scattering cross sections of the selected two rare gases relative to those of helium. However, a sufficiently strong scattered flux from helium could be obtained only at 1607Å where the source intensity, the reflectance of the grating, the transmittances of the LiF windows, and the quantum efficiency of the EMR detector combined to yield a suitably large signal. The ratio of the argon scattering cross section to that of helium at 1607Å was 92.3 ± 7.1. The scattering cross section of helium at this wavelength is $9.9 \times 10^{-27} cm^2$ [74], hence, the cross section for argon at this spectral position is $0.91 \pm 0.07 \times 10^{-24}$ cm^2. This value is in relatively good agreement with theoretical results [74,78,80] but is not sufficiently precise to establish a final distinction as shown in Figure 50. The flux scattered from argon per unit incident flux was also measured at 1215, 1176, 1162, 1146 and 1090Å. Relative scattering cross sections were deduced from these measurements (with the exception of that at 1090Å) by accounting for the variations over this spectral range of the quantum efficiencies of the phototubes and the degree of polarization of the dispersed radiation. The polarization was measured by the method of Rabinovitch, et al. [81]. Although these two corrections were relatively small, they constituted the major contributions to the estimated errors. The results, with appropriate error bars, have been normalized to the reported value of 6.4×10^{-24} cm^2 at 1216Å [76,79] as shown in Figure 50. The increase in the measured cross section at short wavelengths was more rapid than predicted. The measurements at 1090Å indicate that the scattered photon flux increased quadratically with pressure and not linearly as was the case at longer wavelengths (see Figure 51). This might be explained by strong scattering from quasi-molecules, i.e., atoms in the state of collision, the concentration of which increases quadratically with pressure. Rare gas molecules are known to exist and to absorb in the wings of the atomic resonance lines [82]. The linear plots, shown in Figure 51, suggest that such molecules do not introduce measurable errors in the data obtained at wavelengths longer than 1090Å.

Measurements were performed of the flux scattered from krypton at two wavelengths, i.e., 1215 and 1607Å. At 1216Å the scattered flux did

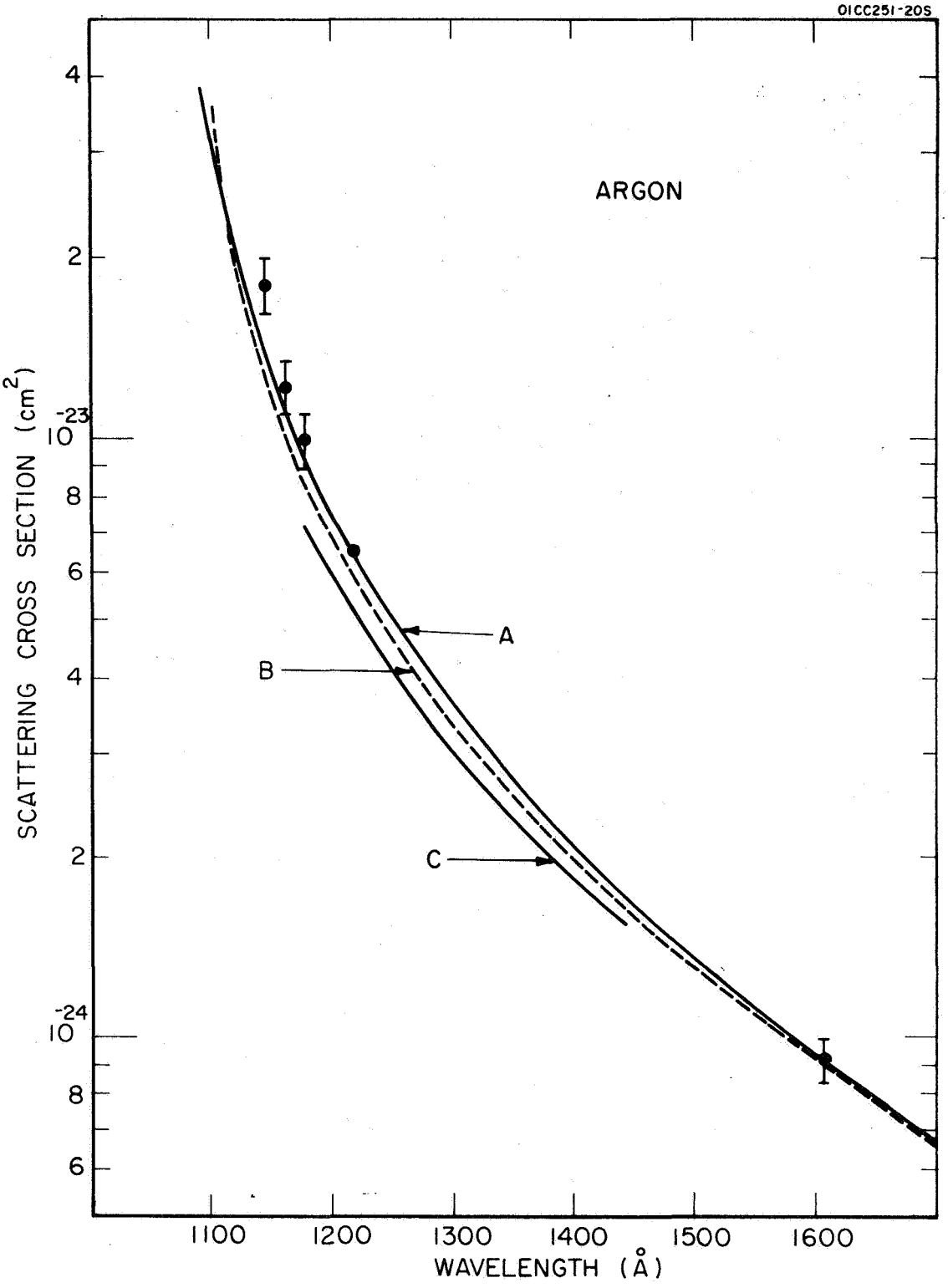

Figure 50. The scattering cross section of argon; curve A from Dalgarno and Kingston [74]; curve B from Kingston [78]; curve C from Liggett and Levinger [80]; points represent present data.

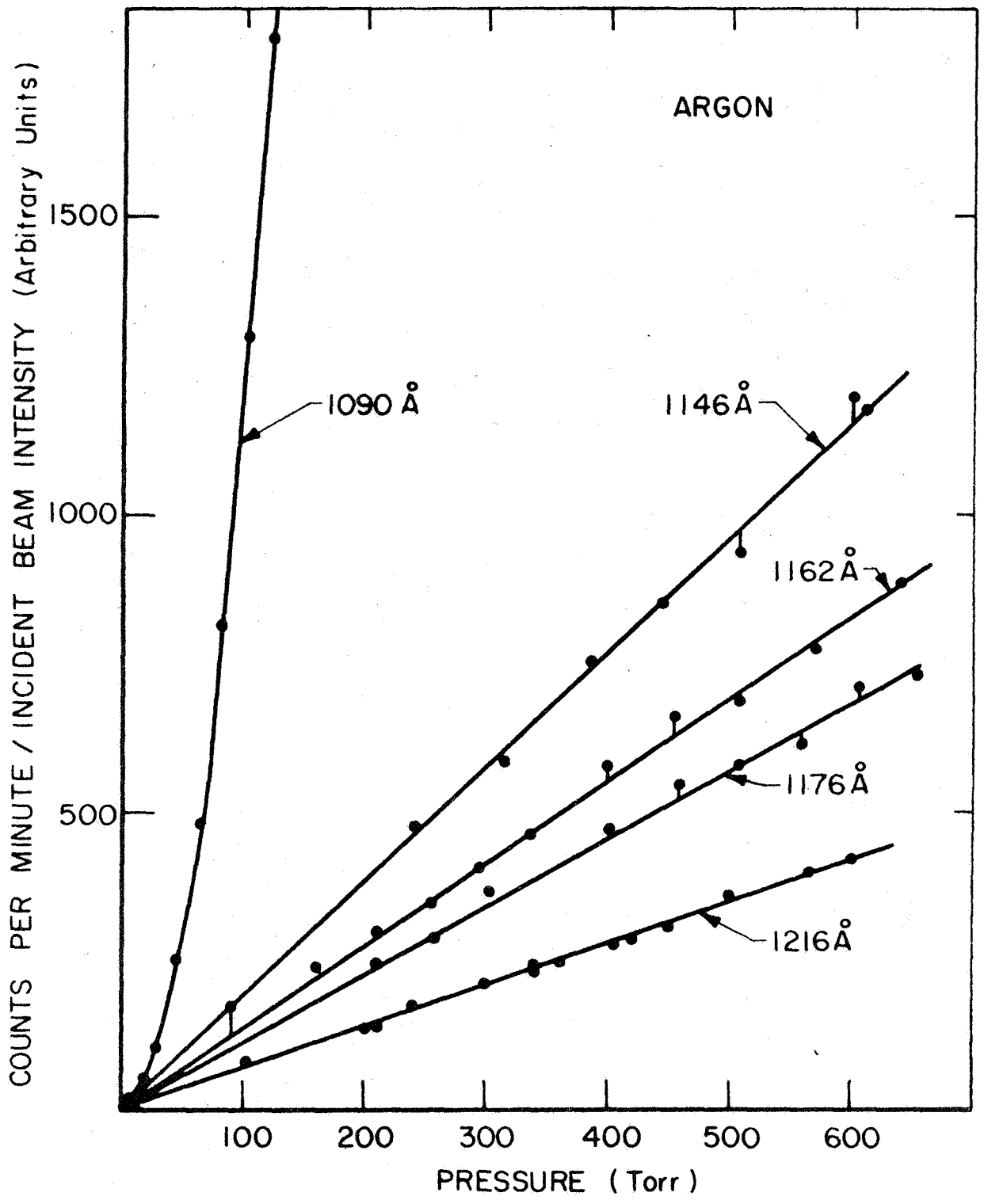

Figure 51. The scattered flux from argon as a function of pressure.

not increase linearly with pressure so that no value for the scattering cross section could be obtained. This result differs from that previously reported [76] where a preliminary and excessively large value was obtained from measurements performed on the basis of undispersed radiation. At 1607Å the measured ratio of the scattering cross section of krypton to that of argon was 3.12 ± 0.16. The scattering cross section of krypton was therefore $2.84 \pm 0.37 \times 10^{-24}$ cm^2. This result can be compared with the values of 2.60×10^{-24} and 2.64×10^{-24} cm^2 obtained, respectively, from the dispersion formula of Kronjager [71] and at 1600Å from the theory of Kingston [78].

b. Laboratory investigation on the selective scattering by CO in the VUV. – The presence of CO (due to solar photodissociation of CO_2) in the upper atmospheres of Venus and Mars may represent an important factor in establishing the VUV albedos of these planets. This point was discussed previously in the present reports where it was demonstrated that resonance-fluorescence radiation (fourth positive bands) due to solar-illuminated CO may be significantly greater than the CO_2 molecular scattering (see Figures 47 and 48). However, since CO displays strong discrete absorption bands (fourth positive band system) in the VUV, a major contributing factor to the VUV albedo may involve the corresponding enhanced molecular scattering within this band system. Unfortunately, in this complex molecular case, no theoretical procedure exists for calculating the scattering efficiency in regions of strong absorption features and additionally no pertinent experimental data are available at present. Thus, it was evident that evaluation of the role of selective molecular scattering in planetary atmospheres required the design and performance of new laboratory experimental programs in this area.

The general features of the experimental apparatus and the procedure employed have been described in detail previously [83]. Briefly, the technique involves the application of the 1/2-meter Seya monochromator to provide the monochromatic (3Å resolution) emission source, I, which is incident on the scattering volume, V, of the suitably designed scattering chamber containing the sample gas. The resultant scattered radiation is then measured by an appropriate photon detection device. In previously reported investigations [83](D-7,D-10,D-11,D-12) the scattered signal was observed at a viewing angle orthogonal to the incident beam. In the present GO measurement program, it was particularly advantageous to employ a viewing angle $54^\circ 43'$ (or the complement angle of $125^\circ 47'$) since, in this specific case, the measured value of the scattered flux can be related directly to the integrated scattering cross section, σ_s, without a priori knowledge of the individual depolarization factor, Δ_u, which is involved in scattering associated with nonspherically symmetric molecules, i.e., CO. On this basis, an improved scattering chamber configuration was designed and fabricated for the present purpose as illustrated schematically in Figure 52. A number of additional modifications are involved, but are described elsewhere (D-13).

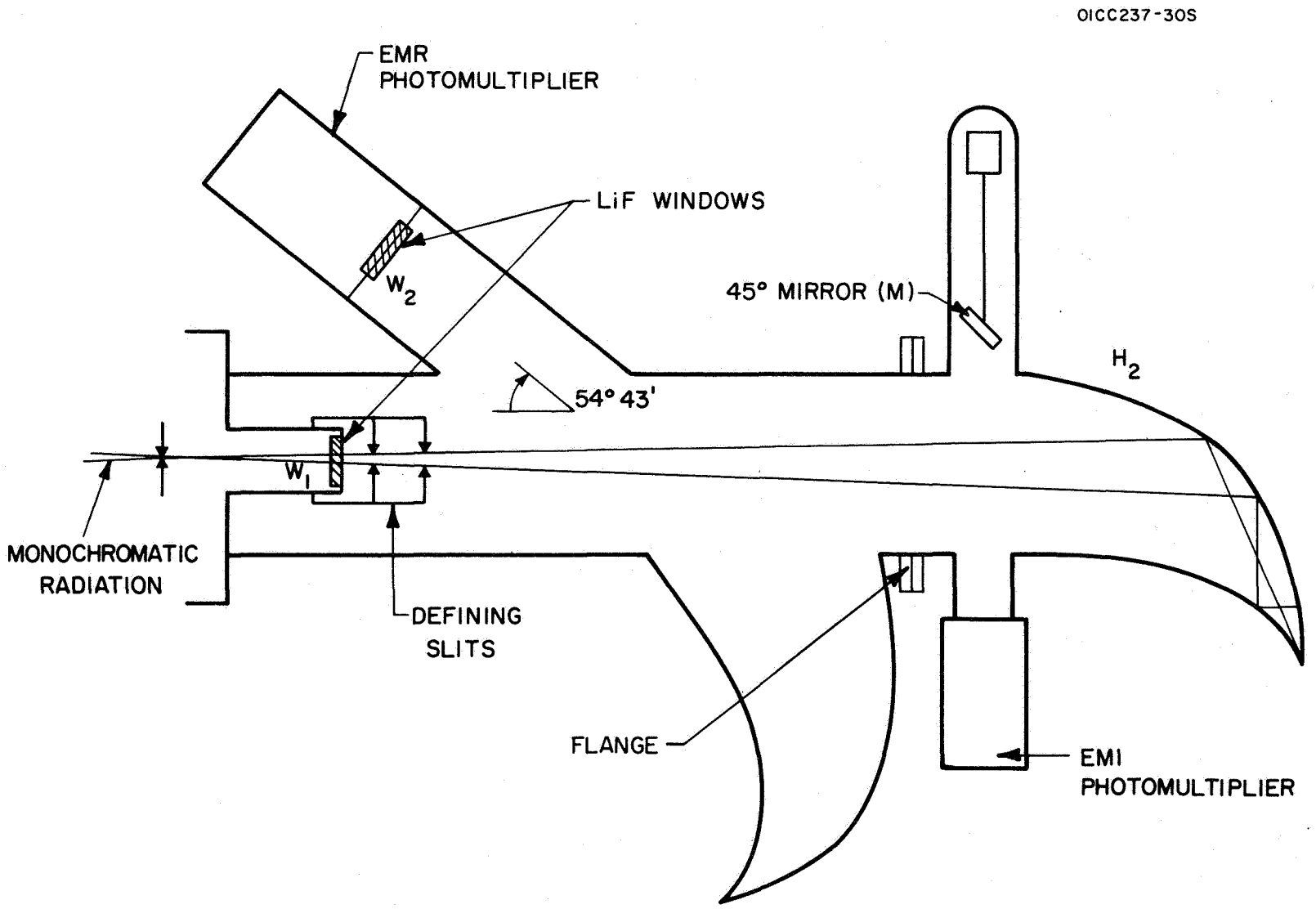

Figure 52. Schematic configuration of $54^{o}43'$ viewing scatter chamber.

The chamber was attached to the exit slit of the monochromator as indicated in the figure. A hydrogen light source was employed wherein the maximum intensity occurred at $\lambda \approx 1607$Å. At this spectral setting, two sets of data runs were performed for CO chamber pressures of 160 mm and 63.6 mm. In each case, the total counts were recorded for an integrated time interval of 20 minutes duration. The measured and derived total (20-minute duration) counts values and their associated random error components (obtained by application of the law of propagation of random errors [84]) are presented in Table 6.

TABLE 6

TOTAL COUNTS AND CORRESPONDING RANDOM ERRORS FOR MEASURED EXPERIMENTAL PARAMETERS

	Experimental Parameter	Count Value $\pm$ Error
(a)	Thermal Component, T	64 ± 8.0
(b)	Background Component, B	476 ± 24.6
(c)	Signal Component, S (160 mm; 1607Å)	3182 ± 66.0
(d)	Signal Component, S (63.4 mm; 1607Å)	1162 ± 48.6
(e)	Ratio of S-Values, R	2.74 ± 0.128

In principle, the above derived R-value should be equivalent to the ratio of the employed pressures within the random error involved. The observed degree of deviation from this expected value provided a measure of the relatively small systematic error component involved in the present investigation. In view of the preliminary nature of these results, it was decided that the indicated capability was sufficient for the present purposes.

Measurement of the relative scattering efficiency as a function of wavelength was obtained by application of the following procedure. It was found that even for the 62.6-cm case, the observed count rate was sufficiently high so that a spectral scan could be performed by employing the Hamner Linear Count Rate Meter, Model H730. Observations were performed at every 2Å interval throughout the investigated wavelength region, and the results were normalized on the assumption that the thermal count remained constant with wavelength whereas the background component varied in direct proportion to the wavelength of the radiation incident upon the scattering volume. To obtain cross section values for each 2Å interval investigated, it was necessary to account for absorption of the exit slit radiation by that portion of the chamber gas sample between the exit slit radiation and the scattering volume, V. For this purpose absorption cross

sections, σ_A, values were obtained by employing the 45-degree mirror and EMI PM tube arrangement illustrated in Figure 52. The resultant σ_A-values are shown in Figure 53 by the solid curve so designated. It was found that at 1607Å, $\sigma_A \approx 3 \times 10^{-21}$ cm^2 in relatively good agreement with the corresponding value by Watanabe, et al. [63]. The spectral variation of the scattering cross section values, σ_s, (shown by the dashed curve in Figure 53) were derived for each 2Å interval. The relative scattering values were then placed on an absolute basis by direct comparison against argon gas which had been calibrated previously on an absolute basis as discussed previously. It was demonstrated that σ_s (CO; 1607Å) $\cong 3 \times 10^{-24}$ cm^2 to within $\pm$ 20 percent.

The observed close correspondence between the strong absorption features (solid curve) and the intensity of the "scattering" signal (dashed curve) may be attributed either to the resonance-fluorescence emission subsequent to the discrete band absorption in the A $^1\Pi$ - X $^1\Sigma^+$ transition or to the enhanced selective scattering anticipated in the close vicinity of absorption features. The former process directly involves the radiative lifetimes, τ_r, of the excited electronic vibrational states; in general, for this system, $\tau_R > 10^{-8}$ sec. Thus, in the absence of "quenching," it might be anticipated that the resonance-fluorescence process would lead to observed scattering cross section values on the order of σ_A, although this was not observed. A detailed analysis (D-13) of the data has shown that the criteria for efficient self-quenching is indeed satisfied in this case so that it appears that true selective scattering does prevail under these experimental conditions. However, this tentative conclusion should be verified by additional experimentation so that any final comment on this issue should be deferred.

Finally, the results of Figure 53 indicate the existence of some interesting anomalies in the present data, i.e., in the vicinities of 1600 and 1490Å. Specifically, relatively strong scattering signals are observed in these two spectral regions of weak absorption. The 1600Å anomaly may be explained by the occurrence of the band head position at 1597Å which corresponds to the A $^1\Pi(v' = 0)$ - X $^1\Sigma^+(v'' = 1)$ transition. Calculations indicate that at 20°C only about 0.025 percent of the chamber CO molecules are in the X $^1\Sigma^+$ $(v'' = 1)$ state so that the observed weak absorption feature can be expected. Notwithstanding, a plausible explanation of this anomaly may involve additional experimental effort and data interpretation in terms of this particle transition. The anomaly in the vicinity of 1490Å has not been resolved to date.

In any case, it is clear that these and additional laboratory data are directly applicable to the interpretation of VUV observations of the atmospheres of Mars and Venus.

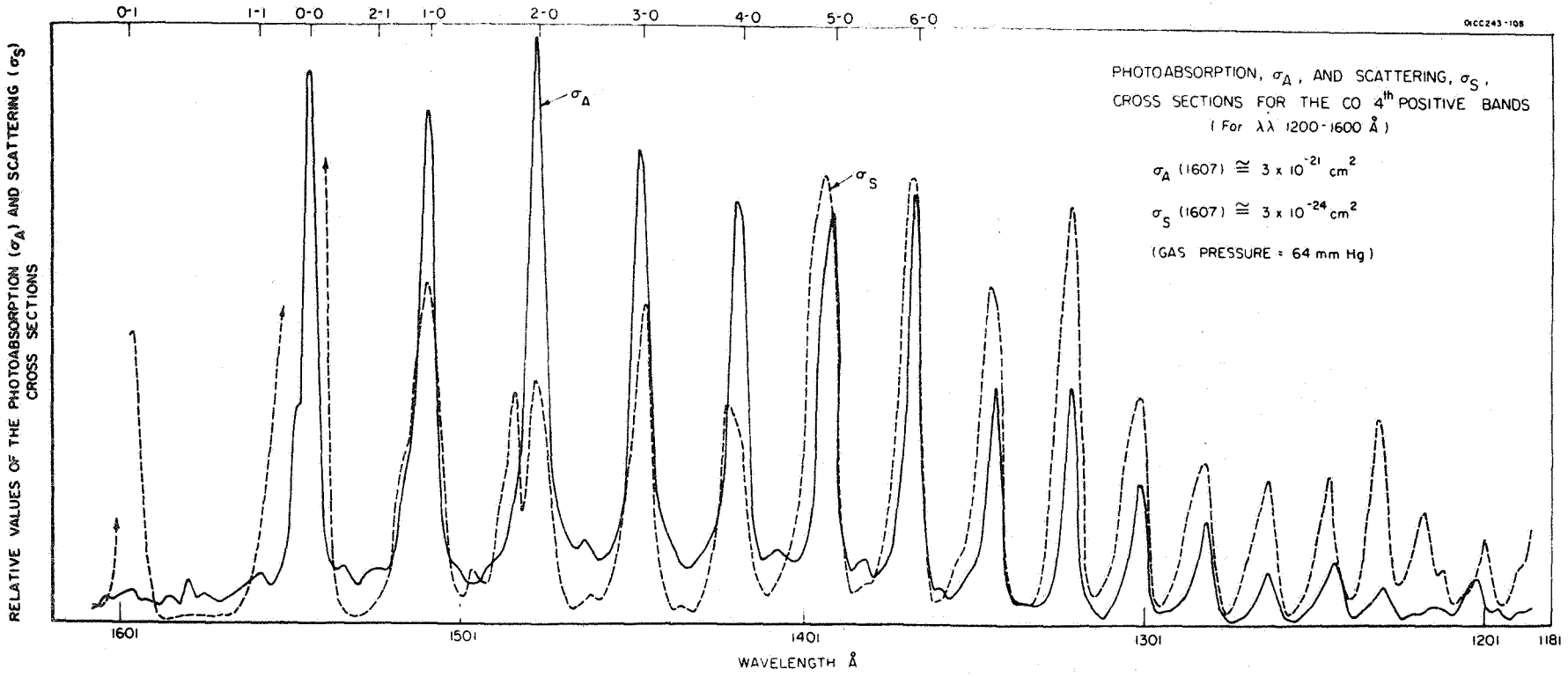

Figure 53. Photoabsorption and scattering cross sections for the CO fourth positive band system.

REFERENCES

1. Connes, J., Connes, P., and Kaplan, L. D., Science 153, 739 (1966).

2. Warneck, P., Appl. Opt. 1, 721 (1962).

3. Okabe, H., J. Opt. Soc. Am. 54, 478 (1964).

4. Sullivan, J. O. and Warneck, P., J. Chem. Phys. 46, 953 (1967).

5. Awtrey, A. D., and Connick, R. E., J. Am. Chem. Soc. 73, 1842 (1951).

6. Thompson, B. A., Harteck, P., and Reeves, R. R., J. Geophys. Res. 68, 643 (1963).

7. Romand, J., Ann. Phys. 4, 527 (1949).

8. Mason, B., The Earth as a Planet, G. P. Keuper, Ed. Vol. II, Chapter 6, University of Chicago Press (1954).

9. Holland, A. and Sullivan, J. O., GCA Technical Report No. 64-20-N, Contract No. NASw-840 (1964).

10. Miller, S. L. and Urey, H. C., Science 130, 245 (1959).

11. Warneck, P., Marmo, F. F., Sullivan, J. O., J. Chem. Phys. 40, 1132 (1964).

12. Bertolacini, R. and Barney, J., Anal. Chem. 29, 281 (1957).

13. Chen, S. W., Acta. Chemica Sinica 24, 187 (1958).

14. Narcisi, R. S. and Bailey, A. D., J. Geophys. Res. 70, 3687 (1965).

15. Paulson, J. F., Ann. Geophys. 20, 75 (1964).

16. Bogess, R. L., Brace, L. H., and Spencer, N. W., J. Geophys. Res. 64, 1627 (1959).

17. Spencer, N. W., Brace, L. H., and Carignan, G. R., J. Geophys. Res. 67, 157 (1962).

18. Brace, L. H., Spencer, N. W., and Carignan, G. R., J. Geophys. Res. 68, 5397 (1963).

19. Bowen, P. J., Boyd, R. L. F., Henderson, C. L. and Willmore, A. P., Proc. Roy. Soc. (London) A281, 526 (1964).

20. Nagy, A. F., Brace, L. H., Carignan, G. R., and Kanal, M., J. Geophys. Res. 68, 6401 (1963).

21. Brace, L. H., Spencer, N. W. and Dalgarno, A., Planet. Space Sci. 13, 647 (1965).

22. Spencer, N. W., Brace, L. H., Carignan, G. R., Taeusch, D. R. and Niemann, H., J. Geophys. Res. 70, 2665 (1965).

23. Hanson, W. B. and Johnson, F. S., Memoires Roy. Soc. Leige, Series 5, 4, 390 (1961).

24. Hanson, W. B., Space Research III, 282 (1963).

25. Dalgarno, A., McElroy, M. B. and Moffet, R. J., Planet. Space Sci. 11, 463 (1963).

26. Geisler, J. E. and Bowhill, S. A., J. Atmos. Terrest. Phys. 27 457 (1965).

27. Evans, J. V., J. Geophys. Res. 70, 1175 (1965).

28. Dalgarno, A., McElroy, M. B. and Walker, J. C. G., Planet. Space Sci. 15, 331 (1967).

29. Kolos, W. and Wolniewicz, L., J. Chem. Phys. 43, 2429 (1965).

30. Bridge, N. J. and Buckingham, A. D., Proc. Roy. Soc. A295, 334 (1966).

31. Dalgarno, A., Henry, R. J. W. and Stewart, A. L., GCA Technical Report No. 64-1-N (1964).

32. Henry, R. J. W., J. Chem. Phys. 44, 4357 (1966).

33. Warneck, P., J. Chem. Phys. 46, 513 (1967).

34. Warneck, P., Planet. Space Sci. 15, 1349 (1967).

35. Warneck, P., J. Chem. Phys. 47, 10 (1967).

36. Warneck, P., J. Geophys. Res. 72, 1651 (1967).

37. Samson, J. A. R. and Weissler, G. L., Phys. Rev. 137A, 381 (1965).

38. Keller, G. E., Martin, D. W. and McDaniel, E. W., Phys. 140A, 1535 (1965).

39. Saporoschenko, M., Phys. Rev. 139A, 352 (1965).

40. Dalgarno, A., McDowell, M. R. C. and Williams, A., Phil. Trans. Roy. Soc. (London) A250, 411 (1958).

41. Dalgarno, A., Trans. Roy. Soc. (London) A250, 428 (1958).

42. Reynolds, R. and Scherb, F., Rev. Sci. Instr. 38, 348 (1967).

43. Samson, J. A. R. in Advances in Atomic and Molecular Physics, Vol. 2, D. R. Bates and I. Estermann, Eds. Academic Press, New York, p. 177 (1966).

44. Jacobus, G. F., Madden, R. P. and Canfield, L. R., J. Opt. Soc. Am. 53, 1084 (1966).

45. Madden, R. P. in Physics of Thin Films, Vol. 1, p. 123, Academic Press, New York (1963).

46. Smith, H. M. and Turner, A. F., Appl. Opt. 4, 147 (1965).

47. Hass, G., Jacobus, G. F., and Hunten, W. R., Meeting Opt. Soc. Am. (October 1966).

48. Samson, J. A. R. and Cairns, R. B., Appl. Opt. 4, 915 (1965).

49. Pines, D., Solid State Physics, Eds. S. F. Seitz and D. Turnbull, Vol. 1, p. 367, Academic Press, New York (1955).

50. Sandström, A. E., Handbuch der Physik, Vol. 30, p. 78, Springer-Verlag, Berlin (1957).

51. Hunten, W. R. and Tousey, R., Le Journal de Physique 25, 148 (1964).

52. Rustgi, O. P., J. Opt. Soc. Am. 55, 630 (1965).

53. Hass, G. A., A. Anorg. W. Allgem. Chem. 254, 96 (1947).

54. Philipp, H. R. and Ehrenreich, H., J. Appl. Phys. 35, 1416 (1964).

55. Samson, J. A. R. and Cairns, R. B., Rev. Sci. Instr. 36, 19 (1965).

56. Marmo, F. F. and Degges, T. C., "A Satellite Experiment on the Detection of Noctilucent Clouds in the VUV Region," presented at AGU Meeting, Washington, D. C. (April 1966).

57. Fiocco, G. and Colombo, G., J. Geophys. Res. 69, 1795 (1964).

58. Mikirov, A. E., Space Research V, 815 (1965).

59. House, F., Ohring, G., Sherman, C. and Tang, W., GCA-TR-67-12-G (August 1967).

60. McElroy, M. B., Astrophys. J., 150, 1125 (1967).

61. Marmo, F. F., and Degges, T. C., "VUV Albedo for Solar Illuminated Planetary Atmospheres," presented at International Symposium on Electromagnetic Sensing from Satellites, Miami, Florida (Nov. 1965).

62. Marmo, F. F., GCA-TR-66-19-N (August 1966).

63. Watanabe, K., Zelikoff, M., and Inn, E. C. Y., AFCRC-TR No. 53 (1953).

64. Thompson, B. A., Harteck, P., and Reeves, R. R., Jr., J. Geophys. Res. 68, 6431 (1963).

65. Barth, C. A., JPL Technical Report No. 32-822 (December 1965).

66. Marmo, F. F., GCA Quarterly Progress Report No. 8, Contract NASW-1283, p. 59 (March 1966).

67. Gill, P. and Heddle, D. W. O., J. Opt. Soc. Am. 53, 847 (1963).

68. Marmo, F. F., GCA-TR-65-16-N, Contract No. NASw-840, p. 104 (1965).

69. Chan, Y. M. and Dalgarno, A., Proc. Roy. Soc. 85, 227 (1965).

70. Quarder, B., Ann de Physik 74, 255 (1924).

71. Kronjager, W., Zs. F. Phys. 98, 17 (1936).

72. Koch, J., Kungl. Fys. Sallskapets Lund Forh. 19, 173 (1949).

73. Korff, S. A., and Breit, G., Rev. Modern Physics 4, 471 (1932).

74. Dalgarno, A., and Kingston, A. E., Proc. Roy. Soc. (London) A259, 424 (1961).

75. Heddle, D. W. O., Jennings, R. E. and Parsons, A. S. L., J. Opt. Soc. Am. 53, 840 (1963).

76. Gill, P. and Heddle, D. W. O., J. Opt. Soc. Am. 53, 847 (1963).

77. Marmo, F. F. and Mikawa, Y., Bull. Am. Phys. Soc. 9, 626 (1964).

78. Kingston, A. E., J. Opt. Soc. Am. 54, 1145 (1964).

79. Shardanand, and Mikawa, Y., J. Quant. Spectrosc. Radiative Trans. 7, 605 (1967).

80. Liggett, G., and Levinger, J. S., J. Opt. Soc. Am. 58, 109 (1968).

81. Rabinovitch, K., Canfield, L. R., and Madden, R. P., Appl. Opt. 4, 1005 (1965).

82. Wilkinson, P. G., J. Quant. Spectrosc. Radiative Trans. 5, 503 (1965).

83. Marmo, F. F., GCA Quarterly Progress Report No. 11, Contract NASW-1283. (December 1967).

84. Mandel, J., The Statistical Analysis of Experimental Data, Interscience, p. 75 (1964).